AN EXPERIMENTAL AND THEORETICAL STUDY OF BUOYANCY-DRIVEN AIR FLOW IN A HALF-SCALE STAIRWELL MODEL

Thesis submitted for the degree of
Doctor of Philosophy

by

Alfred Sorooshkani Zohrabian
BSc(Eng), MSc(Eng)

Department of Mechanical Engineering
Brunel University

November 1989

To my wife Volga

ABSTRACT

The buoyancy-driven air flow and the associated energy transfer within a half-scale stairwell model have been investigated experimentally and theoretically. The experimental work comprised the larger part of the investigation.

The stairwell model consisted of a lower and an upper compartment connected through the stairway. The recirculation of air was maintained by a continuous supply of heat in the lower compartment. Two different cases, referred to as closed and open non-sloping ceiling stairwells, were considered. In the former, the stairwell formed a closed system, and in the latter situation the air was allowed to enter and leave the stairwell through small openings in the lower and upper compartments, a situation which may arise in practice due to the presence of cracks.

The experimental work provided detailed measurements of the velocity and temperature within the stairwell model. Hot-wire anemometers of a temperature-compensated type were used to measure the velocities, and the air temperatures were measured using platinum resistance probes. These measurements, supported by flow visualisation using smoke, provided a detailed description of the flow field.

Due to the symmetry condition which existed in the stairwell, the measurements were carried out in only one-half of the stairwell. The results for both closed and open cases include the velocity and temperature profiles at the throat area (minimum area between the

stairway and the lower compartment ceiling) for various distances from the side wall, mean temperatures in the upper and the lower compartments, volume and mass flows up and down the stairwell. The effect of the heat input rate on these parameters is also included. The results also include the heat losses through various surfaces bounding the system, heat and mass transfer through the stairwell joints and inlet and outlet openings, and the wall temperatures.

The theoretical work was concerned with a numerical prediction of turbulent flow in two-dimensions. The k-ε turbulence model, with the buoyancy terms included, was adopted. The governing equations for mass, momentum, energy and those of the turbulence model were solved using a finite-volume method. The model incorporates the SIMPLE algorithm for the derivation of pressure. The wall-function method was used for the treatment of the flow near the walls. The hybrid discretisation scheme was adopted.

The predicted flow pattern was in good agreement with the pattern established by experiment. The proportion of the heat loss from the upper compartment was also in good agreement with the experiment. The maximum velocities in the throat area were underpredicted. The discrepancy between the prediction and experiment is believed to arise from shortcomings of the turbulence model, the treatment of the near-wall flow and the two-dimensionality of the numerical model.

PUBLICATIONS

1. REYNOLDS, A.J., MOKHTARZADEH-DEHGHAN, M.R., ZOHRABIAN, A.S. (1988) The modelling of stairwell flows, Bldg Environ., Vol. 23, No. 1, pp. 63-66.

2. ZOHRABIAN, A.S., MOKHTARZADEH-DEHGHAN, M.R., REYNOLDS, A.J. (1988) A numerical study of buoyancy-driven flows of mass and energy in a stairwell, 9th AIVC Conference "EFFECTIVE VENTILATION" 12-15 September 1988, Gent, Belgium. Vol. 2, pp. 183-204.

3. ZOHRABIAN, A.S., MOKHTARZADEH-DEHGHAN, M.R., REYNOLDS, A.J., MARRIOTT, B.S.T. (1989) An experimental study of buoyancy-driven flow in a half-scale stairwell model, Bldg Environ., Vol. 24, No. 2, pp. 141-148.

4. ZOHRABIAN, A.S., MOKHTARZADEH-DEHGHAN, M.R., REYNOLDS, A.J. (1989) Buoyancy-driven air flow in a closed half-scale stairwell model: velocity and temperature measurements, 10th AIVC Conference "PROGRESS AND TRENDS IN AIR INFILTRATION AND VENTILATION RESEARCH" 25-28 September 1989, Espoo, Finland, Vol. 2, pp. 145-166.

5. ZOHRABIAN, A.S., MOKHTARZADEH-DEHGHAN, M.R., REYNOLDS, A.J. (1989) Buoyancy-driven air flow in a stairwell model with through-flow. Submitted to "Energy and Buildings".

ACKNOWLEDGEMENTS

I would like to express my deep gratitude to my supervisor, Dr M.R.Mokhtarzadeh-Dehghan, for his guidance, constructive criticism and advice, and continuous support throughout the course of this research.

I am grateful to Professor A.J. Reynolds for many helpful discussions, criticism and advice.

I am thankful to B.S.T. Marriott for his assistance and helpful discussions, at the early stage of the work.

I am grateful to Professor P. Stow,Dr F. Alamdari, Dr.I.P. Jones, Dr A.D. Burns and Dr C. Weber for their valuable discussions, on many aspects of the computational fluid dynamics, during the ICFD Conference in Oxford.

I am grateful to my parents and my wife Volga for their continuous support and encouragement.

I would like to acknowledge the helpful information which I received from the Air Infiltration and Ventilation Centre (AIVC), and Fire Research Station (FRS).

I have benefitted from the questions which arose during my first and third year seminars. I would like to thank Dr A.J. Ward-Smith, Dr B.E. Smith, Dr N. Ladommatos, Dr C. Clark and Dr S.A. Tassou for their fruitful criticism which is deeply appreciated.

I would like to thank the technician staff, G.H. Reading, J. Richardson, C. Barrett, D. Headley, I.T. Gates, J.M.E. Langdon, P. Mathers, H.A. Tarifa and G. Morvay, who assisted me in my experimental work.

I thank Mrs Jean Ingram, Mrs Olive Rolph and Mrs Valerie Berry for their excellent and speedy typing of the thesis

I would like to thank the staff of the Brunel University Computer Centre, in particular Mr R.S. Pank. My thanks also go to the librarians, for their assistance.

I wish to acknowledge the support of the Science and Engineering Research Council; through its 'Energy in Buildings' Specially Promoted Programme this research work was initiated.

CONTENTS

Page

NOMENCLATURE

A	Area (m^2)
a	Coefficient of discretized equations
b,c	Coefficients in the source term
C,c	Internal and external concentrations of tracer gas (ppm)
C_o	Concentration of tracer gas at time t=0
C_μ, C_1, C_2, C_3, C_D	} Constants in the k-ε turbulence model
c_p	Specific heat at constant pressure (J $kg^{-1}K^{-1}$)
DT	Differential temperature (T_H - T_C), (C deg)
E	Log-law integration constant (9.793)
f	Weighting factor of coefficients of discretized equations (Equation 5.10 and 5.15)
f_ϵ	Near-wall k-equation dissipation term parameter (Equation 5.30)
f_r	Under relaxation factor (Equation 5.38)
g	Gravitational acceleration (m s^{-2})
h	One half the height of the stairwell model (1.218 m)
J	Function given by Jayatillaka (Equation 5.34)
K	Heat conductivity (W m^{-1} K^{-1})
k	Turbulence kinetic energy per unit mass (N m kg^{-1})
ℓ	Height of the stairwell model (2.44 m)
$\dot{m}_\ell$	Leakage rate (kg s^{-1})
$\dot{m}_T$	Through-flow rate (kg s^{-1})
$\dot{m}_u, \dot{m}_d$	Upflow and downflow mass flow rates (kg s^{-1})
P	Pressure (N m^{-2})
Pe	Cell Péclet number
$\dot{Q}$	Rate of supply of heat to the stairwell (W)
$\dot{Q}_\ell$	Rate of heat loss from the stairwell (W)

$\dot{Q}_s$	Volume flow rate through leakage ($m^3\ s^{-1}$)
$\dot{q}''$	Wall heat flux ($W\ m^{-2}$)
R	Gas constant ($J\ kg^{-1}K^{-1}$)
R_ϕ	Residual source (Equation 5.39)
$R_{\phi,ref}$	Reference residual source (Equation 5.40)
S_ϕ	Source term for variable ϕ ($S_\phi = b\phi + c$)
S_T	Source term in the energy equation
t	time
t_w	Wet bulb temperature (°C)
T	Temperature (°C)
T_{av}	Average temperature within the stairwell (°C)
T_H, T_C	Mean temperatures of warm upwards-flowing air and cold downwards-flowing air, respectively (°C)
T_R	Mean air temperature in the room (°C)
T_L, T_U	Arithmetic average of the temperatures measured in the lower and upper compartments, respectively (°C)
T_w	Wall temperature (K)
T_P	Temperature at node P next to wall (K)
T_i, T_o	Inlet and outlet air temperatures through openings (°C)
u^+	Non-dimensional velocity in wall region ($u^+ = \dfrac{u}{u_\tau}$)
u_τ	Friction velocity (ms^{-1}), ($u_\tau = \sqrt{\dfrac{\tau_w}{\rho}}$)
u,v	Time averaged velocity components in x- and y-directions, respectively (ms^{-1})
U_{maxu}	Maximum velocity of the flow moving up the stairwell (ms^{-1})
U_{maxd}	Maximum velocity of the flow moving down the stairwell (ms^{-1})
$\dot{V}_i$	Inlet volume flow rate ($m^3\ s^{-1}$)

$\dot{V}_m$ Arithmetic average of the volume flow rates of the upflow and downflow (m^3 s^{-1}), ($\dot{V}_m = \frac{\dot{V}_u + \dot{V}_d}{2}$)

$\dot{V}_T$ Through-flow rate (dm^3 s^{-1})

$\dot{V}_u, \dot{V}_d$ Upflow and downflow volume flow rates (m^3 s^{-1})

V_s Stairwell volume (m^3)

y^+ Non-dimensional distance from wall

y_P Distance from node P to the adjacent wall (m)

x,y Cartesian co-ordinates

w Width of the stairwell (m)

z1,z2,z3 Distances along A'A, D'D and E'E (See Figure 2.2), respectively (m)

GREEK SYMBOLS

β Coefficient of thermal expansion (K^{-1})

Γ_ϕ Diffusion coefficient for variable ϕ ($\Gamma_\phi = \frac{\mu}{\sigma_\phi}$)

ΔT Temperature difference between the upper and lower compartments (C deg)

ε Rate of turbulence energy dissipation per unit mass (N m kg^{-1} s^{-1})

κ Von Kármán constant

λ Constant (Equation 5.40)

μ Molecular viscosity (kg m^{-1} s^{-1})

μ_t Turbulent viscosity (kg m^{-1} s^{-1})

μ_{eff} Effective viscosity ($\mu_{eff} = \mu + \mu_t$)

ν Kinematic viscosity ($\frac{\mu}{\rho}$) , ($m^2 s^{-1}$)

ρ Fluid density (kg m^{-3})

ρ_r Reference density (kg m^{-3})

$\sigma_T, \sigma_{T,t}$ Laminar and turbulent Prandtl numbers, respectively

$\sigma_\varepsilon, \sigma_k$ Constants of turbulence model

τ_w	Wall shear stress (N m^{-2})
ϕ	General dependent variable
δ_{ij}	Kronecker delta (= 1 if i = j; otherwise = 0)

SUBSCRIPTS

a	atmospheric condition
eff	Effective value
i,j	tensor notation
ℓ	leakage
m	model (Appendix E)
n,s,e,w	Control volume faces
P	node P next to wall
P,E,W, N,S	Main node and its east, west, north and south neighbouring nodes, respectively
ref	Reference value
t	Turbulent flow condition
w	Denotes wall

SUPERSCRIPTS

*	Guessed value
'	Correction

DIMENSIONLESS GROUPS

Fr	Froude number	$= \dfrac{\dot{V}_m}{A(gh)^{\frac{1}{2}}}$
Gr	Grashof number	$= \dfrac{g\ \beta\ DT\ \ A\ h}{\nu^2}$
Pr	Prandtl number	$= \dfrac{\mu\ c_p}{K}$

Ra	Rayleigh number	=	Gr.Pr
Re	Reynolds number	=	$\frac{\dot{V}_m}{\nu A^{\frac{1}{2}}}$
St	Stanton number	=	$\frac{\dot{Q}}{\rho c_p T_{av} A (g h)^{\frac{1}{2}}}$

DEFINITIONS

Throat area: The area shown by A-A' in Figure 2.2.

Side wall: The wall defined by ACDEFGHIA in Figure 5.2

Balustrade: One of the upright posts supporting the handrail is called a baluster. This is shown in Figure 1. A complete series of balusters together with the connecting string or handrail is called a balustrade. The balustrade is used to prevent users falling from the side of the stairs. A solid balustrade will also help to make the stairwell shaft into a channel, and air flowing through it will be guided by this balustrade.

Straight flight stairwell: This is the type of stairwell used for this research work. It has no landings and is a useful form of stair when the total rise is not too great, otherwise the absence of landings makes it tiring to ascend (see Figure 1). Where floor heights are great and it is essential to use a straight stair with no turns, it may be necessary to introduce a landing in the length of the stairs. This is in order to keep the number of risers (which are usually not less than two and not more than sixteen, for a stairwell with an elevation not exceeding 42 degrees) in the flights within the limits satisfying the Building Regulations 1976 (IHVE Guide 1970).

CHAPTER ONE

INTRODUCTION

1.1 INTRODUCTION

Since the energy crisis of the 1970's, the insulation of buildings has been improved considerably. As a result, the air conditioning load in buildings, and subsequently the required ventilation rate have been reduced. As a consequence the type of air flow in buildings has changed from forced convection into natural and mixed convection. Buoyancy has then become a strong factor in the indoor air flow.

Buoyancy-driven flow and the associated energy transfer within stairwells are important in relation to energy saving in buildings, thermal comfort, design of air conditioning systems, architectural design, fire prevention and control of contaminant levels in the indoor environment. Although much work has been published on the movement of air within simple geometries such as rooms, the type of flow encountered in stairwells has received relatively little attention, either experimentally or theoretically. It has become apparent that a more complete understanding of the characteristics of the flow within stairwells and its interaction with the surrounding environment is needed. This realisation has led the building and environment industry to direct research towards a fundamental understanding of the buoyancy-driven flows of the type encountered in stairwells.

Earlier experimental investigations have involved studies of interzonal heat and mass transfers by natural convection via a doorway between two adjoining rooms, and of stack effect in tall buildings. Among the first researchers who provided data on the interzonal heat and mass transfer by natural convection were Brown and Solvason (1962), Brown (1962) and Shaw (1971, 1976). Their findings have been extended by the more recent experiments of Marshall (1983, 1985, 1986), who investigated the movement of smoke in a staircase, and of Feustel et al. (1985) and Münch et al. (1986), who studied the stack effect in tall buildings, and more recently of Moodie et al. (1988), who carried out experiments on a one-third scale model of an escalator, to investigate the rapid spread of fire at King's Cross underground station. The above findings have been applied by building designers to improve the fire safety, energy saving and controlling contaminant levels in buildings. However, the dependence of characteristics of the buoyancy-induced recirculating flows within stairwells on parameters such as heating, outside temperature, and heat losses through walls and inlet and outlet openings is largely unknown.

The present study is an extension of the work started by Marriott and Reynolds (1986), which was originated as part of the "Energy in Buildings" Specially Promoted Programme of the Science and Engineering Research Council. Some other aspects of the work are reported by Reynolds (1986), Reynolds et al. (1988), Zohrabian et al. (1988), Zohrabian et al. (1989) and two studies on a one-tenth scale model by Chu (1984) and Maguire (1985).

In the present work air flow and the associated energy transfer in a one-half scale model of a typical domestic stairwell have been investigated experimentally and theoretically. The experimental programme provided detailed measurements of velocity and temperature within the stairwell model. The flow was induced by supply of heat from a source placed in the lower compartment of the stairwell. The measurements, supported by flow visualisation using smoke, provided detailed description of the flow field. The results include volume and mass flow rates of air circulating between the lower and upper compartments, which are presented for various heat input rates. However, the case of an open stairwell and stairwell with adiabatic side walls are also included and the effects on the parameters of interest are discussed. The results also include the rate of heat and mass transfer via leakage.

The velocities were measured using hot-wire anemometers of a temperature compensated type, and the temperatures were measured using platinum resistance probes. The leakage measurement was carried out using a Sieger gas analyser.

The development of more accurate mathematical models and efficient numerical solution methods and the availability of the computer power, presents an attractive alternative to experimental measurements for predicting the flow within complex building geometries such as stairwell (Day [1982], Clarke [1982], Hammond [1982]).

The mathematical model adopted consisted of the governing differential equations of mass, momentum and energy. These are transformed into the discretised form using a finite-volume technique which are then solved using Tri-Diagonal Matrix Algorithm. The model incorporated the SIMPLE algorithm of Patankar and Spalding (1972). A two equation k-ε turbulence model was adopted in which the turbulent viscosity was determined from the solution of the transport equations of the turbulent kinetic energy and its rate of dissipation. The terms modelling the effect of buoyancy were included in the mathematical model. Various discretization schemes were also adopted. The predictions include the components of velocity, temperature, kinetic energy of turbulence and rate of dissipation over the entire flow domain.

It is hoped that detailed studies of this kind would improve the existing experimental data and would lead to development of better mathematical models for prediction of the flow processes of interest. Such models would provide means of examining the effects of key controlling variables without resorting to costly experiments.

1.2 REVIEW OF THE PREVIOUS WORK

1.2.1 Experimental Studies

The survey reported here concentrates on the data and experimental work carried out since 1962. Brown and Solvason (1962) give a review of the earlier work. In most of the experiments to be described here air has been used as the working fluid. Methods of experimentation reported here are tracer gas, pressurisation and hot-wire techniques.

Among the first researchers who have provided experimental data on natural convection across rectangular openings are Brown and Solvason (1962). Their experimental rig consisted of two large sealed adjoining cavities, which were separated from one another by a vertical partition. One side of the test unit was heated and air temperatures on both sides of the partition were measured using copper-constantan thermocouples. They investigated the influence of the differential temperature on the heat transfer through openings. They carried out a series of tests for different differential temperatures, across the opening, ranging from 8 C deg to 47 C deg. They also developed a theory based on Bernoulli's equation. The experimental results were in good agreement with the theory, for Grashof numbers in the range of 10^6 to 10^8.

Shaw (1971) investigated the heat and mass transfer by natural convection, and combined natural and forced convection air flow through rectangular openings, in a vertical partition. The experimental work included measurements of the temperature and velocity profiles across the openings of different door areas of 2.05 m high and from 0.10 m to 0.9 m wide. Measurements of the velocities and temperatures were made by hot wire anemometers and thermocouples, respectively. Air temperature differentials across the opening ranged from 0 to 12 C deg. The volume flow rates were in the range of 0 to 0.3 m^3s^{-1}. Using the Bernoulli's equation already derived by Brown and Solvason (1962), the author predicted volume flow and heat transfer rates by natural convection across the opening. For the case of combined natural convection and forced air flow, the author developed a theory based on dimensional analysis. He found that the characteristic dimensionless numbers for natural convection would be a function of Reynolds and Grashof numbers. The author compared the theory with the experimental results, and also with the experimental results of Brown and Solvason (1962). The experimental results showed good agreement with the theory. The author also pointed out that the type of the flow in both natural convection and combined natural and forced air flow cases was turbulent.

Shaw and Whyte (1974) investigated the air flow through doorways, 0.10 m to 1.40 m wide, with and without the influence of temperature. They used hot wire anemometers and thermocouples to measure air velocities and temperatures. To compare the volumetric flow rates with theory, they used an expression developed earlier in a similar work by one of the authors (Shaw [1971]). Furthermore, in order to prevent the unwanted transfer of air through the doorways, to the room that needed to be isolated, they suggested supply of an excess air. This situation is important in relation with those parts of the hospitals with a high risk of infection, as an important group of bacteria which causes wound infection, can be transferred to these areas through doorways. Using the experimental results, they also derived a theoretical expression from which the amount of air required to prevent the unwanted airflow across the doorways could be determined.

Chu (1984) carried out an extensive survey of different types of stairwells in use. He conducted a series of experiments on a one-tenth scale model of a straight-flight stairwell model. He used a 24 V light bulb as the heat source to generate a recirculating flow within the stairwell model. Jack plug temperature probes were used for temperature measurements. For the velocity measurement he measured the time taken for the smoke to travel a certain distance. The general flow pattern within the stairwell model was observed using smoke. The temperatures at fifteen different positions inside the model were recorded. From the observation of the air flow patterns, he estimated the velocity in the stairwell to be in the range of 0.035 m s^{-1} to 0.12 m s^{-1} and he concluded that the flow in the stairwell was turbulent.

Maguire (1985) studied the air movement within one-tenth scale models of six different staircases. The fluid flow was generated by a heat source, positioned at the lower compartment. He used Zeatron GPE remote reading electronic thermometers to measure the temperature inside the stairwell. For each geometry the effect of balustrade was studied (see Figure 1). The temperatures at sixteen locations inside the stairwell were measured over a period of time. The measurement supported by flow visualisation using smoke, provided detailed description of the flow in the stairwell. He also derived an expression to calculate the differential temperature between the ground floor and the first-floor compartments. In order to have a more efficient dwelling he concluded that the straight-flight type of stairs without covered balustrade gives the least temperature difference between the two floors.

Feustel et al. (1985) adopted a tracer gas technique to study the effects of the wind and buoyancy-induced air flow upon infiltration in a multi-storey building. The concentration of the tracer gas together with the pressure and temperature recorded on several floors were used to determine the air flow in the stairwell. Measured pressure and tracer gas distributions were compared with those from a predictive infiltration computer model for high-rise buildings. The results showed that for a constant ambient air temperature and lower wind speeds, the flow regime in the stairwell was dominated by the buoyancy forces (i.e. air flowing from ground floor to top floor). However, at high wind speeds the air was pressed into the building at the upper floors through the leakages, and this changed the flow direction from the upper to the lower floors. Results of air flow pattern in the stairwell for different ambient air temperatures were also included. The results showed that the lower the ambient temperature, the longer the thermal buoyancy effect would dominate the wind effect. They also included that the air flow through the building could be laminar or turbulent, for example through openings and cracks.

Marshall (1985) using one-fifth scale model of a five-storey staircase, investigated the behaviour of hot gases flowing within the staircase, with the aim of improving the physical basis of the existing computer programs. He used a tracer gas technique to estimate the volume flow rates within the staircase. Based on the experimental results he obtained a simple empirical equation from which (when solved simultaneously with an equation for venting from staircase) the entrainment of air in the stairwell could be found. He suggested that these equations could be incorporated into existing computer programs for predicting the movement of smoke and fire gases within a staircase. He concluded that computer predictive methods could be used in designing smoke control systems or better protection for life safety in buildings.

In another study Marshall (1986), using the same one-fifth scale model of a five storey open shaft, conducted a detailed study into the movement of hot smoky gases in open shafts. The air supply to the fire was isolated from the air flowing into the shaft to enable its flow rate to be measured. Hot gases flowing out of the shafts were also monitored to enable the amount of air entrainment within the shaft to be determined. The experimental results included the description of the behaviour of the hot gases flowing within the shaft for different fire sizes, different ground floor and upper floor openings, and for different heights of the shaft. The results showed that increasing the fire size produced a larger mass flow rate of hot gas entering the ground floor. It was also found that the reduction of the ground floor door opening and shaft height both caused a reduction in mass flow rates. In order to predict the amount of air entrained in the shaft, the author modified a theory previously developed by Morgan and Marshall (1975, 1979) for predicting the mixing of smoke and air in an enclosed multi-level shopping mall. There was a good agreement between the experimental and predicted mass flow rates. The Reynolds number in the model varied, ranging from 5.2×10^3 to 1.3×10^4.

Marriott and Reynolds (1986) carried out a preliminary experimental investigation of the flows of mass and energy on a one-half scale stairwell model. They used the velocity and temperature probes, which were also employed by the author in the present work. However, in their stairwell model, the probes were held in an aluminium holder, positioned at the throat area. This was a disadvantage, since the velocity probes were locked in the aluminium holder and therefore the temperatures could not be measured at the same point as the velocities. Hence they adopted an interpolation technique to obtain the temperatures. For the calculation of the volume flow rates, they assumed uniform distribution of velocity profiles across the entire width of the model. However, their results were not extensive and were only limited to velocity and temperature profiles at the throat area and volume flow rates. They also concluded that probe interference with the flow did not prove to be significant. Furthermore, they suggested the following recommendations for future investigation, (i) to improve the instrumentation and design of the rig, (ii) to use thermocouples for the measurements of the heat flux through the walls.

Münch et al. (1986) studied the buoyancy induced air flow and micro-organisms concentration in a nine-storey hospital stair shaft. The concentration and pressure difference across each of the doorways and windows were used to estimate the air flow and micro-organisms flow rates. To study the influence of the temperature difference between inside and outside the stairwell, on the transportation of the micro-organisms from the lower level to the top, the temperature difference was kept at 19 C deg. The stairwell doors and windows were closed, but allowing air exchange to take place through cracks of the windows and doors. The results showed that the transportation of micro-organisms depended strongly on the temperature difference between inside and outside of the stair shaft. They concluded that the infection rate increased with the height of the hospital. They also predicted the flow theoretically, using a mathematical model based on the transport equations. However, although they suggested that a value of 20,000 for Reynolds number was likely, they treated the flow as laminar and isothermal. The difference between the prediction and measurement of the air flow rate in the stairwell was about 10 per cent.

Mahajan (1987) performed experiments on two full size adjoining rooms to measure interzonal heat and mass transfer by natural convection, in order to improve the existing analytical models. He studied the effect of temperature difference between the rooms on the air flow through openings, under two different conditions. One of the rooms was heated to an average temperature of 32 °C, while the other room was cooled to 19 °C. In the first test, the auxiliary heating and cooling were turned off. In another test the auxiliary heater was left on. The air speed was measured using temperature compensated hot wire anemometers, and thermocouples were employed for the temperature measurement. Heat and mass transfer rates through the doorway were calculated from velocity and temperature data. He also carried out flow visualisation using a smoke generator. The results showed that the flow through the opening was three dimensional and the velocity profile was not symmetrical with respect to the opening's mid-height. He also concluded that the velocity of the air moving from the warmer to the cooler room was generally higher than that moving from the cooler to the warmer. The experimental results were compared with the values predicted by a theory based on the application of Bernoulli's equation.

Riffat and Walker et al. (1988) and Riffat and Eid (1988) carried out experiments to measure air flows up and down the stairwell of a two storey building. Two SF_6 tracer gas systems were used in the experiments. The average error in the measurement of air flows was found to be 1.1 per cent and 1.5 per cent for the two systems. The systems were located one in the downstairs and the other in the upstairs. In order to improve the accuracy of the work, the tracer gas was once released in the downstairs and samples were recorded both in the upstairs and downstairs. The experiment was then repeated, this time releasing the tracer gas in the upstairs. Their results showed that the air flow rate between the floors increased from 105 m^3 hr^{-1} to 180 m^3 hr^{-1} when the temperature difference increased from 0.2 C deg to 4.0 C deg. However, the authors suggested that in winter, downstairs (living room) were heated to a higher temperature than the upstairs (bedroom), and this could cause significant energy loss.

More recently Moodie et al. (1988) carried out experiments on a one-third scale model of an escalator, in order to investigate the case of rapid spread of fire at King's Cross underground station. The escalator model was inclined at 30 degrees and set alight at a point near its base. The tests were conducted in still air conditions. The escalator was made of plywood. Their instrumentation consisted of sixty nine K-type thermocouples for temperature measurements, three ADC infra-red gas analysers, seven pitot tubes (angled to be parallel to the slope of the escalator) and a TSI hot wire anemometer for the measurement of the air velocity in the escalator shaft. These were connected to a data logging system on a microcomputer. The tests were supported by visual observations. The results showed that, following the ignition, the flame was soon established across the full width of the escalator channel. The flame front then remained low in the escalator channel as the fire developed and then progressed up the escalator. The peak temperature was 800 °C at a position below the top of the balustrades (see Figure 1). The air velocity measurements showed that the average velocity increased as the fire developed. The maximum velocity at the top of the escalator was 8 m s^{-1}. Prior to the experimental work, an analytical study of the escalator duct flow was also carried out, which was based on Froude scaling and showed that one-third scale model could provide results representative of the full scale.

Zohrabian et al. (1989) have reported the earlier studies on a half-scale stairwell model, from which the present model was developed. A different heater was used in their study (see section 2.8) and the instrumentation was less flexible. They have included detailed results for a sloping ceiling geometry (see Figure 2.2) which are not included in the present work.

1.2.2 Theoretical Studies

1.2.2.1 Analytical modelling

Analytical techniques have been comprehensively applied to a variety of problems concerning heating and cooling systems and description of the flow within building compartments. The equations derived analytically from first principles can give accurate information on the specific problems for which they are developed. Unfortunately, as problems differ from one study to another, different analytical approaches may be necessary for each study. However, although there is extensive work on the movement of air or smoke within building compartments, it is remarkable that very little information has been published on the air movement and heat transfer within typical domestic stairwells. The only available analytical approach developed for stairwell flows are those of Reynolds (1986) and Reynolds et al. (1988).

Lidwell (1977) used the Bernoulli's equation as recommended by Shaw (1971) and developed it further to predict the exchange of air across doorways. The derived expression was in terms of the temperature differential established between the spaces on both sides of the doorway as a result of the buoyancy forces or excess air supply. Comparing his results with the experimental results of Shaw (1976) and Shaw and Whyte (1974), the author concluded that the theoretical expressions could give a satisfactory quantitative account of the volumetric flow rate across a doorway with temperature differentials of up to 10 C deg.

Nevrala and Probert (1977) developed an analytical modelling of air movements in rooms, using dimensional analysis. They suggested that air movements in closed rooms are predominantly turbulent, the turbulence being of low frequency and of comparatively high amplitude. They believed that turbulence occurs throughout the room, and any heat source in the room tends to increase the general level of turbulence. They suggested that under such conditions the influence of viscous forces was restricted to the boundary regions and they play a relatively minor role in determining the overall air movement pattern. Thus they added that the invariance of Reynolds number between the model and full size flows was not essential. They concluded that accurate prediction of the air flows in full size air conditioned rooms might be obtained from observations made using small models.

Liddament (1983) used a multi-cell mathematical model to investigate the influence of the ventilation on air distribution and heat loss in a single family dwelling. The performance of natural ventilation was assessed for different climatic conditions and for two levels of air tightness. It was shown that the air movement was a function of wind direction and stack effect. However, despite the advantages of stack ventilation, the author concluded that the air change rates were largely uncontrollable in mild climates, where the temperature difference may be insufficient to drive the system. For the case of stack dominated flow, the author included a sample of ventilation rates for a two-storey dwelling.

The modelling of convective heat transfer in rooms has been studied by Howarth (1985). For rooms heated by convective sources, he developed an empirical expression to describe the magnitude of room temperature variation with height. The predicted temperature gradients were compared to the experimental data obtained by Lebrun and Marret (1976).

Reynolds (1986) developed an analytical model for the flow processes within stairwells. The author used the data, obtained from one-half and one-tenth scale models of a domestic stairwell type. He used dimensional analysis and derived dimensionless groups to characterise the recirculating flow within the stairwell. Using the results from the half-scale model and the relationship with the corresponding full-scale equivalent, he concluded that, for one-half scale models, it was possible to determine operation conditions which preserved the essential dynamical features of the motion of the full scale. Also, they can be used to determine the quantitative behaviour of prototype stairwell flows. Furthermore, he added that predictions of air flows in full size stairwells may be obtained from observations made with one-tenth scale models.

In another study Reynolds et al. (1988) extended the earlier work by Reynolds (1986) to include the role of Reynolds number. They used the data from the half-scale stairwell model for this purpose. They defined the differential temperatures in terms of warm upflow and cold downflow and mean temperatures, and derived equations which characterise stairwell type of flows. From the derived expressions it was also found that two-thirds of the heat released from the heater was lost through the walls of the upper compartment.

1.2.2.2 Numerical modelling

An alternative approach to that of the analytical methods is numerical modelling based on finite volume and finite element techniques. The partial differential equations representing the conservation of mass, momentum and energy and equations of the adopted turbulence model are discretized and then solved simultaneously throughout the flow field.

Since there are no previously reported studies of the stairwell flows (except Zohrabian et al [1988]) by numerical prediction, this section is concerned with a review of numerical studies relevant to other aspects of air movement in buildings. These include, air movement within rooms and cavities. The emphasis is given to (i) studies that include comparisons with measurements, thus allowing evaluation of the accuracy of prediction methods and (ii) studies that include the effect of buoyancy. Other studies which are not of immediate interest are briefly summarised in Table 1.

Nielsen et al. (1979) used finite-volume numerical procedure and the k-ε model of turbulence for the prediction of two-dimensional flow in rooms. They also modelled the effect of buoyancy, by introducing the buoyancy terms in the momentum equation for vertical direction, turbulence energy and dissipation rate equations.

They examined the case of cold-air injection with a predominant 'through flow' and relatively small buoyancy effect.

Ideriah (1980) employed the model adopted in the present work to compute turbulent mixed convection in a square cavity, for Reynolds number ranging from 10^4 to 2×10^5. The calculated flow, temperature and turbulence fields were presented and compared with experimental data of Grand (1975). He concluded that the computed results differed from the experimental data by 5 to 30 per cent, with the difference becoming greater when the influence of buoyancy was more pronounced.

Viollet (1981) carried out experimental as well as two-dimensional numerical studies in a liquid-metal fast breeder nuclear reactor. The fluid flowed from the core circulation in a pool-type free surface plenum, and left through heat exchanger windows. Comparing the experimental results with theory, the author suggested that in the buoyancy induced shear flows of this type, the k-ε model can be applied for the prediction of thermal fluid interaction. He concluded that the computation of highly stratified flows with sharp density gradients was possible.

A similar numerical study of the turbulent two-dimensional air flow in a square enclosure was carried out by Fraikin et al. (1980), in which the vertical walls were held at constant temperature distributions. Buoyancy effects were also accounted for. Various model constants were tested and a sensitivity study was carried out to determine the effect of the constants on the results. A comparison with the experimental data was given. The agreement was good.

Markatos et al. (1982) adopted a two-dimensional computational procedure for predicting velocity and temperature distributions in enclosures containing a fire source. The procedure was based on the solution, by finite-volume method, of two dimensional equations for the conservations of mass, momentum, energy and those of the k-ε model of turbulence. They also included the buoyancy effects in the turbulence model. The results were shown to be in reasonable agreement with the experimental data.

In another study Markatos and Pericleous (1984a) presented a two-dimensional computational method, incorporating the k-ε model of turbulence, to obtain solution of the buoyancy-driven turbulent flow in a square cavity. They concluded that more work was required to establish realistic wall-function relations for buoyancy-dominated flows. However the authors suggested that the wall function may still lead to a reasonable prediction of the overall flow structure, of the problem considered.

Ahluwalia and Shoukri (1983) also studied the turbulent mixed convection in an enclosure. The model geometry consisted of a two-dimensional square enclosure with two inlets and one outlet. Heat generation in the core region resulted in a buoyancy induced flow opposite to the recirculating flow caused by the imposed inlet/outlet flow. For predicting the flow, they employed finite-volume numerical procedure, with the buoyant version of the k-ε turbulence model. They suggested that the k-ε model appeared to be adequate for such simulation. They concluded that the results were sensitive to the empirical constants of the turbulence model.

For room ventilation flows, Alamdari (1984) developed a computer code for buoyant flows based on the elliptic code of Pun and Spalding (1977). Computations were presented for a room in which air was injected through a low or high side wall register. The supply of air governed by both cyclic and modulating control was examined. The author recommended that for further improvement of accuracy, the upwind difference-scheme should be replaced by the power-law scheme (Patankar [1980]).

In another study Alamdari et al. (1986) predicted the air flow and convective heat transfer within rectangular enclosures, for which buoyancy effects were significant. Emphasis was placed on meeting the needs of building thermal simulation programs for accurate input data on convective heat transfer. The computation was performed using finite-volume numerical procedure. The authors compared the predicted convective heat transfer coefficients with those suggested by established guides, such as CIBSE and ASHRAE.

Simcox and Schomberg (1988) investigated the flow of gases in an escalator to ascertain why the King's Cross fire spread so rapidly. They used HARWELL-FLOW3D (Burns and Jones et al. [1988]), a software package designed to predict laminar and turbulent flows. The package incorporates the k-ε turbulence model. The boundary conditions for the air velocity were taken from the measurements conducted at the adjacent Victoria line escalator shaft, and the air temperature was set to 15 °C which was recorded on the day of the fire. The 2 MW heat source, which was represented by a temperature of 500 °C was positioned below the handrail and 1.5 m along the stair tread (see Figure 1). The results showed that the hot air flowed parallel to the escalator floor, corkscrewing up the shaft. The highest air velocity caused by the 2 MW heat source was 8 m s^{-1}. As the heat source increased to 7 MW, the pattern of air flow remained the same but air was pulled in from the two adjacent escalator trenches as well as below. The maximum velocity in this case increased to 14 m s^{-1}. The conclusion drawn from these results was that flames stayed just above the steps, corkscrewing up the escalator, and moving faster as air currents pushed them upwards.

Zohrabian et al. (1988) in an earlier study of the two-dimensional buoyancy-induced flow have reported the prediction and comparison with the experimental data obtained using the present half-scale stairwell model. The boundary conditions (i.e. surface temperatures and the heat fluxes) were based on the experimental results obtained when heat loss took place from the side walls. The numerical model did not obviously take into account this heat loss. However, in the present work, the predicted results are obtained using the boundary conditions corresponding to the stairwell with adiabatic side walls.

1.3 PRESENT WORK

1.3.1 Objectives

The specific objectives of the work presented in this thesis were:

1. To improve the understanding of buoyancy-driven air flow and the associated energy transfer within stairwells.
2. To improve the design and instrumentation of an existing rig of a half-scale stairwell model.
3. To provide experimental data for stairwell flows, which are relatively less documented.
4. To provide data for validating computational models.
5. To predict the flow within the stairwell, using the k-ε turbulence model.

1.3.2 Outline of the Thesis

The thesis consists of six chapters, the first of which is the introduction.

Chapter two is concerned with the experimental rig. The stairwell model and its instrumentation are discussed in detail. The type, accuracy and calibration procedure of the velocity and temperature probes are explained. The data logging and processing are also discussed. The experimental procedure is then described, together with the procedure for processing of the experimental data. The remainder of Chapter 2 is related to the measurement of the air leakage in the stairwell.

Chapter three is concerned with the analysis of the experimental results. Visual observations of the flow are described. Velocity and temperature profiles at the throat area for both closed and open stairwell cases are described. The effect of the heat input rate on the velocity and temperature profiles are also included. Furthermore, results include the temperature profiles for two other cross-sections, differential temperatures at the throat area, heat losses through the walls, wall surface temperatures and leakage measurements. The velocity and temperature profiles for a stairwell with insulated side walls are also included. The rest of the Chapter is concerned with volume and mass flows and energy transfer rates, which are presented in tabulated form.

Chapter four is concerned with the discussion of the experimental results.

Chapter five is concerned with the numerical prediction of the stairwell flow. The time-averaged forms of the equations for conservation of mass, momentum, energy and those of turbulence energy and energy dissipation rate are presented for two-dimensional flows. The corresponding discretized forms of the governing differential equations are also presented, and the method of the solution is described. The discretization schemes are then discussed in detail. The remainder of the Chapter is concerned with the boundary conditions and computational details. Finally, the predicted results are presented and compared with the experimental results. The factors affecting the accuracy of the predicted results are also discussed in detail.

The main conclusions and the recommendations for the future work are presented in the closing Chapter six.

CHAPTER TWO

EXPERIMENTAL RIG

2.1 INTRODUCTION

This chapter is concerned with the experimental rig and instrumentation adopted for this research work and gives details of the experimental procedure and processing of the experimental results.

The original stairwell model rig was designed and constructed by Marriott (see Marriott and Reynolds [1986]). This rig was adequate for the basic information sought at that stage, when most of the measurements were concentrated in the throat area. The results obtained using this rig, have been reported in two studies by Marriott and Reynolds (1986) and Zohrabian et al. (1989). But at a later stage the rig was redesigned and reconstructed for the following reasons: (i) to make the flow visualisation possible over the entire flow field, (ii) to be able to measure the velocity and temperature in other parts of the stairwell, rather than only in the throat area, and (iii) to achieve symmetrical boundary conditions.

The air velocity encountered in the stairwell model was small, mainly in the range of 0.05 m s^{-1} to 0.6 m s^{-1}. Recent developments in the hot-wire anemometry enable measurement of velocity down to 0.05 m s^{-1}. They compensate automatically for changes in the ambient air temperature (Doebelin [1983], Sinclair et al. [1982]). The temperature differential in the throat area was in the range of 1.5 C deg. to 11 C deg. The choice of the temperature measuring system was based on its accuracy, simplicity and long term stability (Marriott and Reynolds

[1986]).

2.2 THE STAIRWELL MODEL

The one-half scale stairwell model consisted of lower and upper compartments connected through the stairway. Thirteen steps formed the stairway. The width of the stairwell was 0.608 m. A schematic diagram of the stairwell model is provided in Figure 2.1. Two different geometries were considered, which are referred to as non-sloping-ceiling and sloping-ceiling. The results for the sloping-ceiling geometry have been reported by Zohrabian et al. (1989), and are not repeated here. Figure 2.2 shows the two-dimensional view of the stairwell geometries with the corresponsing dimensions. For non-sloping-ceiling geometry both closed and open cases were studied. In the closed stairwell case, no air was allowed to enter or leave the stairwell. The circulation of air was maintained by a continuous supply of heat to the lower compartment. In the open stairwell case, air was allowed to enter the lower compartment and leave from the upper compartment, each through a rectangular opening measuring 0.01 m x 0.608 m. The area we refer to as the throat area, shown by the broken line A-A' in Figure 2.2, is the area within which most of the measurements were taken. The size of the throat area was 0.462 m^2. The model was composed mainly of Perspex and plywood, mounted within a Dexion frame. Perspex of 10 mm thickness was used for the sides of the model in order to aid visualisation. The ceiling was also made of Perspex of 6 mm thickness in order to allow illumination of the inside of the rig using the light sources located above the stairwell. Sealing of the joints was achieved mainly by foam-backed draught-proofing insulation tape.

A two-way clamp was designed in order to hold the velocity and temperature probes on the side walls. It had an external expanding collet which retained the clamps into the Perspex and an internal contracting collet to retain the probe. The clamp was locked by a screwed cap. Figures 2.3 a-c show the measuring positions of the velocities, temperatures and concentrations within the stairwell model.

The heater was placed in the extreme corner of the lower compartment; see Figure 2.2. It was a 1 kW Dimplex oil-filled electric radiator with heater dimensions 0.570 m x 0.659 m (both sides were exposed to the air). It was mounted 0.045 m from the front wall and 0.01 m above the floor. The front wall was thickened to reduce heat transfer by conduction from the lower compartment. The heat input rate to the radiator was determined from recordings of voltage and current. The accuracy of the heat input rate was about 2 per cent.

In parts of the study, in order to investigate the effect of the heat transfer from the side walls on the velocity and temperature profiles in the stairwell, the stairwell was insulated on both sides. The insulating material consisted of an inner layer of polystyrene of 0.025 m thickness followed by an outer layer of wooden boards of 0.018 m thickness.

2.3 INSTRUMENTATION

The main objective in the development of the instrumentation system adopted for this research work was to give emphasis to the use of microcomputers in the control of data collection. The instrumentation comprised nine velocity probes and ten temperature probes. The output from these being fed through the signal-conditioning to two 16-channel analogue-to-digital converters. These in turn were linked to a controlling Apple II microcomputer using the IEEE interface bus. A printer was used for printing out the results. A schematic diagram of the data-logging system is shown in Figure 2.4.

2.3.1 Velocity Measurement

2.3.1.1 Velocity measuring system

The air velocity probe was designed by Prosser Scientific Instrumentation Ltd to cover the range 0 to 1 m s^{-1}. It was a temperature compensated type and linearised. The probe sensor was located in a bore of 6 mm diameter at the centre of a nearly spherical protecting head. The output from the electronic system, following calibration, was 0 to 10 volts for 0 to 1.0 m s^{-1} velocity. The response time over this range was estimated to be about 1 second. The output from each channel was taken separately by a shielded cable, terminated by a BNC plug to an Analogue-to-Digital converter. The accuracy of the velocity measurement was estimated to be better than 10 per cent for the range of velocities measured within the stairwell.

To measure the velocity the probe head was positioned such that the air was flowing directly through the protecting head. Deviation from this position of more than five degrees in any direction could result in errors in the velocity readings. This was found by setting the probes in the wind tunnel and rotating them through

180 degrees in five degree steps. Figure 2.5 shows the variation of velocity with angle of rotation of the probe. The maximum velocity was recorded when the flow was perpendicular to the hot-wire.

2.3.1.2 Calibration of velocity probes

The calibration of the probes was carried out by Prosser Scientific Instrumentation Ltd, using a low-velocity wind tunnel which was calibrated against a single-channel low velocity system. A brief calibration sequence of a typical probe is as follows:

(i) The wind tunnel was calibrated against a calibrated standard probe.

(ii) The probe under calibration was placed in the tunnel and the output voltage was recorded.

(iii) The calibration Printed Circuit Board was put in the test rig and the flow was simulated by applying the voltage recorded in stage (ii). The circuit was then adjusted for best output linearity.

There was a nearly linear output of 1 volt per 0.1 m s^{-1} for velocities in the range of 0.2 m s^{-1} to 1 m s^{-1} Appendix A contains the results of calibration data for the velocity probes. Figure A.1 shows typical calibration curves for a velocity probe supplied by the manufacturers.

2.3.1.3 Air velocity meter AVM-5031

The multi-channel air velocity meter was supplied by Prosser Scientific Instrumentation Ltd. The equipment consisted of a modular sub-rack system, capable of accepting ten standard Eurocards. Each Eurocard contained the signal conditioning electronics for one air velocity channel. A simple arrangement of paired terminal strips (12 inputs/12 outputs) was placed at the rear of the sub-rack, there being one such pair for each of the ten card positions. The power-supply and monitor module was housed within the sub-rack. The function of the monitor unit was to allow the analogue signal to be patched from each card to a 0-10 V meter for calibration or testing purposes.

2.3.1.4 Recalibration of the velocity probes

Smoke was frequently used during the experiments in order to indicate the probe alignment with the flow. Therefore calibration changes occurred with wear, dust and contamination due to the smoke. The recalibration of velocity probes was carried out in the aerodynamic laboratory at Brunel University. The calibration rig consisted of a wind tunnel, of a working section 0.457 m x 0.457 m, which could be run at speeds of 0.1 m s^{-1} to 30 m s^{-1}. The probes were calibrated against mechanical and electronic micromanometers, using a pitot-static tube. Figure B.1 (Appendix B) shows a typical calibration curve for a velocity probe prior to and after tests. However, to verify the accuracy of the electronic micromanometer, it was calibrated against the mechanical micromanometer. Figure B.2 shows the calibration curve for the electronic micromanometer.

2.3.2 Temperature Measurement

2.3.2.1 Platinum resistance thermometers

The platinum resistance probes were supplied by

TC Ltd. The schematic diagram of the measuring circuit is shown in Figure 2.6. The probe consisted of a four-wire bridge with an additional pair of wires carried alongside the thermometer pair. This additional pair was connected close to the thermometer and the formed loop was introduced into the other side of the bridge circuit, in order to cancel the effect of the two sets of leads. The probe leads were ten metres long.

The platinum resistance thermometer detector elements are nominally 100 ohms at 0 °C, with a fundamental interval of 38.5 ohms. The element consisted of an environmental resistance combination of 99.9 per cent pure strain-free platinum wire fully encased in a high purity ceramic envelope. The detector element of the probe was protected by a stainless steel metal sheath. The sheath was 0.457 m long of 6 mm diameter. The probes were pierced shrouded tip type.

The platinum resistance probes were supplied with operating temperatures between 0 to 200 °C, but it had been calibrated only within the range of 18°C to 50 °C. It was manufactured to German standards specification (DIN 43760). It incorporated 1/5 DIN element. The time constant of the probes was three minutes. This high value resulted from the use of the stainless steel sheath. The accuracy of the 1.5 DIN probe, according to the manufacturer's supplied information, was ± 0.05 °C. The accuracy due to the calibration of the probes, was ± 0.2 °C. Hence the maximum overall error in the temperature measurements was estimated to be ± 0.25 °C.

2.3.2.2 Calibration procedure for temperature measurement system

The temperature probes were calibrated using a constant temperature water bath. The probes, five at a time, were located in a water-proof glass enclosure, together with two mercury thermometers. The enclosure was then submerged in the water bath. Figure 2.7 shows the probe calibration set-up. Appendix C contains the calibrated data for all the probes. Figure C.1 shows a typical calibration curve for platinum resistance probes, prior to and after tests.

2.3.3 Data Logging and Processing

2.3.3.1 Analogue-to-Digital converters

Two CIL Model PC, 16-channel, 12 bit Analogue-to-Digital converters were used. These were, one CIL Model PCI 1000 with 10 volts input for the velocity probes and one PCI 1001 with 100 mV differential input for the temperature probes.

2.3.3.2 Computer program for data logging

The computer program for data logging was written in BASIC. It displayed the results that had just been collected, as well as the average of the last five results. For most of the results presented here, forty readings were taken in approximately twenty seconds, for each of the velocity probes, and one reading for each of the temperature probes. The forty readings of the velocity were then averaged and together with the temperature readings were processed using the calibration data. The procedure was repeated five times and then averaged. This set of results was printed out and used for analysis. The other useful information obtained during this process was maximum and minimum values of velocity and temperature. Figure 2.8 shows the flow chart for the data acquisition system.

2.3.4 Additional Instruments

2.3.4.1 Electronic micromanometer

An electronic micromanometer type MDS FC002 was employed to calibrate the velocity probes in the wind tunnel. It was manufactured by Furness Control Ltd. Its operating range was 0 to 1.99 mm of water gauge. The manufacturer suggested a display accuracy of this device to be within 0.5 per cent with a normal operating frequency response of 50 Hz.

2.3.4.2 The "COMBIST" micromanometer

This manometer was used for the calibration of the velocity probes alongside the electronic micromanometer. The instrument was designed by the National Physical Laboratory and manufactured by Combustion Instruments Ltd. It comprised a shallow U-tube system. The left-hand limb of the U-tube was in the form of an inclined sight-glass tube. The right-hand limb consisted of a reservoir which could be raised or lowered so as to tilt the instrument about an axis coinciding with the centre line of the sight tube. The height of the reservoir in relation to the sight tube was adjusted by means of a micrometer. Another micrometer was provided for the precision sighting of the null point.

The instrument was compact and easily adaptable. The response was rapid and there was practically no zero drift. The micromanometer was sensitive to 0.01 mm w.g. (equivalent to ± 0.01 m s^{-1} with an operating range of 0 to 10 mm w.g.

2.3.4.3 Microprocessor thermometer and selector unit

The model 6101 microprocessor thermometer was supplied by Comark Electronic Ltd, with a calibration curve for temperatures in the range of 10 °C to 60 °C. The calibration was in accordance with BS 4937 using equipment traceable to British Calibration Services Certification to National Standards. Uncertainty of measurements was estimated to be less than 7 microvolts. The response time of the instrument was 1 second. It gave direct temperature reading in °C. The thermometer was characterised to accept input from type-K thermocouples. It had ten inputs via miniature thermocouple sockets mounted on an isothermal block and selected by a front panel switch.

In order to measure the surface temperatures at 57 locations inside and outside the stairwell, a type K selector unit was incorporated. It was a 1694 PF Model selector unit supplied by Comark Electronic Ltd. It was manually operated.

2.3.4.4 Thermocouples

The thermocouples were used for surface temperature measurements. They were self-adhesive patch type, supplied by TC Ltd. They were standard, type K, suitable for operating up to 250 °C. The thermocouples were supplied with a lead length of two metres and were calibrated against a mercury thermometer.

In the measurement of the surface temperature, generally two conditions have to be satisfied, (i) the sensitive element must be brought to the same temperature as that of the surface and (ii) its presence must not alter the temperature of the surface by conducting heat away from it.

For the implementation of the thermocouples two different methods were used, as suggested by Hall (1966). In the case of plywood the best method was to bury thermocouples at the surface, whereas for the Perspex the junction of the thermocouple was pegged into the surface and wires were led away along the surface.

2.3.4.5 Ventilation smoke tube

The smoke tube was employed to determine the direction of the flow within the stairwell. It was supplied by MSA Ltd. The instrument consisted of two parts, an aspirator bulb and a glass tube containing a chemical which produced white smoke when in contact with air. For the visualisation of the flow within the stairwell, a portable smoke generator, manufactured by Taylor Electronic Ltd. was used. The oil was heated by a thermostatically controlled electric heater, vaporised, and then released out of the outlet nozzle using a CO_2 gas cylinder.

2.3.4.6 Air velocity meters

While the velocity probes were employed to measure the velocity in the throat area, it was sometimes necessary to measure the velocity in other parts of the stairwell. For this reason two additional air velocity meters were also used during the course of an experiment. One was AVM 1650 supplied by TSI Ltd. It was a constant temperature hot-wire anemometer, with an operating range of 0 to 3.0 $m\ s^{-1}$. The other meter was manufactured by PSI Ltd, with the same operating range as the previous meter.

2.4 EXPERIMENTAL PROCEDURE

The heater was left on for four to five hours in order to establish a steady-state condition within the stairwell. The stairwell rig was placed in a room with no windows and therefore variation of the outside temperature had a negligible effect on conditions inside the room. During the so-called steady-state conditions, variation of the averaged velocity and temperature were 0.001 $m\ s^{-1}$ per hour and 0.09 °C hr^{-1} respectively.

At the start of a test, the flow pattern was made visible locally using smoke, and the velocity probe was aligned with the flow direction. Measurements of the velocity and temperature in the stairwell were then carried out.

2.5 PROCESSING OF THE EXPERIMENTAL RESULTS

2.5.1 Volume Flow and Mass Transfer Rates

The volume flow and mass transfer rates for warm upflow and cold downflow through the throat area were calculated from the velocity and temperature data taken at twenty locations along the height of the throat area and at six various distances from the side wall. The calculation procedure was as follows:

i) The velocity and temperature were measured at twenty locations along the height of the throat area at w/2, 5w/12, w/3, w/4, w/6 and w/12 distances from the side wall.

ii) The local density and specific heat capacity were calculated, using the atmospheric pressure, the average temperature in the stairwell and the humidity of the air (see Appendix F).

iii) For each distance from the side wall, the area under the velocity profile was calculated, using Simpson's summation technique. This was done for upflow and downflow separately.

iv) An integration was performed, employing Simpson's rule, across the width of the stairwell, using values calculated in stage (iii). This resulted in the volume flow rates in the upflow and downflow regions, respectively.

v) The mass flow rate through the warm upflow and cold downflow was calculated by repeating the procedures (i) to (iv), but in addition at stage (iii) the local velocity was multiplied by the corresponding local density, before applying the integration method.

2.5.2 Heat Losses Through the Stairwell Walls

In the case of the closed stairwell the heat losses through the stairwell walls were mainly by conduction. The heat losses through the walls were calculated using the surface temperatures measured on the two sides of the corresponding walls and the thermal heat conductivity of the material. For this purpose 118 thermocouples were used, of which half were used to measure the internal surface temperatures and the rest for the external surface temperatures. The sensors were deployed over 59 regions (24 in the lower compartment, 9 in the stairway and 26 in the upper compartment) as shown in Figure 2.3b. Owing to the condition of symmetry which existed in the stairwell, thermocouples were placed on only one-half of the stairwell, it being assumed that the same amount of heat flowed through the other half. This was verified by an experiment in which the surface temperatures were measured on both sides of the stairwell. The thermal conductivity of Perspex and the plywood were taken as 0.21 W m^{-1} $°C^{-1}$ and 0.14 W m^{-1} $°C^{-1}$ respectively (see Porges [1971]).

2.6 AIR LEAKAGE MEASUREMENT

2.6.1 Sieger IRGA-120 Gas Analyser

Air leakage may occur through tiny cracks of 0.2 mm wide or smaller. The Sieger gas analyser was employed to measure the air leakage in the stairwell. It was manufactured by J & J Sieger Ltd.

The accuracy of the instrument was estimated to be ± 1 per cent of the full-scale deflection. Response time of the analyser was approximately 20 s for the overall system, depending on the gas flow rate and the sample cell volume. The gas analyser was calibrated by the manufacturer for two different low and high calibration ranges, using CO_2 tracer gas.

2.6.2 Measurement Procedure

The tracer decay method has been used to measure the air leakage in the stairwell. Before use, the Sieger had to warm up for approximately two hours with the instrument set to stand-by mode. After the warm-up period, the machine was switched to operate mode and the Test/Sample switch was set to Sample. The CO_2 tracer gas was released in the stairwell using PVC tubing, where it was mixed with air using a fan. To ensure that a uniform concentration had been achieved in the stairwell, samples were taken at several locations in the lower and upper compartments, as shown in Figure 2.3c, and compared with each other. After a mixing period of 30 minutes, which was sufficient to achieve uniform concentration, the fan was switched off and the samples were taken every ten minutes for a total experimental time of about two hours.

2.7 HUMIDITY MEASUREMENT

The measurement of relative humidity was needed to calculate the local density and specific heat capacity within the stairwell model. The measurements were carried out using a KM 8001 relative humidity meter, supplied by Kane-May Measuring Instruments. The KM 8001 probe used a thin-film capacitive sensor for humidity measurement. The accuracy of the instrument was estimated to ± 2 per cent, with an operating range of 0 to 97 per cent RH.

2.8 DISCUSSION

The heat source used by Marriott and Reynolds (1986) and by the author in the earlier stages of the work (see Zohrabian et al. [1989]), consisted of 12 x 100 W bulbs, in rows of three, positioned inside a wooden box. The top lid of the box was composed of 21 strips of width 0.025 m, any combination of which could be removed. The output from the bulbs was controlled by the same 6 A Variac, as used for the present study. The Variac could then be adjusted to give the required heat input rate. However, as explained in section 2.2, in the present study a commercial Dimplex oil-filled radiator was used. Measurement of the heater surface temperature at four locations on each surface, showed that it remained reasonably uniform. Results for various heat input rates, showed that the difference between the maximum and minimum values of the surface temperatures was less than 4 C deg.

The Perspex ceiling of the upper compartment allowed illumination of the inside of the rig. This was achieved using a light source located above the stairwell. The results showed that the heat emitted from the light source could significantly affect the flow within the model, if it was left on for a long period.

It can be seen from Figure 2.3a that the measurements were concentrated in the throat area, from the belief that the flow conditions at this area could have crucial effects on the flow in the other parts.

In section 2.3, it was mentioned that there were nine velocity probes and ten temperature probes. For the greater part of the tests, these were located in the throat area. Of the throat area's depth (A-A' in Figure 2.2) of 0.760 m, 0.115 m were taken up by the probes, that is about 15 per cent of the total. Therefore, tests were carried out to determine whether the temperature and velocity probes themselves affected the flow processes within the model. Different probe arrangements were also tried by Marriott and Reynolds (1986). The conclusion was that the probe interference with the flow was insignificant.

In subsection 2.3.1.4, it was explained that the probes required recalibration, as calibration changes could have occurred due to contamination with smoke and dust. The recalibration results, prior to and after the tests, showed that the effect of contamination on calibration data was between two per cent to ten per cent, for velocities in the range of 0.1 m s^{-1} to 0.6 m s^{-1} respectively.

In subsection 2.3.2.2, it was mentioned that the temperature probes were calibrated against mercury thermometers. The calibration was carried out up to 50 °C, as given in Appendix C. However, for the case of 900 W heat input rate, the temperatures at the top of the throat area exceeded the limit of calibration data by up to 6 °C. The temperatures above 50 °C were therefore found by extrapolation.

In subsection 2.3.3.2, it was mentioned that a quoted value for velocity represented the average of 40 readings in approximately 20 s. This value was then referred to as the steady-state value. However, a closer look at the activity sensed by a probe indicated an unsteady behaviour. For example, for heat input rate of 600 W, the velocity variation at the top of the throat area in the warm upflow fluctuated between 0.2 m s^{-1} to 0.5 m s^{-1} over a time period of 2 s. The fluctuations were more severe in the cold downflow, near the stairs.

In section 2.4, it was mentioned that the velocity measurements were taken first by establishing the direction of the flow with the aid of flow visualisation, and then rotating the probe until it recorded the maximum value. This indicated the probe alignment with the flow. Tests indicated that the measured velocities were, to a good approximation, perpendicular to the throat area, except for those measured by six probes located at the top of the throat area, near the ceiling. This is shown in Figure 2.10. The broken lines represent the velocities actually measured. However, for the calculation of the volume flow rates (see section 2.5) the component of the velocity normal to the throat area was used. The angle between the velocities normal to the throat area and those in the direction of the flow were measured, using a pointer clamped on the probe which moved on a protractor. Furthermore, it was mentioned that a steady-state condition was achieved within a period of four to five hours. Figure 2.11 shows the differential temperatures, DT, at the throat area as a function of time and for various heat input rates. The results indicate that DT increases rapidly during the first three hours, and it becomes nearly constant after about five hours.

It was mentioned in subsection 2.6.2 that the air leakage through the stairwell joints was measured, using CO_2 tracer gas. However, it should be indicated that, although this method is quick and results are easy to interpret, it has a disadvantage that no information on the position of the leakage can be obtained (see Sinclair et al. [1982]).

In subsection 2.5.2, it was mentioned that the heat losses from the stairwell walls were mainly by conduction. However, in both closed and open stairwell cases heat was also transferred through stairwell joints and inlet and outlet openings by convection. The rate of heat transfer through the inlet and outlet openings was obtained by multiplying the mass flow rate of the flow through by the specific heat of air and the difference between the temperature measured at the inlet and outlet openings.

CHAPTER THREE

EXPERIMENTAL RESULTS

3.1 INTRODUCTION

This chapter is concerned with the experimental results. Visual observations of the flow are reported. The velocity and temperature distributions at the throat area for closed and open non-sloping ceiling stairwells are presented. The temperature distributions at two other cross-sections and mean values in the upper and lower compartments are also included. The results also include circulating volume and mass flow rates and the effect of heat input rate on the above parameters. The rest of the chapter is concerned with the heat losses through the walls, surface temperatures and leakage measurement through the stairwell joints.

3.2 VISUAL OBSERVATIONS

The general flow pattern within the stairwell was visualised with the aid of smoke injected locally in various parts of the model. A two-dimensional view of the flow pattern for a closed stairwell is shown in Figure 3.1. Three regions can be distinguished. The first is in the lower compartment which indicates a rising column of air followed by a nearly parallel flow along the ceiling. A small recirculation zone, between this compartment and the throat area, can also be seen. The returning cold air enters the lower part of the heater. The second region is the upper compartment within which two large recirculation zones can be seen. The air enters this region and moves towards the ceiling where it divides into two streams which form the recirculation zones. The third region is the throat area, on which the investigation has been focused. Here, an upflow of the warm air and a downflow of the cold air at different temperatures move in opposite directions.

Rapid mixing, indicated by smoke dispersion, was observed in the central regions of the upper and lower compartments and the stairway. The stairs are of comparable size to the other dimensions of the stairwell. They cause local smaller-scale separation and recirculation zones.

Figure 3.2 shows the flow pattern within the open stairwell. This is the case when air enters the stairwell, through an opening in the lower compartment, and leaves the upper compartment through another opening. The flow visualisation indicates that air was drawn in through the opening in the lower compartment, owing to the temperature difference between the inside and the outside of the stairwell. The air flowed a short distance along the floor and then rose along the heated surfaces of the heater. The general flow pattern in the stairwell is similar to that of the closed stairwell case.

3.3 RESULTS FOR THE CLOSED STAIRWELL CASE

3.3.1 Velocity and Temperature Profiles in the Throat Area

3.3.1.1 Various heat input rates

Tests with different heat input rates were designed to provide information on the effects of variation of heat input rate $\dot{Q}$, on the flow rate $\dot{V}_m$, and the differential temperature DT. This information was important as they represent the characteristics of the flow. The results are presented for heat input rates of 100 W, 300 W, 600 W and 900 W.

Figures 3.3 and 3.4 show, respectively, the velocity and temperature distributions at various distances from the side wall and for various heat input rates. The results indicate two distinct regions: one associated with the warm upflow, located in the upper part of the throat area, and one with the cold downflow, located in the lower part. The velocity profiles indicate an increase in velocity to a maximum very close to the ceiling, after which it drops to zero at the ceiling. The results show that, the maximum velocity varies from about 0.24 m s^{-1} at 100 W to about 0.54 m s^{-1} with 900 W heat input rate. Figure 3.4 shows that the temperature varies from its lowest value near the stairs to a maximum very near to the ceiling of the throat area. The same behaviour can be seen for other heat input rates. As expected, the increase in heat input rate has resulted in an increase in velocity and temperature of the recirculating flow. The temperature data also show that the maximum temperature varies from approximately 31 °C at 100 W to about 56 °C at 900 W heat input rate.

3.3.1.2 Various distances from the side wall

These tests were carried out in order to investigate the three-dimensional behaviour of the flow within the stairwell model. Although the measurements were carried out for six different distances from the side wall (at w/2, 5w/12, w/3, w/4, w/6 and w/12, see Table 3.1), for clarity of the Figures only results for w/2, w/3 and w/6 distances from the side wall are presented here.

Figures 3.5 and 3.6 show the velocity and temperature profiles at various distances from the side wall, respectively. The profiles for temperatures, show higher temperatures for higher heat input rates. Also, the temperature profiles show a higher degree of uniformity across the throat area for higher heat inputs. This uniformity is even more pronounced in the upper region of the throat area. However, it is interesting to note that although, as expected, the lowest temperatures were measured at position w/6, the highest temperatures were not recorded at the mid-plane (w/2) of the stairwell (except for 100 W heat input rate), but at w/3. This indicates the complex flow behaviour near the stairs. Figure 3.5 shows that the velocity profiles from one-half to one-sixth of the stairwell width, i.e. two-thirds of the width of the stairwell, are not drastically different, and an assumption of uniformity over much of the cross-section may not be ruled out entirely.

3.3.2 Comparison of the Temperature Profiles at Different Cross-sections of the Stairwell

Figures 3.7 to 3.10 show the temperature profiles at three cross-sections DD', AA' and EE', as shown in Figure 2.2, for various heat input rates, and at various distances from the side wall.

Results show that at cross-section DD', the temperature varies from a minimum near to the floor, to a maximum near to the ceiling. It is interesting to note that in over two-thirds of the cross-section the temperature remains uniform. At AA', the throat area, the warm upflow and cold downflow can clearly be distinguished. At cross-section EE', however, the strong buoyant layer leaving the lower compartment advances further (approximately one-half of the opening EE') parallel to the lower compartment ceiling, before flowing into the upper compartment.

3.3.3 The Difference Between the Temperatures in the Upper and Lower Compartments

The results for closed stairwell indicated that T, the difference between the average of five temperatures measured in each of the upper and lower compartments, varied with heat input rate as

$$\Delta T \; \alpha \; \dot{Q}^{n} \tag{3.1}$$

where n = 0.79. This is in fair agreement with the value of 0.75 adopted by Reynolds (1986).

3.4 RESULTS FOR THE OPEN STAIRWELL CASE

3.4.1 Velocity and Temperature Profiles in the Throat Area

3.4.1.1 Various heat input rates

Figures 3.11 and 3.12 show the velocity and temperature profiles at various distances from the side wall, for various heat input rates. Similar to those for the closed-stairwell case, the results indicate distinct regions of warm upflow and cold downflow. The velocity and temperature also increase as the heat input rate increases. However, the rate of increase is much higher in the upflow than in the downflow. As expected, the temperature profiles show lower values near the stairs and higher values near the ceiling. The maximum velocity varies from about 0.21 m s^{-1} for 100 W to about 0.48 ms^{-1} for 900 W heat input rate. Similarly, the temperature profiles show that the maximum temperature varies from approximately 30 °C at 100 W to 53 °C at 900 W input rate.

3.4.1.2 Various distances from the side wall

Figures 3.13 and 3.14 show velocity and temperature profiles, respectively, at various distances from the side wall, for various heat input rates. The temperature profiles were nearly uniform over the whole width of the stairwell. The degree of uniformity was greater in the upflow compared with the downflow. One should also note the higher temperature gradient in the upflow compared with that in the downflow, as mentioned in the subsection 3.4.1.1.

3.4.2 Comparison of the Temperature Profiles at Different Cross-sections of the Stairwell

Figures 3.15 to 3.18 show the temperature profiles at three cross-sections DD', AA' and EE', for various heat input rates and at various distances from the side wall. The results indicate that the temperature profiles are similar to those of the closed stairwell case. However, generally lower temperatures have been obtained.

3.5 COMPARISON BETWEEN THE RESULTS FOR THE CLOSED AND OPEN STAIRWELLS

Figures 3.19 and 3.20 provide comparisons between velocity and temperature profiles at the throat area for open and closed stairwell cases, at one-half width of the stairwell. The results indicate that the velocities and temperatures are higher in the closed case, in both upflow and downflow regions. The difference is more significant for the lower heat input rates.

Figures 3.21 and 3.22 show the temperature profiles at cross-sections DD' and EE', respectively. The results indicate that the temperature profiles are similar in both cases but they show higher temperatures in the closed stairwell case.

3.6 LEAKAGE MEASUREMENT

Tables 3.1 to 3.4 show the tracer-decay test results for various heat input rates. Figure 3.23 shows a typical curve of the CO_2 tracer-gas concentration against time (for a 100 W heat input rate), which is often plotted for practical purposes. The negative slope of the line is equal to the air change rate, given by

$$\dot{Q}_s/V_s = \text{Air change rate} \tag{3.3}$$

where V_s is the stairwell volume, and $\dot{Q}_s$ is the volume flow rate through leakage.

The complete derivation of equation 3.3 is given in Appendix D. For the actual volumetric air flow rate, or air leakage rate in this case, the stairwell volume is multiplied by the air change rate. Table 3.5 gives the air leakage rates through the stairwell joints, for various heat input rates. The results indicate that the leakage rate increases with heat input rate. It should be noted that the calculation of leakage mass flow rate was based on the arithmetic average of T_{av} and room temperature. However, the calculation of heat flow rate was based on the difference between T_{av} and the room temperature.

3.7 MAXIMUM VELOCITIES, MEAN TEMPERATURES AND FLOW RATES AT THE THROAT AREA

Tables 3.6 and 3.7 show the maximum velocities and mean temperatures in the upflow and downflow streams at various distances from the side wall and for various heat input rates. The results indicate that the maximum air velocity across the throat area varies slightly; this can be attributed to the three-dimensional nature of the flow. Also, the results show that the velocities are higher in the closed case.

The calculation of the mean temperatures T_H and T_C was based on the arithmetic mean of the temperatures measured in the warm upflow and in the cold downflow regions of the throat area, respectively. The results indicate higher temperatures for the closed stairwell case.

Tables 3.8 and 3.9 show the volume and mass flow rates for the closed and open stairwell cases and for various heat input rates. The results show that the volume and mass flow rates increase as the heat input rate increases. For the closed stairwell case, the variation of the volume flow rate $\dot{V}_m$, with the heat input rate $\dot{Q}$ can be written in the following form, as suggested by Reynolds (1986)

$$\dot{V}_m \propto \dot{Q}^n \qquad (3.2)$$

From the experimental results, it was found that n=0.22. This is in agreement with the previous results (Zohrabian et al. [1989]) and also is generally consistent with the model described by Reynolds (1986), in which the value of 0.25 was suggested.

Assuming that the inflow and the outflow through cracks take place in the lower and upper compartments, respectively, one expects that $\dot{m}_u = \dot{m}_d + \dot{m}_\ell$. The results of Table 3.8 show that the two sides of the above relationship differ by about 2 per cent for 100 W, 300 W and 600 W heat input rates and about 5 per cent for 900 W heat input rate. Similarly, for the open stairwell case, one expects that $\dot{m}_u = \dot{m}_d + \dot{m}_T$. The results given in Table 3.9 show a discrepancy of less than 2 per cent for 100 W and 300 W heat input rates and about 8 per cent for 600 W and 900 W heat input rates. The possible reasons for these discrepancies are given in section 4.5.

3.8 RATE OF HEAT LOSS THROUGH THE STAIRWELL

Tables 3.10 and 3.11 give the rate of heat loss from the stairwell walls, stairwell joints and inlet and outlet openings for various heat input rates, for closed and open stairwell cases. The results shown in Figures 3.24a and 3.24b indicate that the heat losses through the several stairwell boundaries vary approximately linearly with the heat input rate. The results also indicate that for the closed stairwell case over 50 per cent of the heat is lost through the stairwell side walls. Also for the closed stairwell case, the rate of heat loss through stairwell joints was less than 1 per cent for 100 W to 900 W heat input rates. For the open stairwell case, the heat transfer by convection through openings was about 10 per cent for various heat input rates.

3.9 EFFECT OF HEAT TRANSFER THROUGH THE SIDE WALLS

Figures 3.25 and 3.26 show, respectively, the velocity and temperature distributions, at the throat area, for 300 W and 600 W heat input rates. The results indicate higher velocities and temperatures, both in the warm upflow and in the cold downflow streams, in the case of insulated side walls.

Table 3.12 shows the rate of heat loss from the stairwell, with insulated side walls. The results show a substantial increase in the rate of heat transfer through the other walls. For example, the rate of heat transfer through the upper compartment ceiling has tripled.

CHAPTER FOUR

DISCUSSION OF THE EXPERIMENTAL RESULTS

4.1 CHARACTERISTICS OF THE FLOW

The model of the stairwell examined here is a simplified configuration compared with various designs in use. A simpler flow has also resulted by positioning the heater at the left-hand side end of the lower compartment, as shown in Figure 2.1. In practice it may be placed at one side, therefore causing a flow with strong three-dimensional behaviour. The reduction from full scale to half scale is considered unlikely to have affected significantly the essential flow processes (see Reynolds [1986]). The flow in the closed stairwell investigated here is of a purely free-convection type, while for an open stairwell a more complex mixed-convection flow exists. However, even in these simplified conditions, the flow was found to be complex.

In spite of the complex behaviour within the stairwell, with present instrumentation and also with the aid of flow visualisation, a general picture of the flow has been established and the nature and overall characteristics of the flow have been understood. The flow is three-dimensional with considerable temporal variation. Rapid mixing indicated by smoke dispersion was observed in the central regions of the upper and lower compartments and the stairway. There are at least three recirculation zones, one in the lower and two in the upper compartment, as shown in Figure 3.1. The sharp corner at the junction between the lower and upper compartments causes flow separation and instabilities. The stairs are of comparable size to the other dimensions of the stairwell. They cause local smaller-scale separation and recirculation zones. In the throat area two layers of fluid, one above the other and at different temperatures move in opposite directions. Heat and mass are exchanged as the two layers interact. Considerable difficulty was encountered in establishing even the flow direction in this region.

4.2 CHARACTERISTIC DIMENSIONLESS NUMBERS

The characteristic dimensionless numbers relevant to the natural convection in closed and open stairwell flows are the Froude, Stanton, Reynolds and Grashof numbers. Tables 4.1 and 4.2 give values of the dimensionless numbers for both closed and open half-scale stairwell geometries. Full discussion of their range for the half-scale model is also discussed by Reynolds (1987) and Reynolds et al. (1988). The corresponding values for full-scale stairwells can be found using the scaling principles set out by Reynolds (1986). These are based effectively on Froude scaling. For example, for a Froude number about 1.4 times the prototype value, requires that the ratio of the energy input of the model to the prototype be 0.24. With this Froude scaling, the magnitudes of the temperatures and velocities become identical in full and model scales (see Appendix E). Using this scaling for various heat input rates, the dimensionless numbers at the throat area were in the ranges:

$$0.01385 < Fr < 0.03130 \;,\; 0.1765 \times 10^{-3} < St < 1.5845 \times 10^{-3}$$

$$2060 < Re < 4400 \;,\; 9.7330 \times 10^{7} < Gr < 3.8190 \times 10^{8}$$

on the half scale and

$$0.00989 < Fr < 0.0224 , \quad 0.130 \times 10^{-3} < St < 1.167 \times 10^{-3}$$

$$4160 < Re < 8900 , \quad 8.024 \times 10^{8} < Gr < 3.148 \times 10^{9}$$

on the equivalent full scale.

Table 4.3 compares the temperature differential, type of the flow, Grashof numbers and Reynolds numbers as given by previous researchers. It can be seen that the dimensionless numbers for the half scale stairwell flow are within the range of those obtained for similar type of flows. However, it should be noted that:

(i) The calculation of the dimensionless numbers was based on the parameters measured at the throat area, the area of the throat and height of the stairwell model.

(ii) The fluid properties were evaluated at the arithmetic mean temperature of forty-five readings distributed within the upper and lower compartments, including the stairway.

(iii) The temperature differential DT, in the definition of the Grashof number, was derived from the temperatures measured at the throat area. The temperature differential may also be defined as the difference between the mean temperatures in the lower and upper compartments, as explained by Reynolds et al. (1988). However, the experimental results have shown that the two temperature differentials differ by only about 4 per cent.

(iv) The volume flow rates used for the calculation of the Reynolds and Froude numbers are arithmetic averages of the upflow and downflow flow rates.

The flow characteristics in the lower compartment may be understood by reference to the Rayleigh number. One of the most common, and simplest natural convective problems occurs when a vertical plane surface transfers heat to a cooler and still surrounding fluid. This is the case close to the heater, where, depending upon fluid properties and the thermal gradient, transition to turbulent flow occurs when Rayleigh number equals approximately 10^9 (Donald and Leighton [1977]). For example, for 100 W to 900 W heat input rates, the Rayleigh number, based on the heater height, the difference between the surface temperature of the heater and that of the surrounding fluid, and the fluid properties evaluated at the arithmetic mean of the temperatures measured in the lower compartment, was found to be within the range 4.361×10^8 and 1.763×10^9, respectively.

4.3 THE VELOCITY AND TEMPERATURE DISTRIBUTIONS IN THE THROAT AREA

The results indicate that the velocity profile along the height of the throat area (AA' in Figure 2.2) is not symmetrical with respect to the mid-height of the throat area (see Figure 2.10). This asymmetric velocity distribution is apparently due to the different boundary conditions at the top and bottom of the throat area and nature of approaching flow. Furthermore, the position of the zero velocity does not coincide with the mid-height of the throat area. This was established by flow visualisation. It was observed that the plane of the zero velocity was not stationary, but shifted upwards and downwards with respect to the mid-height of the throat area. However, the mean flow was approximately symmetrical with respect to the vertical mid-plane of the stairwell. This was established by measuring temperatures and velocities at the throat area at w/2, w/3 and w/6 distances from both side walls of the stairwell. There was a discrepancy of less than 2 per cent between the temperatures and less than 3 per cent between the velocities measured from the two sides. Therefore, a condition of symmetry was assumed with respect to the vertical mid-plane of the throat area, and the measurements were carried out in only one-half of the stairwell.

4.4 THE EFFECT OF DIFFERENT HEAT SOURCES

As explained in section 2.8, in the earlier studies (Zohrabian et al. [1989]) the heat source consisted of light bulbs. Although the two heat sources were quite different, the results showed that, with the same heat input rate, the velocities were only up to 10 per cent higher than those obtained using the present heater. The temperatures were nearly the same in both cases.

4.5 FLOW RATES AND FACTORS AFFECTING THEIR ACCURACY

Tables 3.8 and 3.9 give the flow rates in the upflow and downflow, at the throat area for various heat input rates and for both closed and open cases. As mentioned in section 3.7, the results indicate a discrepancy between the upflow and downflow rates (having considered the leakage and through-flow). This discrepancy can be attributed to the following reasons:

(i) Errors in the measurement of velocity.

(ii) Calculation of the volume and mass flow rates using Simpson's rule.

(iii) Failure of the point of zero velocity to coincide with the mid-height of the throat area (as was mentioned in section 4.3), as assumed for the calculation of volume flow rates.

(iv) Design of the velocity probes, which prevented measurement of velocity closer than 10 mm from the wall. The velocities at distances closer than 10 mm to the wall, were measured using a less accurate velocity meter (see section 2.3.4.6).

(v) Errors in the calculation of mass flow rates through inlet and outlet openings (for open stairwell case).

4.6 COMPARISON OF THE VOLUME FLOW RATES WITH PUBLISHED DATA

The volume flow rates generated by various heat input rates were in the range of 0.022 m^3 s^{-1} to 0.050 m^3 s^{-1} for the half-scale (see Table 3.8) and about 0.089 m^3 s^{-1} to 0.20 m^3 s^{-1} for the equivalent full scale. The results for the open stairwell case were in the range of 0.017 m^3 s^{-1} to 0.042 m^3 s^{-1} for the half-scale (see Table 3.9).

These values can be compared with the results reported by other investigators. The measurement of the air flow between the floors of a two storey building has been carried out by Riffat and Walker et al.

(1988). They found that the air flow between the floors was within the range of 0.029 m^3 s^{-1} to 0.05 m^3 s^{-1} for the temperature difference (between upper and lower floors) in the range of 0.2 C deg. to 4 C deg. A rather similar investigation, based on a multi-cell theory, was carried out by Liddament (1983). He found that in stack-dominated flows (zero external wind speed), the air flow between the floors was within the range of 0.024 m^3 s^{-1} to 0.033 m^3 s^{-1}. The present results show reasonable agreement with the above published data, for low heat input rates which result in flow rates more comparable to those occurring in real situations. However, one should note that no direct comparison between the flow rates in the stairwell model and those which occur in real houses is possible, since in real situations the lower and upper compartments comprise several rooms, which are absent in the stairwell model.

4.7 HEAT TRANSFER THROUGH THE STAIRWELL WALLS AND JOINTS

The heat transfer rates through the stairwell walls and joints for two different cases of closed and open stairwell cases, and for various heat input rates are given in Tables 3.10 and 3.11. The results indicate that more than half of the heat input to the stairwell is lost through the side walls. The results for the case of closed stairwell also indicate that there is a difference of less than 3 per cent between the measured heat input rate to the stairwell and the measured heat loss through the stairwell walls and joints. This discrepancy in the heat balance can be attributed to the following facts:

(i) The calculation of the heat loss was based on the surface temperatures measured at the mid-plane of the stairwell, and were assumed uniform across its width. However, limited measurements showed that, for a heat input of 600 W, the surface temperature varied by 0.4 C deg.

(ii) The heat input rate to the radiator was determined from recordings of voltage and current. The accuracy of the heat input rate was about 2 per cent.

In the case of open stairwell, the discrepancy between the measured heat input rate and measured heat loss from the stairwell can be attributed to the same factors mentioned above. Additionally there were errors in the measurement of the inlet and outlet velocities through the openings.

In order to investigate the effect of the heat transfer rate through the side walls on the velocity and temperature profiles at the throat area, the side walls of the stairwell were insulated. Table 3.12 gives the heat transfer rates for this case. The results shown in Figures 3.26a and b indicated that insulation of the side walls resulted in an increase in temperatures in the throat area of approximately 3 C deg. for 300 W and between 5 C deg. to 8 C deg. for 600 W heat input rates, respectively. Also, the velocities at the throat area have increased by up to 13 per cent in the upflow and up to 15 per cent in the downflow for 300 W and 600 W heat input rates, respectively. These are shown in Figure 3.25a and b. The results also indicated that insulation of the side walls resulted in a significant increase in the rate of heat transfer through the other walls. For example, the rate of heat transfer through the upper-compartment ceiling increased by about 60 per cent for both 300 W and 600 W heat input rates. Furthermore, the Reynolds number increased by 20 per cent, and the Grashof number by about 6 per cent, respectively.

It should be noted that, the values of leakage given in Table 3.12 was obtained using interpolation, from the average temperatures and leakage rates measured for the stairwell with no insulated side walls.

4.8 FLOW RATES THROUGH THE INLET AND OUTLET OPENINGS

In the case of open stairwell, the model was placed in a room with no windows. The driving mechanism responsible for the flow through the stairwell inlet was considered to be the buoyancy force resulting from the difference between the room temperature and that inside the stairwell. Experimental results showed that, for heat input rates of 100 W to 900 W, this temperature difference changed from 4 C deg. to 17 C deg. This resulted in velocities at the inlet and outlet in the range of 0.40 m s^{-1} to 1.05 m s^{-1}, respectively. The experiments showed that the velocity, measured at several locations along the width of the inlet and outlet openings, was uniform over much of the width of the stairwell.

4.9 EFFECT OF THE SIZE OF THE INLET AND OUTLET OPENING AREAS ON THE FLOW

With the configuration adopted for the open stairwell, the resulting flow entering and leaving the stairwell was about one-tenth of the circulating flow rate. However, the experimental results (supported by flow visualisation) showed that, if the inlet flow rate exceeded a certain limit (attained by increasing the inlet and exit opening areas) an alternative flow pattern would develop within the stairwell. For example, for the 600 W heat input rate and an inlet area of 0.06 m x 0.608 m (six times bigger), no downflow from the upper to the lower compartment was observed.

4.10 EFFECT OF THE STAIRWELL GEOMETRY

The effect of the stairwell geometry on the flow, temperature distribution and volume flow rates may be realized with reference to the results obtained for the sloping ceiling geometry. These are reported in detail by Zohrabian (1986) and Zohrabian et al. (1989) and are only briefly mentioned here. Figure 4.1 shows the two dimensional view of the flow pattern in the sloping ceiling geometry. The flow pattern is similar to that of the non-sloping ceiling. However, in the region where the flow enters the upper compartment through a sudden enlargement, the dispersion of smoke was more rapid for the non-sloping than for the sloping ceiling geometry. The results also indicated that the sloping ceiling had significant effect on the velocity and temperature profiles at the throat area. For the sloping ceiling, the maximum velocities were approximately 20 per cent higher in the warm upflow, but slightly lower in the cold downflow. Also, the velocity profiles at different distances from the side wall indicated that the degree of uniformity was much greater for the sloping ceiling than for the non-sloping ceiling. Furthermore, for various heat input rates adopted in this study, there was a reduction in temperature of up to 5 °C in the region near to the ceiling and up to 2 °C near to the stairs, respectively. The effect of the sloping ceiling on the volume flow rate was an increase of about 2.4 per cent for heat input rate of 100 W, and 9.8 per cent for heat input rate of 600 W.

Also, based on the experimental results, it was found that the flow rate was proportional to the heat input rate to the power of 0.25. This was in good agreement with that suggested by Reynolds (1986).

4.11 APPLICATIONS

There are several fields of study to which the results of this research work may be applied.

Consider for example, the heat loss in residential dwellings, public buildings and multi-storey shops and restaurants where the floors are heated to different temperatures. Figure 4.2 shows the volume flow rate against the differential temperature in the case of the open stairwell. Results show that the flow rates between the compartments increase as the differential temperature increases. During the winter period when higher temperature differences between the floors exist, the air flow between the floors can cause significant energy loss. In the case of a half-scale stairwell model, the results for various heat input rates have shown that 53 to 66 per cent of the heat is lost from the upper compartment.

To use the stairwell as an effective means for smoke control, full advantage must be taken of the stack effect potential of the stairwell. This means that adequate ventilation openings must be available at the bottom and the top of the stairwell, as described by Langdon-Thomas (1972) and Marchant (1972). The results of the open stairwell as mentioned earlier, indicate that the size of the opening has a strong influence on the flow movement within the stairwell. Using different sizes of the inlet and exit openings, it was observed that the formerly recirculating flow within the stairwell changed to a one-way upwards flow. This means that the ventilation at the top and bottom of the stairwell would assist smoke clearance if the inlet flow were strong enough to force the recirculating flow up the stairs to the top vent.

The general movement of air within a stairwell is also important in private dwellings, hotels and public buildings such as underground stations, in relation to fire safety. Fires in general account annually for thousands of deaths and several millions of property loss, due to the smoke and hot gases. Therefore, it is essential to know of the movement of smoke within the stairwell, especially in tall buildings. The experimental results published by Zohrabian et al. (1989) have shown that sloping ceiling geometry speeds up the migration of smoke from the lower to the upper compartment, hence it helps in the spread of fire. Also, during the winter when the temperature differences between the floors, and between the inside and outside of buildings are large, the spread of fire will be more rapid.

Most rooms in hospital buildings are connected by corridors and stairwells, through which air flows from one floor to another. The principal reasons for natural air movement are in general due to thermal buoyancy and wind pressures. The importance of movement of micro-organisms in hospital stairshafts has been shown by several workers in recent years. The measurements by Münch et al. (1986) indicated that transport of micro-organisms depends strongly on the temperature differential within the stairwell. The effect of wind pressure on the flow within the stairwell was absent in the present study. This was achieved by placing the stairwell rig in a room with no connection to the outside. The present experimental measurements, flow visualisation and air movement prediction, show that air flows from the lower floor to the higher, and the volumetric flow rate increases either by increasing the heat input rate or changing the stairwell geometry. Hence micro-organisms as well as toxic agents, which can be responsible for wound infection, can be transferred to the upper floors in the hospital buildings, through the stairwell. Therefore, special arrangement or appropriate stairwell design is needed in order to minimize the flow of micro-organisms to the higher floors.

The inter-zonal energy transfer by natural convection, within stairwells and the way that they connect different floors of domestic houses by means of warm upflow and cold downflow, is important in relation to energy saving in buildings, as described by Reynolds (1986).

Therefore, an efficient stairwell design is necessary. For this purpose, a number of key questions concerning environmental conditions within stairwells should be considered. For example:

- What are the environmental conditions associated with possible leakage?
- What are the likely air movement profiles within the stairwell?
- What are the magnitudes and where are the possible locations of the maximum and minimum temperatures within the stairwell?
- What are the effects of the heat transfer through the walls on the air movement and temperature?
- What are the effects of the different stairwell geometries?

It is hoped that the present experimental results would help in answering the above questions.

CHAPTER FIVE

NUMERICAL MODELLING OF THE STAIRWELL FLOW

5.1 INTRODUCTION

This chapter is concerned with the mathematical model which was adopted for the calculation of two-dimensional flow and heat transfer in the stairwell.

The time-averaged equations for turbulent flow are presented. The partial differential equations of mass, momentum, energy and those of two-equation k-ε model of turbulence are given. The discretization scheme adopted for this work and the solution procedure of the discretization equations are described.

The boundary conditions for the differential equations are specified and two approaches in the modelling of near wall flows are also discussed. This is followed by a description of the computational details such as, convergence, grid dependence tests, under-relaxation factors, computer time and initial conditions. Factors affecting the accuracy of the predicted results are also discussed. Finally, results are discussed and compared with experimental results.

There are a number of commercially available computer programs (for details see Appendix G) which can be used for studies of this type. None of these programs were available to the author until recently. The program used by the author (FLOW.FORTRAN, see section 5.6 originated from TEACH-T computer program. Although, this program lacks many of the capabilities of the available codes, the author, by modifying the above program to suit the present study, has gained considerable insight into the way such programs are written.

5.2 THE MATHEMATICAL MODEL

5.2.1. Time-Averaged Equations for Turbulent Flow

The governing equations for steady, two-dimensional turbulent flows in terms of time averaged properties, in tensor notation, are written as :

Continuity

$$\frac{\partial}{\partial x_i} (\rho \, u_i) = 0 \tag{5.1}$$

Momentum

$$\frac{\partial}{\partial x_j} (\rho \, \overline{u_i u_j}) = \frac{\partial}{\partial x_j} \left\{ \mu \left(\frac{\partial u_i}{\partial x_j} + \frac{\partial u_j}{\partial x_i} \right) + \rho \, \overline{u'_i u'_j} \right\} - \frac{\partial p}{\partial x_j} + S \tag{5.2}$$

Energy

$$\frac{\partial}{\partial x_j} (\rho \, \overline{T \, u_j}) = \frac{\partial}{\partial x_j} \left\{ \frac{\mu}{\sigma_T} \frac{\partial T}{\partial x_j} - \rho \, \overline{u'_j \, T'} \right\} + S_T \tag{5.3}$$

where

p	is the time-averaged static pressure
S, S_T	source terms

u_i, u_j Time averaged velocity components in the x- and y-directions, respectively.

u'_i, u'_j fluctuating part of u_i and u_j

T' fluctuating part of T

5.2.2 <u>Turbulence Model</u>

The equations 5.2 and 5.3 contain two expressions which are known as Reynolds stresses $\rho\ \overline{u'_i u'_j}$ and turbulent heat fluxes $\rho\ \overline{T'u'_j}$. The mathematical formulation which relates these expressions to the mean properties of the flow is known as turbulence model.

The choice of the turbulence model depends on the applicability, accuracy and computational economy. Detailed information about various turbulence models, which have been developed for natural and forced convection flows, is provided by Launder and Spalding (1972a), Lumly (1972), Gibson and Launder (1974), Launder and Spalding (1974), Reynolds (1974), Reynolds (1976), Rodi (1980), Kumar (1983), Lakshminarayana (1986), Gosman and Issa (1987) and Markatos (1986) who has outlined the main features and advantages and disadvantages of several turbulence models.

In this study the k-ε model was employed, which will be described in sub-section 5.2.2.1. Studies using the k-ε model have been applied to a variety of engineering problems similar to that of the stairwell. Nielsen et al. (1979) and Alamdari et al. (1986) studied buoyancy-affected flows in ventilated rooms. Ideriah (1980), Markatos et al. (1982) and Fraikin et al. (1990) predicted buoyancy-induced flows in cavities. In another study Markatos (1983) predicted the air flow and heat transfer in television studios. Markatos et al. (1984b, 1984c), Cox and Kumar (1983, 1984, Cox (1984), Cox et al. (1986), Kumar and Cox (1985) and Kumar et al. (1986) used the Fire Research Station computer program (known as JASMINE) to analyse the smoke movement in enclosures. Chen et al. (1988) have adopted the computer code PHOENICS, using the k-ε model, to study buoyancy-driven air movement in a room with ventilation. More recently, Simcox and Schomberg (1988), using the HARWELL-FLOW3D program, investigated the flow of gases in an escalator to ascertain why the King's Cross fire spread so rapidly. These tests have shown the the model provides an adequate prediction of the flow for engineering purposes.

In general, the k-ε model is the simplest model for flows where the length-scale cannot be specified empirically, for example in recirculating flows, Rodi (1980). It is the most widely tested and successfully applied turbulence model. The k-ε model offers a good compromise between the range of applicability, accuracy and computational economy. It has also been suggested by Markatos (1986) that the predictions, using the k-ε model, agree fairly well with experimental data for flows influenced by buoyancy and low Reynolds number effects.

5.2.2.1. The k-ε model

The turbulence model incorporated in the present work is the high Reynolds number k-ε eddy viscosity model of Harlow and

Nakayama (1968) as developed by Jones and Launder (1972), Launder and Spalding (1974), Ideriah (1980) and Rodi (1980).

In the k-ε model the Reynolds stresses are related to the mean velocity gradients via a turbulent viscosity

$$- \rho \overline{u'_i u'_j} = \mu_t \left(\frac{\partial u_i}{\partial x_j} + \frac{\partial u_j}{\partial x_i} \right) - \frac{2}{3} \rho k \delta_{ij} \tag{5.4}$$

Where μ_t is calculated from

$$\mu_t = C_\mu \rho k^2/\varepsilon \tag{5.5}$$

Where C_μ is an empirical constant, given in Table 5.1.

Based on the concept of eddy diffusivity, $\rho \overline{T'u'_j}$ in the energy equation can be replaced by

$$- \rho \overline{T'u'_j} = \frac{\mu_t}{\sigma_{\phi,t}} \frac{\partial T}{\partial x_j} \tag{5.6}$$

5.2.3. The Governing Equations in Differential Form

In a two-dimensional Cartesian coordinate system, the conservation differential equations for continuity, momentum and energy, and those of turbulence energy, k, and its rate of dissipation, ε, can be written in the general form

$$\frac{\partial}{\partial x}(\rho u\phi) + \frac{\partial}{\partial y}(\rho v\phi) = \frac{\partial}{\partial x}\left(\Gamma_\phi \frac{\partial \phi}{\partial x}\right) + \frac{\partial}{\partial y}\left(\Gamma_\phi \frac{\partial \phi}{\partial y}\right) + S_\phi \tag{5.7}$$

where ϕ, Γ_ϕ and S_ϕ are given in Table 5.1.

5.3. THE DISCRETIZED EQUATIONS AND SOLUTION PROCEDURE

5.3.1. The Governing Equations In Discretized Form

The first step in deriving the discretized equations is to adopt an appropriate grid system. The staggered grid system was adopted in the present study as suggested by Patankar and Spalding (1972). This is shown in Figure 5.1. In such a system the scalar variables (p, T, k, ε) are stored at the grid nodes, while u and v are stored at the mid-point between the two adjacent nodes. The staggered storage of velocities enables easy computation of mass fluxes and pressure gradients.

The governing equations in discretized form are obtained by integration of the differential equations over the corresponding control volumes, and with the aid of a discretisation scheme. The schemes chosen for this study are described in section 5.3.2. As a result the discretized form of the governing equations of thermal energy, turbulence energy and energy dissipation rate can be written as:

ϕ - transport (ϕ = T, k, ε)

$$(a_P - b)\ \phi_P = \sum_n a_n\ \phi_n + c \tag{5.8}$$

where $a_P = \Sigma_n a_n$; $a_n = \rho_n\ v_n\ A_n\ f_n$ (5.9)

and Σ_n denotes summation over neighbours N,S,E,W. A denotes the area of the control volume faces, for example north face as given in equation (5.9)

The symbol f_n represents a weighting factor, which is determined according to the chosen scheme. For example, in the hybrid difference scheme for the north boundary of the cell, it can be written as (see for example Gosman and Ideriah [1976], Ideriah [1977] and Patankar [1980]):

$$f_n = \begin{cases} 1/2\ (1 + 2\ Pe_n^{-1}) & \text{for} \quad -2 < Pe_n < 2 \\ 0 & \text{for} \quad Pe_n \geq 2 \\ 1 & \text{for} \quad Pe_n \leq 2 \end{cases} \tag{5.10}$$

where Pe is the local cell Péclet number, defined as :

$$Pe_n = \frac{\rho_n v_n \delta x_{we}}{\Gamma_n} \tag{5.11}$$

where

$$\rho_n = \frac{\rho_N + \rho_P}{2} \quad ; \quad \Gamma_n = \frac{\Gamma_N + \Gamma_P}{2} \tag{5.12}$$

and δx_{we} is the distance as shown in Figure 5.1.

The approach to drive the discretized form of the equations for components of velocity, u and v, is similar to that for scalar variables, noting that the control volumes for u and v are displaced as shown in Figure 5.1. The result is:

u - momentum

$$(a_P - b)\, u_P = \Sigma_n\, a_n\, u_n + A_{ew}\,(p_W - p_P) + c \tag{5.13}$$

v - momentum

$$(a_P - b)\, v_P = \Sigma_n\, a_n\, v_n + A_{ns}\,(p_S - p_P) + c \tag{5.14}$$

where a_P and a_n are defined in equation 5.9, and A_{ew} is the area of east/west wall of the control volume, and A_{ns} is the area of north/south wall of control volume.

The weighting factor f_n, for the north boundary of the u-cell is written as:

$$f_n = \begin{cases} 1/2\,(1 + 2\,Re_n^{-1}) & \text{for} \quad -2 < Re_n < 2 \\ 0 & \text{for} \quad Re_n \geq 2 \\ 1 & \text{for} \quad Re_n \leq 2 \end{cases} \tag{5.15}$$

where $Re_n = \dfrac{\rho_n\, v_n\, \delta x_{WP}}{\mu_n}$ and $\rho_n\, v_n$ is calculated at the mid-point of the north boundary. δx_{WP} is the distance between nodes P and W (see Figure 5.1)

5.3.2. The Discretization Schemes

A detailed description of the different discretization schemes, their mathematical formulation and shortcomings in terms of accuracy and stability are described by Patankar (1980), Leschziner (1980), Han et al. (1981), and Patel et al. (1985a and 1985b). In this study, several schemes have been considered for comparison. These are central-difference, hybrid and power law schemes. However, the results are presented using the hybrid scheme.

In the central-difference scheme a piecewise-linear variation for ϕ is assumed between the grid nodes. According to Patankar (1980), the central-difference scheme gives accurate results for $|Pe|<2$. Outside this limit the scheme is inaccurate (see also Patel et al. [1985b] and Gosman et al. [1969]).

In the upwind scheme the value of ϕ at an interface of the adjacent cells is assumed to be equal to the value of ϕ at the grid node on the upwind side.

The hybrid scheme was developed by Spalding (1972). This scheme is a combination of the central-difference and the upwind schemes. For $|Pe|<2$ it is identical to the central-difference, while outside this range, as convection dominates diffusion, it reduces to the upwind scheme.

The power-law scheme approximates closely the exponential (exact) variation of the property between the two grid nodes. According to Patankar (1980), it is premature to ignore the diffusion effects, as soon as the Péclet number exceeds 2, as is the case in the upwind scheme. This scheme has the following advantages: (i) it is not expensive to compute, and (ii) at $|Pe| > 10$ the power-law scheme becomes identical with the upwind scheme. However, this scheme requires higher computer time than the hybrid scheme.

When the streamlines and mesh lines are steeply inclined, the above schemes lead to false diffusion. The remedy for the present study was to increase the number of grid lines, as suggested by Gosman et al. (1969) and Patankar (1980). However, to overcome this shortcoming a new formulation known as QUICK (Quadratic Upwind Differencing) was developed by Leonard (1979), which eliminates false diffusion but often fails to converge (Patankar [1988]).

5.3.3. The Procedure for Solution of the Discretized Equations

The main variables in equations 5.8, 5.13 and 5.14 are u, v, k, ε and T. The remaining unknown variable, i.e. pressure, has no equation of its own. To derive the pressure, a special procedure known as SIMPLE (Semi-Implicit Method for Pressure-linked Equations) was used (see for example Patankar and Spalding [1972], Ideriah [1979] and Patankar [1980]). The procedure is based on an iterative solution of the governing equations, by which the variables, including pressure, are guessed over the entire field of solution and then corrected as the iteration proceeds. According to this procedure the continuity equation is used to derive an additional equation known as the pressure correction equation. The main variable in this equation is the pressure-correction (p'), which when added to the guessed (current) value of the pressure (p^*) results in an improved value of the pressure ($p = p^* + p'$). This equation is written in the same form as the equations for other scalar variables (T, k and ε). The six discretised equations are solved simultaneously using the line-by-line method and TDMA (Tri-Diagonal Matrix Algorithm), in the following sequence: u, v, p', T, k, ε.

5.4. BOUNDARY CONDITIONS

The usual boundary conditions are the non-slip condition for the velocity, the wall temperature and the wall heat flux. However, other modifications to the discretized equations are necessary to account for the contribution of the wall to the adjacent cell, for example in the form of the shear-stress force. Also, the equations for turbulence energy and energy dissipation rate have to be modified, as the form given in Table 5.1 is only suitable for high Reynolds number flows. If a wall thermal boundary condition is in the form of a given temperature, the wall-heat flux has to be calculated. Two of the approaches usually adopted for the special treatment near the walls are the low Reynolds number models, as described for example by Jones and Launder (1972, 1973), Rodi (1980), Patel et al. (1985c) and the "wall function" method. The first approach (not adopted in this study) requires a very fine grid within the wall layer which makes it unsuitable for complex geometries such as the stairwell. The second approach (adopted in this study) is based on the assumption that a wall layer has formed at the wall. The boundary-layer equations are then used for the calculation of various parameters such as wall shear stress and heat flux. A brief description of the near wall treatment is given below. The details of the wall function method are described in many sources, see for example Patankar and Spalding (1967), Ng and Spalding (1972), Launder and Spalding (1972b, 1974) and Ciofalo and Collins (1987).

5.4.1. Wall Treatment for Velocities

The k-ε model employed in this study is applicable to high Reynolds number flows, thus it is not valid for the viscous sublayer, where the local Reynolds number becomes very small. Near to the walls, there exists a steep variation of flow properties, and as explained earlier, this requires a very fine grid. Therefore, a special treatment of the near wall flow, known as the wall function method may be used.

Experiments have shown that in wall flows, the region near to the wall is made up of three layers, namely (see for example, Tennekes and Lumley [1973] and Kay and Nedderman [1985]):

(i) viscous sublayer where viscous forces are dominant.

Here $$u = f(y, \tau_w, \mu)$$

And $$\frac{\mu u}{\tau_w y} = 1 \qquad (5.16)$$

(ii) buffer layer where viscous and turbulence forces are of comparable magnitude.

Here

$$u = f(y, \tau_w, \rho, \mu)$$

And

$$\frac{u}{u_\tau} = u^+ = f\left(\frac{u_\tau y}{\nu}\right) = f(y^+) \qquad (5.17)$$

Where

$$u_\tau = \sqrt{\frac{\tau_w}{\rho}} \quad \text{and} \quad y^+ = \frac{\rho\, u_\tau\, y}{\mu} \qquad (5.18)$$

(iii) fully turbulent layer where the flow is completely turbulent and viscous forces are negligible.

Here $\quad \dfrac{du}{dy} = f(y, \tau_w, \rho)$

And $\dfrac{y}{u_\tau} \dfrac{du}{dy} = \text{constant} = \dfrac{1}{\kappa} \qquad (5.19)$

Thus $u^+ = \dfrac{1}{\kappa} \ln (E\, y^+) \qquad (5.20)$

where κ is Von Kármán constant that depends on the magnitude of the variation of the shear stress across the layer and on the roughness of the wall.

For this study, the buffer layer is ignored by defining a point at $y^+ = 11.63$, where the linear velocity profile in the viscous sublayer meets the logarithmic profile of the turbulent layer. Hence, it is assumed that viscous sublayer is extended to $y^+ \leq 11.63$ and the fully turbulent layer to $y^+ \geq 11.63$.

This can be expressed as follows:

For

$$y^+ \leq 11.63 \ , \quad \frac{\mu_t}{\mu} << 1 \quad , \tau = \tau_w \ , \quad \text{hence} \quad u^+ = y^+ \tag{5.21}$$

For

$$y^+ > 11.63 \ , \quad \frac{\mu_t}{\mu} >> 1 \quad , \tau = \tau_w \ , \text{ hence } u^+ = \frac{1}{\kappa} \ln \ (Ey) \tag{5.22}$$

Equations 5.19 and 5.20 describe the wall functions for velocity which are used for the nodes adjacent to the walls. However, in turbulent flows, it is advantageous to ensure that the evaluation of flow properties is carried out in the logarithmic region, i.e. the value of y_p^+ should be kept above 11.63.

An expression for the wall shear stress τ_w can be written as (see Ideriah [1980])

$$\tau_w = \rho \ C_\mu^{\frac{1}{4}} \ k_p^{\frac{1}{2}} \ \kappa \ u_p / \ln \ (E \ y_p^+) \tag{5.23}$$

where

$$y_P^+ = \rho y_P \; C_\mu^{\frac{1}{4}} \; k_P^{\frac{1}{2}} \; / \; \mu \tag{5.24}$$

5.4.2. Wall Treatment For k And ε

In the inertial sublayer ($y^+ = 30$ to 400), where the flow is assumed to be fully turbulent, the local rate of production of k is balanced by the viscous dissipation rate ε. It can be shown that

$$k = \frac{\tau_w}{\rho \, C_\mu^{\frac{1}{2}}} \tag{5.25}$$

and

$$\varepsilon = C_\mu^{3/4} \, k^{3/2} \; / \; \kappa \, y \tag{5.26}$$

Equation 5.26 is used to calculate the rate of energy dissipation for the nodes adjacent to the walls. However, the near wall turbulence energy is found from its normal transport equation, but with the following modifications:

(i) The diffusion of k to the wall is set to zero

$$\left(\frac{\partial k}{\partial y}\right)_{wall} = 0 \tag{5.27}$$

(ii) The generation term, G_k, given in Table 5.1, is modified to account for the wall shear stress as given by equation 5.23,

$$\int_{vol} \mu_t \left(\frac{\partial u}{\partial y} + \frac{\partial v}{\partial x}\right)^2 dV = \tau_w \, u_P \, dV / y_P \tag{5.28}$$

where dV is the volume of the scalar cell, shown in Figure 5.1.

(iii) For extension to 'buffer' and viscous sublayer, ε is modified to:

$$\int_{vol} \varepsilon dV = C_\mu^{3/4} \; k_P^{3/2} \; u_P^+ \; \frac{dV}{y_P} \qquad (5.29)$$

Hence, the dissipation term, $C_D\rho\varepsilon$ is also modified as :

$$C_D \; \rho \int_{vol} \varepsilon dV = f_\varepsilon \; C_D \; \rho \; C_\mu^{3/4} \; k_P^{3/2} \; u_P^+ \; \frac{dV}{y_P} \qquad (5.30)$$

Where

$$u_P^+ = y_P^+ \; , \qquad \text{for } y_P^+ \leq 11.63$$

$$u_P^+ = \frac{1}{\kappa} \ln (E \, y_P^+) \quad \text{for } y_P^+ \geq 11.63 \qquad (5.31)$$

and $\qquad f_\varepsilon = 1.0$

5.4.3. Wall Treatment for Temperature

Similar to the argument in the above section, for $y_P^+ \leq 11.63$ the transport of heat is assumed to be solely due to molecular activity. For $y_P^+ > 11.63$, the transport is assumed to be entirely due to turbulence. It should be noted that a constant heat-flux across the layer is assumed.

It can be shown that the heat flux can be calculated from the following equations.

If $y_P^+ \leq 11.63$

$$\dot{q}_W'' = \mu \, c_P \, (T_W - T_P) \, / \, \sigma_T \, y_P \qquad (5.32)$$

If $y_P^+ > 11.63$

$$\dot{q}_w'' = \rho \; c_p \; C_\mu^{\frac{1}{4}} \; k_P^{\frac{1}{2}} \; (T_w - T_P) \; / \; T_P^+ \tag{5.33}$$

Where

$$T_P^+ = \sigma_{T,t} \; [\; u_P^+ + J \;] \tag{5.34}$$

J is a function given by Jayatillaka (1969) based on experimental data for smooth surfaces;

$$J = 9.24 \left\{ \left[\frac{\sigma_T}{\sigma_{T,t}} \right]^{\frac{3}{4}} - 1 \right\} \left\{ 1 + 0.28 \exp \left[- 0.007 \; \frac{\sigma_T}{\sigma_{T,t}} \right] \right\} \tag{5.35}$$

For the heater the heat flux was known, (see Table 5.2). It was assumed that an equal amount of heat was transferred to the air from each of the two sides, that facing into the room and that facing the wall, see Figure 2.2. The heat flux was introduced directly in the energy equation via the source terms b and c in equation 5.8. For the stairwell walls the wall temperatures were known and therefore the heat flux was calculated using equations 5.32 to 5.35.

5.5. COMPUTATIONAL DETAILS

5.5.1. The Grid

The accuracy and economy of the calculations are influenced strongly by the specification of the grid lines or, in other words, cell numbers . For accuracy, the grid lines should be concentrated in areas where steep gradients of velocity and temperature occur, and reduce where the gradients are small. However, for the stairwell problem the minimum grid size was restricted, as at least two grid lines were necessary for each step of the stairs and a reasonable number for the upper and the lower compartments. The maximum grid size was also limited, if the computer time and cost were to be kept to an acceptable level.

The effect of the grid size can be realized with reference to Figure 5.3, which shows examples of grid sizes employed. The results showed that the effect of grid sizes on the parameters of interest, mainly in the throat area, were small. The calculations were therefore carried out using a 68 x 50 grid of non-uniform intervals as shown in Figure 5.3b which provided a compromise between accuracy and computer time. The number of grid lines adopted in each region of the stairwell is shown in Table 5.3. Note that, due to the staggered grid, the walls are located half-way between the adjacent grid lines.

5.5.2. Boundary and Initial Conditions

Special treatment of near wall flows as described in section 5.4 were applied to the nodes adjacent to the walls. They were incorporated via the coefficients b and c of the source terms (see for example equation 5.8) and by setting the appropriate coefficients of the discretised equations to zero. The energy dissipation was obtained from equation 5.26.

The wall boundary conditions for velocity, temperature and heat flux were incorporated by setting the velocities to zero, temperatures as specified in Table 5.2 and heat fluxes as given in Table 3.12. Note that the results presented here were obtained using the wall temperatures as the boundary condition for the stairwell walls and heat fluxes for the heater surface.

The specification of the initial conditions for all variables can be an important factor in ensuring both fast convergence and numerical stability. It is often advantageous to use the previous solutions for a new run. However, the crudest initial conditions for the variables were as follows: u was set to 0.1 m s^{-1} at the extreme end of the lower compartment (AC in Figure 5.2). The u-velocities in other locations were computed from the continuity equation. The temperature was set to 20 °C. v and p were set to zero. The turbulence energy and energy dissipation rate were obtained from

$$k = 0.03\, u^2 \tag{5.36}$$

$$\varepsilon = k^{3/2} / 0.005\, \ell \tag{5.37}$$

where ℓ is the height of the stairwell.

5.5.3. <u>Physical Properties</u>

The physical properties of air were calculated using the local temperatures, and the density was obtained from, $\rho = p_{ref} / R\,T$ (see Markatos [1983], Markatos et al. [1984a], Whittle [1986], Malin [1987]).

5.5.4. Under-Relaxation Factors

Another factor affecting the computing time and also numerical stability was under-relaxation factor, f_r, which was used in conjunction with the solution of the discretised equations. It was defined as

$$\phi_{new} = f_r \phi + (1 - f_r)\, \phi_{old} \tag{5.38}$$

where ϕ is the current value and ϕ_{old} and ϕ_{new} are the values before and after relaxation.

In this study the following values of f_r were employed: 0.5 for u and v, 0.7 for k, ε as well as μ_t, and 1.0 for P' and T. The only available method for choosing the most appropriate under-relaxation factors was that of trial and error. Also, it was necessary to solve the discretised equations more than once, during each iteration. This is known as "sweeping" through the computational field. In this study two sweeps (from west to east of the flow domain) were carried out for all variables except pressure correction for which five sweeps were used.

5.5.5. Convergence

The criterion for convergence in studies of this type is to check the gradual reduction of the sum of the residual sources of all the cells. Referring to equation 5.8, the residual sources are obtained from

$$R_\phi = (a_P - b)\, \phi_P - \Sigma_n \; a_n \, \phi_n - c \tag{5.39}$$

An exact solution would lead to zero residuals. The sum of the residual sources are normally compared with a suitable reference value $R_{\phi,ref}$. For example, for an open system, the sum of mass residuals is compared with the inflow of mass into the flow domain. Therefore, it is required that

$$\Sigma \left| R_{\phi} \right| < \lambda R_{\phi,ref} \tag{5.40}$$

where λ is a constant, having a small value (say 0.001). However in this study, in the absence of such an obvious reference value, the variation of the sum of the residual sources (for each variable) was plotted against the number of iterations and examined. The results showed considerable fluctuations at first followed by a gradual stabilization and decrease. The computation stopped when

(i) The sum of the residual sources for the u- and v-momentum equations and the mass conservation equation reduced to a relatively small value.

(ii) The computed values of each variable, at selected nodes, reached steady values.

For the results presented here, about 800 iterations were needed for a converged solution to be achieved. Furthermore, although the converged solution gave an indication of the extent to which the numerical solution of the equations have been achieved, it was also found useful to ensure that energy was conserved within the stairwell boundaries (Holmes et al. [1987]). For example, for the converged solution, in the case of 300 W heat input rate, the difference between the heat input rate (from the heat source) and the heat output rate (through the stairwell walls) was less than 1 per cent.

5.5.6. Accuracy

The accuracy of the numerical solution, in general, is influenced by the following factors:

(i) The degree to which the solution satisfies the discretised equations - This can be assessed by the level of the residual-sources. For a satisfactory solution the residual sources should be of order 10^{-3} of the reference value (see equation 5.40).

(ii) The conditions imposed at the boundaries - The physical boundary conditions can influence the final results and should be modelled realistically.

(iii) The degree to which the solution depends on the grid arrangement - A grid-independence test should be obtained, such that no significant change is observed with further increasing of the grid lines.

(iv) The adequacy of the turbulence model - This can have major influence on the accuracy of the solution. The accuracy can be assessed in comparison with experiment.

(v) Round-off errors arise because computers only carry out calculations to a limited number of significant figures. However, this error is not important as calculations of the same problem with 6, 8 and 16 significant figures make negligible difference in the results (Gosman et al. [1969]).

5.5.7. Computer Time

The computing time per iteration was 4 to 5 seconds on a Pyramid 9820 computer. This merely gives an idea of the computing time involved because the computing time, in general, depends on many factors. The type of computer and grid size are obviously important. But it also depends on how efficiently the computer program is written and how the initial conditions are defined. Using information from previous runs for the initial conditions reduces the computing time considerably.

5.6. THE COMPUTER PROGRAM

The two-dimensional results presented here were obtained using a modified version of a computer program called FLOW-FORTRAN (see Appendix G). Figure 5.4 illustrates the flow-chart of the present computer program. It indicates the sequence of the operations and briefly indicates their function.

5.7. RESULTS AND DISCUSSION

The two-dimensional numerical model adopted in the present study is a simple representation of the flow phenomena within the half-scale stairwell model. The experimental work on the half-scale stairwell model showed that the flow was three-dimensional and unsteady. There were a number of separation and recirculation zones. The relative importance of viscosity varies dramatically throughout the field, being very large in corners and near the steps, and relatively small in the body of the flow. An additional difficulty in modelling the flow is the great variety of heat transfer processes which must be described in adequately realistic fashion. There is heat transfer from every surface and the nature of the flow changes profoundly around the boundaries of the field.

The two-dimensional approach adopted here, therefore, only gives a general picture of the actual flow. A three-dimensional approach should provide a better solution. However, any model is based on a set of assumptions which may be violated in one way or another in these wide-ranging conditions. The flow pattern predicted for 300 W heat input rate is shown in Figure 5.5. This shows close agreement with the pattern established in the experimental work, as shown in Figure 3.1. The predicted flow pattern was similar for 600 W heat input rate (not shown here). The main features of the flow are the rising column of warm air along the heated walls of the heater, followed by a nearly parallel flow along the ceiling of the lower compartment. As the air flows into the upper compartment, part of it forms a recirculation zone and the other part moves towards the ceiling and, after a circulation in the upper compartment, flows down along the steps to the lower part of the heater.

The predicted velocity profiles at the throat area, using the hybrid scheme, is shown in Figure 5.6. The experimental values are also included. This figure shows that the maximum velocities are underpredicted in the upflow, and in the lower region of the downflow. However, in comparing the two, one should bear in mind that the experimental results are obtained in three-dimensional flow. The difference may also be attributed, apart from the inadequacy of the mathematical model, to the experimental error inherent in the data. Also, it should be noted that the measurement of the wall temperatures showed that they varied along each wall, while average values were adopted in this study. This approach was chosen because a single value is probably what is available to a designer.

Figures 5.7a-b show, respectively, the velocity contours for 600 W and 300 W heat input rates. In both cases results show higher velocities near the heater, near the ceiling of the first floor compartment and along the stairs. However, comparing the two cases, results indicate higher velocities for the higher heat input rate.

Figures 5.8a-b show the contour plot of the predicted temperature field for 300 W heat input rate . The range of temperatures in the throat area obtained by computation was 52 °C to 62 °C for the case of 300 W heat input rate, as shown in Figure 5.8a. This was high compared with the measured values, which were in the range of 33 °C to 41 °C.

The overprediction of the temperature may be related to the turbulence model, as similar over-prediction has been reported by Alamdari et al. (1986), Markatos et al. (1982) and Hoffmann and Markatos (1988). However, the authors of the first study suggested that a factor (f_ε) might be introduced into the dissipation term of the turbulence energy equation to reduce the rate of dissipation of turbulence energy near the walls (see equation 5.30). In this study introduction of $f_\varepsilon = 0.05$ reduced the overall temperature by about 12 °C. This is shown in Figure 5.8b. But, this in turn affected the velocities at the throat area. The velocities were lower in the upflow by 15 per cent and higher in the downflow by 9 per cent.

For the results presented here, the measured surface temperatures were introduced as the wall boundary conditions, except the heater. But heat fluxes can also be used as boundary conditions, if they are available, as is the case in the present study. This situation was also examined. Specifying the heat fluxes (see Table 3.12) as boundary conditions resulted in underestimation of the temperature throughout the stairwell, compared with experimental data. For example, in the case of 300 W heat input rate, the temperatures at the throat area were underpredicted by 4 °C to 6 °C. The effect on the velocities was not significant in the lower and upper compartments. However, the maximum velocity in the upflow was increased by 3 per cent and the maximum velocity in the downflow was reduced by 15 per cent, compared with the predicted results shown in Figure 5.6.

The results obtained using two different discretization schemes (see sub-section 5.3.2), namely, the power law and the hybrid schemes, not shown here but reported by Zohrabian et al. (1988), indicated that the difference between the two predicted results was not appreciable. The central-difference scheme was also applied. However, this did not lead to a converged solution. The choice of discretization scheme is closely related to the range of cell Péclet number. The Péclet numbers were in the range of -20 to 20 in the lower compartment, and -10 to 10 in the upper compartment. Higher values were obtained near the heater and close to the walls, and much smaller values in the central regions of the recirculation zones. The range of Péclet numbers indicates the reason for failure of the central-difference scheme.

Reference values of the air properties were calculated at the ambient temperature T = 293 K. However, to verify the effect of the reference temperature on the results, it was varied from 10 °C to 50 °C. Examination of the rsults showed that, the effect of the reference temperature on the parameters of interest was not significant.

An examination of the experimental results for the stairwell with insulated side walls and for various heat input rates showed that 52 to 57 per cent of the heat loss took place through the upper compartment. The prediction, however, overestimated this heat loss indicating a value of 65 per cent.

Figures 5.9a-b show the contour plot of the predicted turbulence energy. The results show high turbulence energy in the central region of the stairway, near the throat area. The results also indicate that the turbulence was much higher in the downflow near to the stairs than in the upflow. For example, in the locations where the maximum upflow and downflow velocities were measured, the values of turbulence energy were about 2.752×10^{-3} N m kg^{-1} and 8.527×10^{-3} N m kg^{-1} respectively, the difference being about 67 per cent. Also, the turbulence energy, on the average, was about 35 per cent higher in the upper compartment than in the lower compartment. Furthermore, reduction of the heat input rate from 600 W to 300 W reduced the turbulence energy at the throat area by about 30 per cent.

Figures 5.10a-b show the predicted energy dissipation rate for 600 W and 300 W heat input rates, respectively. The predicted results are similar to those of turbulence energy, showing higher values near the central region of the stairway. Also, results indicate higher values for higher heat input rates.

The comparison has been made here only between the velocities and temperatures, predicted and measured. Some investigatory tests were carried out to obtain an idea of the order of magnitude of the turbulence intensities and turbulence energy. Unfortunately, the available DISA equipment was not of a temperature compensated type and therefore the measurements were subjected to an unknown degree of error. However, the results were promising as they indicated that the regions of high turbulence were predicted correctly by the model, and also the magnitude of the turbulence energy near the ceiling of the lower compartment was within 10 per cent of the computed values.

A sensitivity test was carried out in order to determine the influence of the constants in the turbulence model on the calculated results. The constants C_μ, σ_k and σ_ε were not included in the test since they have been optimized against experiments and have been used with success in many applications, involving buoyancy, for example, Fraikin et al. (1980) and Plumb and Kennedy (1977). These constants with present values have also been adopted in HARWELL-FLOW3D (Burns and Jones et al. [1988]).

The constants C_1 and C_2 were varied by ± 20 per cent and C_3 by ± 30 per cent, from those values given at Table 5.1. The effects of the above constants on the parameters u, v, T, k and ε at the top and bottom of the throat area were investigated.

The variation of C_1 by ± 20 per cent affected the maximum velocities at the throat area by up to 28 per cent. The effect on the temperatures was less than 10 per cent. However, its effect on the turbulence quantities k and ε were up to 70 per cent.

The variation of C_2 by ± 20 per cent affected the parameters k and ε strongly by up to 30 per cent, but other parameters u, v and T were affected by less than 20 per cent. For the case of C_2 = 1.54, the convergence was slow.

The effect of the variation of C_3, by ± 30 per cent, did not significantly influence the higher values of velocities at the throat area, while the effect on the lower velocities were significant. A similar study of the effect of C_3 was also undertaken by Markatos et al. (1982), and they found no significant difference in the prediction with C_3 in the range of 1.0 to 0.3.

In the buoyancy term of the k-ε model, a constant value is given to $\sigma_{T,t}$. But $\sigma_{T,t}$ should be variable in a problem where buoyancy is important (Fraikin et al. [1980]), and its value gives a good description of the turbulent heat flux. The results of the variation of $\sigma_{T,t}$ by ± 30 per cent has shown that all the parameters were affected by less than 10 per cent, except turbulent kinetic energy and energy dissipation rate, where the effects were up to 33 per cent. In the case of $\sigma_{T,t}$ = 1.3 the convergence was very slow.

CHAPTER SIX

CONCLUDING REMARKS

6.1 INTRODUCTION

In this the final Chapter an overview of the present study is given in Section 6.2, where the work presented in the thesis is summarized and the main achievements are identified. Section 6.3 provides recommendations for areas requiring further investigation.

6.2 OVERALL SUMMARY AND CONCLUSIONS OF THE STUDY

6.2.1 Experiment

The experimental study of the buoyancy-driven air flow within the stairwell model included flow visualisation and measurements of temperature and velocity. Using these experiments, with the help of flow visualisation, the flow within the stairwell was described more comprehensively than in previously reported experiments.

The experiments confirmed that the flow was three-dimensional, unsteady, and involved rapid mixing in the central region of the stairwell. There were a number of separation, reattachment and circulation zones which contributed to the complex flow situation. The flow visualisation also revealed features inside the main recirculating flow, such as the presence of the two interacting layers of warm upflow and cold downflow in the stairway between which heat and mass exchange took place. Furthermore, visualisation using smoke, supported the velocity measurements by confirming the correction of the probe alignment with the flow direction. The velocity and temperature distributions were approximately symmetrical with respect to the mid-plane of the stairwell model. However, the velocity profile along the height of the throat area was not symmetrical with respect to the mid-height of the throat area.

The air flow between the lower and upper compartments was found to increase with increase in temperature differential.

The heat transfer rate through the stairwell side walls was found to be more than 50 per cent of the heat input rate to the system. Comparing the results with those obtained from the stairwell with insulated side walls, it was found that the heat transfer through the side walls had significant effect on the velocity and temperature profiles. Furthermore, a study of the heat losses from the walls of various parts of the stairwell showed that 53 to 66 per cent of the heat input rate was lost in the upper compartment.

In the case of an open stairwell, experimental results supported by flow visualisation revealed that the inlet opening area had a strong influence on the circulation within the stairwell and, depending on the size of the opening, an alternative flow regime could develop.

The present results showed that the flow pattern in the open stairwell was similar to that in the closed stairwell (with no through-flow). However, the air velocity and temperature at the throat area were smaller in the open case for a given heat input.

Comparing the results of sloping and non-sloping ceiling geometries, it was found that the effect of the former geometry was to reduce the mean temperature and to increase the velocity and volume flow rates (in both warm upflow and cold downflow) at the throat area.

For the closed stairwell case, the total volume flow rate of the recirculating flow varied as $\dot{V}_m \alpha \dot{Q}^{0.22}$. A similar relationship was obtained for the dependence of mean temperature difference ΔT on the heat input rate, with n = 0.79.

In the closed stairwell case, the measured air-leakage through the stairwell joints proved to be insignificant. The results indicated that the leakage rate increased as the heat input rate increased. In the open stairwell case, the rate of heat transfer via convection through the inlet and outlet openings was about one-tenth of the heat input rate to the stairwell.

Analytical studies of the flows of energy and mass through the stairwell, based on Froude scaling, should provide representative modelling of the characteristics parameters governing the buoyancy-driven flows, and that the half-scale model can provide results representative of the full scale.

6.2.2 Two-Dimensional Prediction

The predictions with the standard k-ε turbulence model appears to be adequate in obtaining some basic information on the flow characteristics in the stairwell. The predicted flow reproduced all the expected features of the flow, including the warm upflow and cold downflow streams along the steps, and recirculating and separation regions in the upper and lower compartments, as established by experiments on the half-scale stairwell model.

However, comparing with the experimental values of the velocity at the throat area, it was found that the upflow and downflow velocities were underpredicted. The discrepancy was at its highest at the top and bottom of the throat area. The temperature was overpredicted, but it was possible to reduce the temperature level by introduction of a constant (less than 1.0) in the dissipation term of the k-equation, when applied to the wall region. Adopting heat fluxes through the walls as boundary conditions, instead of wall temperatures, resulted in under-estimation of temperature. It seems likely that the turbulence model was partly responsible for these shortcomings.

The overall heat balance was satisfied with less than one per cent error, and furthermore, the prediction of the heat loss from the upper compartment was in good agreement with the experiment.

6.3 RECOMMENDATIONS FOR FUTURE WORK

The present study could be extended in several specific directions both experimentally and theoretically. These are associated with experimentation, turbulence modelling and computational improvements. These aspects are discussed in the following subsections.

6.3.1 Experimentation

To provide experimental data against which to compare predicted flow patterns and thereby enable improvements in the calculation procedure and turbulence modelling, extension of the experimental study is recommended along the following lines:

i) Related to the flow field, specially at the throat area, measurements of all three mean velocity components and kinetic energy are suggested. A convenient instrument for performing these measurements would be DISA normal hot-wire and X-wire, temperature compensated probes, which have the advantages, relative to the probe used in the present study, of having a better response time for detecting turbulence fluctuations.

(ii) The measurements should also be directed to provide information on the flow in the regions of particular interest, namely, the central regions of the lower and upper compartments and near the boundaries of the recirculating flow.

(iii) Further work could include study of temperature and velocity profiles by varying certain aspects of the stairwell model which have been kept constant in the present study. These are the position of the heat source, inlet and outlet opening areas and their positions.

6.3.2 Numerical Prediction

The experimental results indicate that more accurate modelling of the flow within the stairwell requires a three-dimensional numerical model. Any of the three-dimensional programs currently available (see Appendix G) should provide a starting point to indicate the areas which require further improvement. Then, a specially tailored three-dimensional program incorporating suggested improvements, can be developed for the stairwell flow, from the present two-dimensional program.

The application of the k-ε turbulence model to bouyancy-driven recirculating flow, led to a reasonable prediction. The discrepancies between the predicted and experimental results can be attributed partly to the turbulence model (which are valid for fully turbulent flows), and partly due to the use of wall functions. There is a need for the development and incorporation of a more realistic turbulence model and near-wall modelling, capable of predicting the recirculating and separated flows within the stairwell over the lower range of Reynolds numbers. The future work, therefore, should be directed towards improving the wall function method and incorporation of higher level turbulence models such as Reynolds stress models.

Further investigations should also be directed in the following areas:

i) Efforts should be made to improve the numerical stability and speed of convergence of the present procedure. This may be achieved by using other algorithms than SIMPLE, which was used in the present study. Examples are SIMPLER (Patankar [1980, 1981]), SIMPLEC (Van Doormaal and Raithby [1984]), PISO (Issa [1985]).

ii) The discretisation scheme most commonly used in control volume method is the hybrid difference scheme. This scheme provides the best compromise between good convergence and accuracy (Patankar [1975]). Other schemes such as QUICK (Leonard [1979]) and Higher Upwind scheme HUW (Wilkes and Thomson [1983], Burns et al. [1987]) may also be used.

REFERENCES

AHLUWALIA, A.K. and SHOUKRI, M. (1983)
Numerical simulation of turbulent mixed convection flows, The American Society of Mech. Eng. 83- WA/HT- 13.

ALAMDARI, F. (1984)
Convective heat transfer within mechanically ventilated building spaces, PhD thesis, Cranfield Institute of Technology, School of Mechanical Engineering.

ALAMDARI, F., HAMMOND, G.P. and MOHAMMAD, W.S. (1986)
Computation of air flow and convective heat transfer within space-conditioned, rectangular enclosures, Proceedings of the 5th International Symposium on the use of computers for environmental engineering related to buildings, Bath, 7-9 July 1986, CIBSE 1986, pp. 191-205.

BROWN, W.G. and SOLVASON, K.R. (1962)
Natural convection through rectangular openings in partitions-Vertical Partitions, Int. J. Heat Mass Transfer, Vol. 5, pp. 859-868.

BROWN, W.G. (1962)
Natural convection through rectangular openings in partitions - Horizontal partitions, Int. J. Heat Mass Transfer, Vol. 5, pp. 869-878.

BURNS, A.D., INGRAM, D., JONES, I.P., KIGHTLEY, J.R., LO, S. and WILKES, N.S. (1987)
Flow 3D: The development and application of Release 2, UKAEA-AERE R 12693, HL87/1244.

BURNS, A.D., JONES, I.P., KIGHTLEY, J.R. and WILKES, N.S. (1988)
HARWELL-FLOW 3D-Flow modelling software, Computer Science and System Division, Harwell Laboratory Oxfordshire, OX11ORA.

CHARLESWORTH, P.S. (1988)
Air exchange rate and airtightness measurement techniques - An application guide, Air Infiltration and Ventilation Centre, University of Warwick Science Park, Barclays Venture Centre, Sir William Lyons Road, Coventry, CV4 7EZ, Chapter 2, pp. 2.3-2.9.

CHEN, Q., JAN VANDER, K. and MAYERS, A. (1988)
Measurements and computations of ventilation efficiency and temperature efficiency in a ventilated room, Energy and Building, Vol. 12, pp. 85-99.

CHU, D.D.H. (1984)
Assessment and characterisation of airflow in domestic stairwell, MSc Thesis, Brunel University.

CIOFALO, M. and COLLINS, M.W. (1987)
k-ε Predictions of heat transfer in turbulent recirculating flows using an improved wall treatment, submitted to Numerical Heat Transfer, Oct. 1987.

CLARKE, J.A. (1982)
Computer applications in the design of energy-conscious buildings, Vol. 14, No. 1, pp. 3-9.

COX, G. and KUMAR, S. (1983)
Computer modelling of fire, BRE Information paper, IP 2/83.

COX, G. and KUMAR, S. (1984)
The mathematical modelling of fire in forced ventilated enclosures, 18th DOE Nuclear Airborne Waste Management and Air Cleaning Conf., Baltimore, pp. 629-639.

COX, G. (1984)
Simulating fires in buildings by computer - The state of the art, 10th Int. Association of Forensic Science meeting, Oxford, pp. 175-188.

COX, G., KUMAR, S. and MARKATOS, N.C. (1986)
Some field model validation studies, Fire Safety Science-Proc. of the first Int. Symposium, Hemisphere 1986, pp. 159-171.

DAVIDSON, L. (1986)
One-equations turbulence models in flows near walls, Chalmers University of Technology, Department of Applied Thermodynamics and Fluid Mechanics.

DAY, B. (1982)
Computation of the dynamic thermal performance of buildings: Computer aided design, Vol. 14, pp. 49-54.

DOEBELIN, E.O. (1983)
Measurement Systems, Application and Design, Third Edition, McGraw Hill Publication.

DONALD, R.P. and LEIGHTON, E.S. (1977)
Theory and problems of heat transfer, Schaum's Outline Series, McGraw Hill Publication.

FANG, J.B., GROT, R.A. and KURABUCHI, T. (1988)
Application of mathematicl modelling to the ventilation of building ventilation system, 9th AIVC Conference "EFFECTIVE VENTILATION" 12-15 September 1988, Novolel, Gent., Belgium.

FEUSTEL, H., ZUERCHER, CH., DIAMOND, R., DICKINSON, B., GRIMSRUD, D., and LIPSCHUTZ, R. (1985)
Temperature and wind-induced air flow patterns in a staircase: Computer modelling and experimental verification, Energy and Buildings, 8, pp. 105-122.

FONTAINE, J.R. and DELLAGI, F. (1987)
Dynamical and contaminant flow simulation inside ventilated industrial premises 1: Numerical methods, Int. Conference, Stockholm 10-12 June.

FRAIKIN, M.P., PORTIER, J.J., FRAIKIN, C.J. (1980)
Application of k-ε turbulence model to an enclosed buoyancy driven recirculating flow, Am. Soci. Mech. Engrs., ASME paper No. 80-HT-68, pp. 1-11.

GIBSON, M.M. and LAUNDER, B.E. (1974)
On the calculation of horizontal non-equilibrium turbulent shear flows under gravitation influence, Imperial College, HT Section.

GOSMAN, A.D., PUN, W.M., RUNCHAL, A.K., SPALDING, D.B. and WOLFSTEIN, M. (1969)
Heat and mass transfer in recirculating flows, Academic Press, London.

GOSMAN, A.D. and IDERIAH, F.J.K. (1976)
A general computer program for 2-D turbulent recirculating flows, Imperial College, London.

GOSMAN, A.D. and ISSA, R.A. (1987)
Computational fluid dynamics and heat mass transfer, Lecture Notes, Imperial College, London.

GRAND, D. (1975)
Contribution a l'etude des courant de recirculation, PhD thesis, L' Universite Scientifique et Medicale et Institut Nationale, Polytechnique, Grenoble.

HALL, J.A. (1966)
The measurement of temperature, Chapman and Hall Ltd., London.

HAMMOND, G.P. (1982)
Appropriate calculation methods for thermo-fluid problems related to buildings, SERC Seminar: "What next in Energy in Building Research?", Rodney Lodge, Bristol University, 19-21 September.

HAN, T., HUMPHREY, A.C. and LAUNDER, B.E. (1981)
A comparison of hybrid and quadratic-upstream differencing in high Reynolds number elliptic flows, Comp. Meth. in Applied Mech. Eng., 29, pp. 81-85.

HARLOW, F.H. and NAKAYAMA, P.I. (1968)
Transport of turbulence energy decay rate, University of California, Los Almos Science Lab., 1968, LA 3854.

HOLMES, M.J. and WHITTLE, G.E. (1987)
How accurate are the predictions of complex air movement models? The Chartered Ins. of Build. Serv. Engrs., Vol. 8, No.2, pp. 29-31.

HOFFMANN, N. and MARKATOS, N.C. (1988)
Thermal radiation effects on fires in enclosures, Appl. Maths. Modelling, Vol. 12, pp. 129-140.

HOWARTH, A.T. (1985)
The prediction of air temperature variations in naturally ventilated rooms with convective heating, Building Services Engineering Research and Technology, Vol. 6, No. 4, pp. 169-175.

HUMPHREY, J.A.C. and TO, W.M. (1986)
Numerical simulation of buoyant, turbulent flow - II. Free and mixed convection in a heated cavity, Int. J. Heat Mass Transfer, Vol. 29, No. 4, pp. 593-610.

IDERIAH, F.J.K. (1977)
Turbulent natural and forced convection in plumes and cavities, Ph.D. Thesis, Imperial College.

IDERIAH, F.J.K. (1979)
A numerical procedure for calculating partly elliptic flows, J. Mech. Eng. Sci., Vol. 21, No. 6, pp. 373-380.

IDERIAH, F.J.K. (1980)
Prediction of turbulent cavity flow driven by buoyancy and shear, J. Mech. Eng. Sci., Vol. 22, No. 6, pp. 287-295.

ISSA, R.I. (1985)
Solution of the implicity discretized fluid flow equations by operator splitting, Journal of Computational Physics, Vol. 62, pp. 40-65.

JAYATILLAKA, C.V.L. (1969)
The influence of Prandtl number and surface roughness on the resistance of the laminar sub layer to momentum and heat transfer, Progress in Heat and Mass Transfer, Vol. 1, Pergamon Press, London.

JONES, W.P. and LAUNDER, B.E. (1972)
The prediction of laminarization with a two equation model of turbulence, Int. J. Heat and Mass Transfer, 15, pp. 301-314.

JONES, W.P. and LAUNDER, B.E. (1973)
The calculation of low-Reynolds-number phenomena with a two equation model of turbulence, Int. J. Heat and Mass Transfer, 16, pp. 1119-1130.

JONES, W.P. (1973)
Air conditioning engineering, 3rd edition, Edward Arnold, London.

KATO, S. and MURAKAMI, S. (1988)
New ventilation efficiency scales based on spatial distribution of contaminant concentration aided by numerical simulation, 8th International Symposium on Contamination Control, Milan, Sept. 9-12, pp. 781-791.

KAY, J.M. and NEDDERMAN, R.M. (1985)
Fluid mechanics and transfer processes, Cambridge University Press.

KUMAR, S. (1983)
Mathematical modelling of natural convection in fire - A state of the art review of the field modelling of variable density turbulent flow, Fire and Materials, Vol. 7, No. 1, pp. 1-24.

KUMAR, S. and COX, G. (1985)
Mathematical modelling of fire in road tunnels, 5th Int. Conference on the Aerodynamics and Ventilation of Vehicle Tunnels, Lille.

KUMAR, S., HOFFMANN, N. and COX, G. (1986)
Some validation of JASMINE for fires in hospital wards, in numerical simulation of fluid flow and heat/mass transfer processes, Eds. Markatos, N.C. et al., Springer Verlag, Berlin, pp. 159-169.

LAKSHMINARAYANA, B. (1986)
Turbulence modelling for complex shear flows, AIAA Journal, Vol. 24, No. 12, pp. 1900-1917.

LANGDON-THOMAS, G.J. (1972)
Fire safety in buildings, A & C Black Limited Publication.

LAUNDER, B.E. and SPALDING, D.B. (1972a)
Lectures in mathematical models of turbulence, Academic Press, London.

LAUNDER, B.E. and SPALDING, D.B. (1972b)
Turbulence models and their application to the prediction of internal flows, Heat and Fluid Flow, 2. No. 1, pp. 43-54.

LAUNDER, B.E. and SPALDING, D.B. (1974)
The numerical computation of turbulent flows, Computer Methods in Applied Mechanics and Eng., Vol. 3, pp. 269-289.

LEBRUN, J. and MARRET, D. (1976)
Convection exchanges inside a dwelling room in winter, International Seminar of ICHMT, Dubrovnik.

LEONARD, B.P. (1979)
A stable and accurate convective modelling procedure based on quadratic upstream interpolation, Computer Methods in Applied Mechanics and Engineering, 19, pp. 59-98.

LESCHZINER, M.A. (1980)
Practical evaluation of three finite-difference schemes for the computation of steady-state recirculating flows, Computer Methods in Applied Mechanics and Engineering, 23, pp. 293-312.

LIDDAMENT, M.W. (1983)
Modelling the influence of ventilation strategies on distribution and heat loss in a single family dwelling. Proceedings of the 2nd International Congress on building energy Management. 30 May - 3 June 1983, Iowa USA.

LIDWELL, O.M. (1977)
Air exchange through doorways. The effect of temperature difference, turbulence and ventilation flow, J. Hyg. Comb., Vol. 79, pp. 141-154.

LUMLEY, J.L. (1972)
A model for computation of stratified turbulent flows, Symp. on Stratified flows, Novosibrisk, USSR.

MAHAJAN, BAL M. (1987)
Measurement of interzonal heat and mass transfer by natural convection, Solar Energy, Vol. 38, No. 6, pp. 437-446.

MAGUIRE, D.H. (1985)
Air movement in domestic stairwell, MSc Thesis, Brunel University.

MALIN, M.R. (1987)
The decay of mean and turbulent quantities in vertical forced plumes, Appl. Math. Modelling, Vol. 11, pp. 301-314.

MARCHANT, E.W. (1972)
Fire and building, MIP Co. Ltd., Publication.

MARKATOS, N.C., MALIN, M.R. and COX, G. (1982)
Mathematical modelling of buoyancy-induced smoke flow in enclosures, Int. J. Heat Mass Transfer, Vol. 25, No. 1, pp. 63-75.

MARKATOS, N.C. (1983)
Computer analysis of building-ventilation and heating problems, 2nd Int. PLEA Conference, Crete 28 June-1 July 1983, Passive and Low Energy Architecture, Edited by S. Yannas, pp. 667-675.

MARKATOS, N.C. and PERICLEOUS, K.A. (1984a)
Laminar and turbulent natural convection in an enclosed cavity, Int. J. Heat Mass Transfer, Vol. 27, No. 5, pp. 755-772.

MARKATOS, N.C. and COX, G. (1984b)
Hydrodynamics and heat transfer in enclosures containing a fire source, PCH, Physicochemical Hydrodynamics, 5, No. 1, pp. 53-66.

MARKATOS, N.C. and PERICLEOUS, K.A. (1984c)
An investigation of three dimensional fires in enclosures, 21st National Heat Transfer Conference, Seattle, pp. 115-124.

MARKATOS, N.C. (1986)
State of Art Review - The Mathematical modelling of turbulent flows, Appl. Maths. Modell., Vol. 10, pp. 190-220.

MARSHALL, N.R. (1983)
Movement of smoke and fire gases in stairwell, BRE News, 59, Spring Issue, p. 13.

MARSHALL, N.R. (1985)
The behaviour of hot gases flowing within a staircase, Fire Safety Journal, 9, pp. 245-255.

MARSHALL, N.R. (1986)
Air entrainment into smoke and hot gases in open shafts, Fire Safety Journal, 10, pp. 37-46.

MARRIOTT, B.S.T. and REYNOLDS, A.J. (1986)
Flows of mass and energy through a stairwell - Experimental studies, Report FM 86/1, Dept. of Mech. Eng. Brunel University.

MATHEWS, E.H. and MERJER, J.P. (1987)
Numerical modelling of wind loading on a film clad greenhouse, Build. and Environ., Vol. 22, No. 2, pp. 129-134.

MOKHTARZADEH-DEHGHAN, M.R., EL-TELBANY, M.M.M. and REYNOLDS, A.J. (1989)
Transfer rates in single-sided ventilation. To be published in Building and Environment.

MOODIE, K., JAGGER, S.F., BETTIS, R.J. and BECKETT, H. (1988)
Fire at King's Cross underground station - Scale model fire growth tests, Health and Safety Executive, Research and Lab. Services, Harpur Hill, Buxton, Derbyshire. SK17 9JN.

MORGAN, H.P. and MARSHALL, N.R. (1975)
Smoke hazards in covered, multi-level shopping malls - An experimentally based theory for smoke production. Current Paper 48/72, Building Research Establishment, Borehamwood.

MORGAN, H.P. and MARSHALL, N.R. (1979)
Smoke control measurements in a covered two-storey shopping mall having balconies as pedestrian walk ways, BRS Paper CP11/79.

MÜNCH, W., RÜDEN, H., SCHKALLE, Y.D. and THIELE, F. (1986)
Flow of micro-organisms in a hospital stair-shaft - Full scale measurements and mathematical model, Energy and Buildings, 9, pp. 253-262.

NIELSEN, P.V., RESTIVO, A. and WHITELAW, J.H. (1979)
Buoyancy affected flows in ventilated rooms, Numerical Heat Transfer, Vol. 2, pp. 115-127.

NEVRALA, D.J. and PROBERT, S.D. (1977)
Modelling of air movement in rooms, Journal of Mech. Eng. Science, Vol. 19, No. 6.

NG, H. and SPALDING, D.B. (1972)
Some application of a model of turbulence to boundary layers near walls, Physics of Fluids, 15, pp. 20-30.

OZOE, H., MOURI, A., HIRAMITSU, M., CHURCHILL, S.W. and LIOR, N. (1986)
Numerical calculation of three-dimensional turbulent natural convection in a cubical enclosure using a two-equation model for turbulence, Journal of Heat Transfer, Vol. 108, pp. 806-813.

PATANKAR, S.V. and SPALDING, D.B. (1967)
Heat and mass transfer in boundary layers, Morgan-Grampian, London.

PATANKAR, S.V. and SPALDING, D.B. (1972)
A calculation procedure for three-dimensional parabolic flows, Int. J. Heat Mass Transfer, 15, pp. 1787-1806.

PATANKAR, S.V. (1975)
A numerical prediction of 3-D flows, Studies in Convection, Vol. 1, Academic Press, London. pp. 1-78.

PATANKAR, S.V. (1980)
Numerical heat transfer and fluid flow, McGraw Hill, New York.

PATANKAR, S.V. (1981)
A calculation procedure for two-dimensional elliptic situation, Numerical Heat Transfer, Vol. 4, pp. 409-425.

PATANKAR, S.V. (1988)
Recent developments in computational heat transfer, Journal of Heat Transfer, November 1988, Vol. 110, pp. 1037-1046.

PATEL, M.K., MARKATOS, N.C. and CROSS, M.A. (1985a)
Methods for reducing false-diffusion errors in convection-diffusion problems, Appl. Math. Model., 9, pp. 302-306.

PATEL, M.K., MARKATOS, N.C. and CROSS, M.A. (1985b)
A critical evaluation of seven discretization schemes for convection-diffusion equations, Int. J. Numerical Meth. Fluids, 5, pp. 225-244.

PATEL, V.C., RODI, W. and SCHEUERER, G. (1985c)
Turbulence models for near-wall and low-Reynolds number flows: A review, AIAA J., Vol. 23, No. 9, pp. 1308-1319.

PERICLEOUS, K.A., WORTHINGTON, D.R.E. and COX, G. (1987)
The field modelling of fire in an air supported structure, An information/discussion paper prepared for CHAM seminar, "Fire and Smoke Hazard Analysis and Energy Conservation in Buildings", 7th July 1988.

PLUMB, O.A. and KENNEDY, L.A. (1977)
Application of a k-ε turbulence model to natural convection from a vertical isothermal surface, J. of Heat Transfer, Feb. 1977, pp. 79-85.

PORGES, F. (1971)
Handbook of Heating, Ventilating and Air Conditioning, 6th edition, Newman-Butterworths.

PUN, W.M. and SPALDING, D.B. (1977)
A general computer program for two-dimensional elliptic flows, Imperial College, Mechanical Engineering Dept., Report HTS/76/2.

QINGYAN, C. and JAN VANDER, K. (1988)
Accuracy - A program for combined problems of energy analysis, indoor airflow, and air quality, ASHRAE Transaction, Vol. 94, part 2.

REYNOLDS, A.J. (1974)
Turbulent flows in engineering, John Wiley and Sons Publication.

REYNOLDS, A.J. (1986)
The scaling of flows of energy and mass through stairwells, Build. and Envir., Vol. 21, part 3/4, pp. 149-153.

REYNOLDS, A.J. (1987)
Modelling of flow driven by buoyancy and imposed pressure differential, Analytical studies, FM 87/1, Dept. of Mechanical Engineering, Brunel University.

REYNOLDS, A.J., MOKHTARZADEH-DEHGHAN, M.R. and ZOHRABIAN, A.S. (1988)
The modelling of stairwell flows, Build. and Envir., Vol. 23, No. 1, pp. 63-66.

REYNOLDS, W.C. (1976)
Computation of turbulent flows, Annual Review of Fluid Mechanics, Vol. 8, pp. 183-208.

RIFFAT, S.B., WALKER, J. and LITTLER, J. (1988)
Zone to zone tracer gas measurement: Laboratory calibration and values of air flows up and down stairs in houses. 9th AIVC Conference "EFFECTIVE VENTILATION" 12-15 September 1988. Novotel, Gent, Belgium, Vol. 2, pp. 85-101.

RIFFAT, S.B. and EID, M. (1988)
Measurement of air flow between the floors of houses using a portable SF_6 system, Energy and Buildings, 12, pp. 67-75.

RODI, W. (1980)
Turbulence models and their application in hydraulics - A state of the art review, Book Publication of Int. Associ. for Hydraulic Research, Delft, Netherlands.

SCHWARZ, M.P. and TURNER, W.J. (1988)
Applicability of the standard k-ε turbulence model to gas-stirred baths, Appl. Math. Modelling, Vol. 12, pp. 273-279.

SHAW, B.H. (1971)
Heat and mass transfer by natural convection and combined natural and forced air flow through large rectangular openings in a vertical partition, Instn. Mech. Engrs., C117/71, pp. 31-39.

SHAW, B.H. and WHYTE, W. (1974)
Air movement through doorways - the influence of temperature and its control by forced airflow, BSE, Vol. 42, pp. 210-218.

SHAW, B.H. (1976)
Heat and mass transfer by convection through large rectangular openings in vertical partitions, PhD thesis, Dept. of Mechanical Engineering, University of Glasgow.

SIMCOX, S. and SCHOMBERG, M. (1988)
Tunnel of fire, Science and Business, Nov. - Dec. Issue.

SINCLAIR, V.J. CROOME, D.J. and CATHAIN, C.S.O. (1982)
A review of possible techniques to measure ventilation in occupied spaces. University of Bath, School of Architecture and Building Engineering.

SPALDING, D.B. (1972)
A novel finite-difference formulation for differential expressions involving both first and second derivatives, Int. J. Num. Methods Eng., Vol. 4, pp. 551-559.

TENNEKES, H. and LUMLEY, J.L. (1973)
A first course in turbulence, MIT Press, Cambridge Mass.

TIMMONS, M.B. and BAUGHMAN (1981)
Similitude analysis of ventilation by the stack effect from an open ridge livestock structure, Transactions of ASAE, pp. 1030-1034.

TO, W.M. and HUMPHREY, J.A.C. (1986)
Numerical simulation of buoyant, turbulent flow-free convection along a heated vertical flat plate, Int. J. Heat Mass Transfer, Vol. 29, No. 4, pp. 573-592.

VAN DOORMAAL, J.P. and RAITHBY, G.D. (1984)
Enhancement of the SIMPLE method for predicting incompressible fluid flows, Numerical Heat Transfer, Vol. 7, pp. 147-163.

VIOLLET, P.L. (1981)
On the modelling of turbulent heat and mass transfer for the computation of buoyancy affected flows, Numerical Meth. in Laminar and turbulent Flow Proc., 2nd Int. Conf., Venice Italy, July 13-16, C. Taylor, B.A. Schrefler Swansea, U.K., Pineridge Press Ltd., Section 4, Flow with Heat Transfer, Paper 3, pp. 569-580.

WHITTLE, G.E. (1986)
Computation of air movement and convective heat transfer within buildings, Int. J. of Ambient Energy, Vol. 7, No. 3, pp. 151-164.

WILKES, N.S. and THOMPSON, C.P. (1983)
An evaluation of higher-order differencing for elliptic flow problems, AERE-CSS 137.

ZOHRABIAN, A.S., (1986)
A study of heat and buoyancy-driven fluid flow in a stairwell, Internal report, Dept. of Mechanical Engineering, Brunel University.

ZOHRABIAN, A.S., MOKHTARZADEH-DEHGHAN, M.R., REYNOLDS, A.J. (1988)
A numerical study of buoyancy-driven flows of mass and energy in a stairwell. 9th AIVC Conference "EFFECTIVE VENTILATION" 12-15 September 1988. Novotel, Gent, Belgium, Vol. 2, pp. 183-204.

ZOHRABIAN, A.S., MOKHTARZADEH-DEHGHAN, M.R., REYNOLDS, A.J. and MARRIOTT, B.S.T. (1989)
An experimental study of buoyancy-driven flow in a half-scale stairwell model, Bldg Environ., Vol. 24, No. 2, pp. 141-148.

AUTHOR	TURBULENCE MODEL AND METHOD OF SOLUTION.	APPLICATION
Davidson (1986)	one equation and k-ε models; SIMPLE[1], finite volume; hybrid scheme.	Flow over flate plate, flow in a plane channel, plane wall jet with zero free stream velocity.
Fang et al. (1988)	k-ε (buoyant version); MAC[2], finite volume.	3D turbulent buoyant flow emerging from an air diffuser in an air-conditioned, ventilated room.
Fontaine et al. (1987)	k-ε, SIMPLE algorithm; finite volume; hybrid scheme.	Flow simulation inside ventilated industrial premises.
Humphrey and To (1986) To and Humphrey (1986)	k-ε and ARSM[3] finite volume; hybrid, upwind and central difference schemes.	Free and mixed convection, low Reynolds number flow in a heated cavity and on a heated vertical flat plate.
Kato et al. (1988)	k-ε; finite volume.	To evaluate the ventilation effectiveness - by means of distribution of the contaminant concentration.

Table 1 Some of the recent publications on room air flow and flow near walls.

Table 1 contd.

Malin (1987)	k-W model (buoyant version); SIMPLE ; finite volume; PHOENICS.	Prediction of the decay of mean turbulent quantities in vertical forced plumes.
Mathews et al. (1987)	k-ε; SIMPLE; finite volume.	To predict wind loading on a film clad greenhouse.
Mokhtarzadeh-Dehghan et al. (1989)	k-ε (buoyant version); SIMPLE; finite volume.	Transfer rates in single-sided ventilation.
Ozoe et al. (1986)	k-ε (buoyant version); SIMPLE procedure; hybrid and upwind schemes.	3-D turbulent natural convection in a cubical enclosure, heated on the floor and cooled on part of the vertical wall.
Pericleous et al. (1987)	k-ε (buoyant version); SIMPLEST; using JASMINE and PHOENICS codes.	Prediction of temperature distribution and smoke movement in a sports building covered by an air supported dome.
Qingyan et al. (1988)	k-ε (buoyant version); upwind scheme; using PHOENICS and ACCURACY[4] codes.	Prediction of temperature and concentration distribution in offices.
Schwarz et al. (1988)	k-ε (buoyant version); using PHOENICS code.	To simulate the flow field in gas-stirred baths

1: SIMPLE: Semi-Implicit Method for Pressure-Linked Equations.

2: MAC : Marker-and-Cell method.

3: ARSM : Algebraic Reynolds Stress Models.

4: ACCURACY : A Computer program, for energy analysis, room air temperature and contamination field predictions.

TIME t (min)	ACTUAL CONCENTRATION C (ppm)	ADJUSTED CONCENTRATION C-c (ppm)	ln(C-c)
0	2920	2770	7.926
10	2900	2750	7.919
20	2850	2700	7.901
30	2800	2650	7.882
40	2770	2620	7.871
50	2720	2570	7.852
60	2710	2560	7.848
70	2680	2530	7.836
80	2650	2500	7.824
90	2620	2470	7.812
100	2600	2450	7.804
110	2580	2430	7.796
120	2560	2410	7.787

Table 3.1 Tracer decay test results.
Heat input rate = 100 W
(see Figure 3.23).

TIME t (min)	ACTUAL CONCENTRATION C (ppm)	ADJUSTED CONCENTRATION C-c (ppm)	ln(C-c)
0	640	490	6.194
10	630	480	6.174
20	620	470	6.153
30	610	460	6.131
40	600	450	6.109
50	595	445	6.098
60	585	435	6.075
70	580	430	6.064
80	575	425	6.052
90	570	420	6.040
100	565	415	6.028
110	560	410	6.016
120	555	405	6.004

Table 3.2 Tracer decay test results.
Heat input rate = 300 W.

TIME t (min)	ACTUAL CONCENTRATION C (ppm)	ADJUSTED CONCENTRATION C-c (ppm)	ln(C-c)
0	740	560	6.328
10	735	555	6.319
20	725	545	6.301
30	715	535	6.282
40	705	525	6.263
50	695	515	6.244
60	685	505	6.225
70	670	490	6.194
80	665	485	6.184
90	660	480	6.174
100	650	470	6.153
110	642	462	6.136
120	635	455	6.120

Table 3.3 Tracer decay test results.
Heat inout rate = 600 W.

TIME t (min)	ACTUAL CONCENTRATION C (ppm)	ADJUSTED CONCENTRATION C-c (ppm)	ln(C-c)
0	860	580	6.363
10	845	565	6.337
20	825	545	6.301
30	810	530	6.273
40	795	515	6.244
50	780	500	6.215
60	765	485	6.184
70	750	470	6.153
80	740	460	6.131
90	730	450	6.109
100	720	440	6.087
110	710	430	6.064
120	700	420	6.040

Table 3.4 Tracer decay test results.
Heat input rate = 900 W.

HEAT INPUT RATE (W)	AIR CHANGE RATE (hr^{-1})	LEAKAGE RATE ($m^3\ s^{-1}$)	LEAKAGE RATE ($kg\ s^{-1}$)	ROOM TEMP. (°C)	EXTERNAL CONCENTRATION (PPM)
$\dot{Q}$	$\dot{Q}_m/V_m$	$\dot{Q}_m$	$\dot{m}$	T_R	C
100	0.0659	5.42×10^{-5}	6.45×10^{-5}	19.5	150-160
300	0.0998	8.21×10^{-5}	9.69×10^{-5}	21.0	150-160
600	0.1085	8.92×10^{-5}	1.04×10^{-4}	21.5	180
900	0.1575	1.29×10^{-4}	1.49×10^{-4}	21.5	280

Table 3.5 Rate of leakage, through the stairwell joints, for various heat input rates (closed stairwell case).

CLOSED STAIRWELL CASE					
DISTANCE FROM SIDE WALL (m)	$\dot{Q}$ (W)	U_{maxu} ($m\ s^{-1}$)	U_{maxd} ($m\ s^{-1}$)	T_H (°C)	T_C (°C)
w/2	100	0.17	0.24	29.7	28.3
	300	0.28	0.31	35.4	32.1
	600	0.36	0.36	43.6	36.8
	900	0.42	0.54	50.1	41.8
5w/12	100	0.16	0.23	29.8	28.0
	300	0.27	0.27	35.5	31.6
	600	0.34	0.36	43.6	37.3
	900	0.41	0.54	50.4	41.5
w/3	100	0.17	0.22	29.7	27.8
	300	0.27	0.27	35.5	31.6
	600	0.34	0.36	43.4	37.2
	900	0.46	0.50	50.7	41.1
w/4	100	0.17	0.21	29.8	27.3
	300	0.26	0.23	35.5	31.1
	600	0.32	0.32	43.2	37.0
	900	0.38	0.47	50.6	42.5
w/6	100	0.17	0.18	28.0	26.8
	300	0.24	0.21	35.0	30.2
	600	0.31	0.31	42.5	36.2
	900	0.35	0.47	49.6	41.4
w/12	100	0.17	0.16	27.6	26.0
	300	0.24	0.18	32.8	28.2
	600	0.31	0.31	39.9	34.7
	900	0.31	0.47	46.3	37.7

Table 3.6 Maximum velocities and mean temperatures in the upflow and downflow streams (at the throat area) at w/2, 5w/12, w/3, w/4, w/6, w/12 for various heat input rates.

OPEN STAIRWELL CASE					
DISTANCE FROM SIDE WALL (m)	$\dot{Q}$ (W)	U_{maxu} ($m\ s^{-1}$)	U_{maxd} ($m\ s^{-1}$)	T_H (°C)	T_C (°C)
w/2	100	0.17	0.21	28.3	26.7
	300	0.25	0.31	32.7	29.4
	600	0.32	0.38	42.5	36.1
	900	0.38	0.48	48.3	38.3
5w/12	100	0.17	0.20	28.2	26.3
	300	0.26	0.29	32.6	29.3
	600	0.33	0.38	43.0	36.6
	900	0.38	0.45	48.3	38.8
w/3	100	0.18	0.19	28.3	26.1
	300	0.26	0.27	32.8	29.2
	600	0.34	0.38	42.7	36.7
	900	0.38	0.42	48.3	38.6
w/4	100	0.18	0.18	28.1	26.1
	300	0.25	0.24	32.3	28.6
	600	0.34	0.39	42.7	36.7
	900	0.38	0.39	48.5	38.3
w/6	100	0.18	0.17	28.1	25.7
	300	0.24	0.23	32.3	28.0
	600	0.33	0.35	41.9	36.0
	900	0.37	0.32	47.9	37.4
w/12	100	0.15	0.15	27.6	25.1
	300	0.24	0.21	30.3	26.8
	600	0.31	0.29	40.0	33.8
	900	0.36	0.30	45.5	35.2

Table 3.7 Maximum velocities and mean temperatures in the upflow and downflow streams (at the throat area) at w/2, 5w/12, w/3, w/4, w/6, w/12 for various heat input rates.

HEAT INPUT RATE $\dot{Q}$ (W)	UP-FLOW VOLUME-FLOW $\dot{V}_u$ ($m^3\ s^{-1}$)	DOWN-FLOW VOLUME-FLOW $\dot{V}_d$ ($m^3\ s^{-1}$)	AVERAGE VOLUME-FLOW $\dot{V}_m$ ($dm^3\ s^{-1}$)	MASS FLOW RATE $\dot{m}_u$ ($kg\ s^{-1}$)	($\dot{m}_d + \dot{m}_\ell$) ($kg\ s^{-1}$)
100	0.0223	0.0220	22.15	0.0251	0.0245
300	0.0297	0.0288	29.25	0.0327	0.0322
600	0.0378	0.0382	38.00	0.0410	0.0415
900	0.0490	0.0512	50.10	0.0515	0.0543

Table 3.8 Volume and mass flow rates in the up-flow and down-flow, at throat area for various heat input rates and for closed stairwell case.

HEAT INPUT RATE $\dot{Q}$ (W)	UP-FLOW VOLUME-FLOW $\dot{V}_u$ ($m^3\ s^{-1}$)	DOWN-FLOW VOLUME-FLOW $\dot{V}_d$ ($m^3\ s^{-1}$)	THROUGH-FLOW $\dot{m}_T$ ($kg\ s^{-1}$)	MASS FLOW RATE $\dot{m}_u$ ($kg\ s^{-1}$)	($\dot{m}_d + \dot{m}_T$) ($kg\ s^{-1}$)
100	0.0191	0.0144	2.899×10^{-3}	0.0223	0.0227
300	0.0275	0.0237	4.484×10^{-3}	0.0317	0.0320
600	0.0362	0.0352	6.200×10^{-3}	0.0431	0.0463
900	0.0431	0.0403	7.223×10^{-3}	0.0479	0.0522

Table 3.9 Volume and mass flow rates in the up-flow and down-flow at throat area and through-flow for various heat input rates and for open stairwell case.

CORRESPONDING WALL	100 (W)	300 (W)	600 (W)	900 (W)
AC	15.6	39.8	67.4	95.6
CD	4.7	17.1	41.5	45.5
DE	3.0	7.3	18.2	23.1
EF	6.3	29.4	58.7	83.0
FG	3.7	9.6	18.1	26.7
GH	2.5	6.1	12.1	18.7
HI+IA	5.5	16.8	33.5	42.8
SIDE WALLS	58.6	164.0	350.4	583.9
LEAKAGE	0.6	1.1	1.8	3.1
TOTAL LOSS MEASURED	100.5	291.4	601.7	922.4

Table 3.10 Rate of heat loss from the stairwell for various heat input rates and for closed stairwell case (for definition of walls see Figure 5.2)

CORRESPONDING WALL	100 (W)	300 (W)	600 (W)	900 (W)
AC	15.5	34.1	61.4	89.3
CD	5.3	18.8	38.5	48.4
DE	4.2	8.2	12.1	18.8
EF	6.3	30.6	47.2	77.8
FG	3.7	9.6	19.7	22.9
GH	1.5	3.0	12.1	17.0
HI	6.5	13.0	19.0	21.5
IA	4.6	10.5	17.6	21.0
SIDE WALLS	47.8	149.7	336.0	544.7
THROUGH-FLOW	9.6	25.1	67.6	98.7
TOTAL LOSS MEASURED	105.0	302.6	631.2	960.1

Table 3.11 Rate of heat loss from the stairwell for various heat input rates and for open stairwell case (for definition of walls see Figure 5.2)

CORRESPONDING WALL	300 (W)	600 (W)
AC	46.2	85.0
CD	33.6	66.2
DE	15.2	38.9
EF	76.6	178.7
FG	21.3	42.2
GH	14.1	38.4
HI	42.8	67.1
IA	37.0	67.5
LEAKAGE	1.6	2.5
TOTAL LOSS MEASURED	288.4	586.5

Table 3.12 Rate of heat loss from the stairwell, with insulated side walls and for closed stairwell case. (For definition of walls see Figure 5.2).

$\dot{Q}$ (W)	T_{av} (°C)	$\dot{V}_m$ ($dm^3\ s^{-1}$)	1000 x Fr	1000 x St	Re	Gr	DT (C deg)
100	28.1	22.15	13.85	0.1765	2060	9.733×10^7	1.7
300	31.8	29.25	18.33	0.5287	2650	2.179×10^8	4.1
600	38.9	38.00	23.81	1.0567	3300	2.945×10^8	6.1
900	41.9	50.10	31.31	1.5845	4400	3.819×10^8	8.6

Table 4.1 Basic performance characteristics of the closed-stairwell case.

$\dot{Q}$ (W)	T_{av} (°C)	T_i (°C)	T_o (°C)	$\dot{V}_T$ ($dm^3 s^{-1}$)	1000 x Fr	1000 x St	DT (C deg)
100	25.8	21.8	25.4	2.432	13.7	0.1764	2.4
300	29.6	23.7	29.6	3.800	17.3	0.5290	3.5
600	37.9	24.9	36.7	5.320	25.5	1.0590	6.0
900	40.4	24.9	38.6	6.232	29.2	1.5880	10.1

Table 4.2 Basic performance characteristics of the open-stairwell case.

RANGE OF GRASHOF NUMBER	RANGE OF REYNOLDS NUMBER	RANGE OF DT (C deg)	CONVECTION TYPE	SOURCE
10^6 <Gr< 10^8	-	8-47	Natural and Forced	Brown and Solvason (1962
10^8 <Gr< 10^{11}	-	0-12	Natural and Forced	Shaw (1971)
$21.1x10^8$<Gr<$74.9x10^8$	2680<Re<10560	1.8-2.8	Natural	Timmons et al. (1981)
10^7 <Gr< 10^8	-	-	Natural	Fraikin et al. (1980)
10^8 <Gr< 10^{10}	-	0.5-13	Natural	Riffat and Eid (1988)
-	5200<Re<13000	-	Natural	Marshall (1985)

Table 4.3 Comparison of temperature differential, type of flow, Grashof and Reynolds numbers, in previous research.

Equation	ϕ	Γ_ϕ	S_ϕ
Continuity	1	0	-
u-momentum	u	μ_{eff}	$-\frac{\partial p}{\partial x} + \frac{\partial}{\partial x}(\mu_{eff}\frac{\partial u}{\partial x}) + \frac{\partial}{\partial y}(\mu_{eff}\frac{\partial v}{\partial x})$
v-momentum	v	μ_{eff}	$-\frac{\partial p}{\partial y} + \frac{\partial}{\partial x}(\mu_{eff}\frac{\partial u}{\partial y}) + \frac{\partial}{\partial y}(\mu_{eff}\frac{\partial v}{\partial y}) + g(\rho_r-\rho)$
Turbulent Energy	k	$\frac{\mu_{eff}}{\sigma_k}$	$G_k - C_D\,\rho\,\varepsilon + \rho\,g\,\beta\,\overline{v'T'}$
Energy Dissipation	ε	$\frac{\mu_{eff}}{\sigma_\varepsilon}$	$C_1\,\frac{\varepsilon}{k}\,G_k - C_2\,\rho\,\frac{\varepsilon^2}{k} + C_3\,\rho\,\frac{\varepsilon}{k}\,g\,\beta\,\overline{v'T'}$
Energy equation	T	Γ_{eff}	S_T

$$\Gamma_{eff} = \frac{\mu}{\sigma_T} + \frac{\mu_t}{\sigma_{T,t}}\,,\quad \mu_{eff} = \mu + \mu_t\,,\quad -\rho\,\overline{v'T'} = \Gamma_{T,t}\,\frac{\partial T}{\partial y}$$

$$G_k = \mu_t\left\{2\left[\left(\frac{\partial u}{\partial x}\right)^2 + \left(\frac{\partial v}{\partial y}\right)^2\right] + \left(\frac{\partial u}{\partial y} + \frac{\partial v}{\partial x}\right)^2\right\}\,,\quad \rho = \frac{P_{ref}}{R\,T}$$

The empirical constants have been adopted from Launder and Spalding (1972, 1974) and take the following values :

$C_\mu = 0.09,\ C_D = 1.0,\ C_1 = 1.44,\ C_2 = 1.92,\ C_3 = 1.0,\ \sigma_k = 1.0,\ \sigma_\varepsilon = 1.3$

Table 5.1 The differential equations of the mathematical model.

WALL	AB	BC	CK	KD	DE	EF	FG	GH	HI	IJ	JA
Temp. (°C)	54.4	39.0	37.2	35.9	29.7	30.6	29.8	28.7	30.5	34.6	37.7
Heat flux from the two walls of the heater = 798.7 W m^{-2}											

(a)

WALL	AB	BC	CK	KD	DE	EF	FG	GH	HI	IJ	JA
Temp. (°C)	75.8	49.3	47.2	44.0	33.5	34.5	34.5	33.4	33.0	37.7	43.8
Heat flux from the two walls of the heater = 1597.3 Wm^{-2}											

(b)

Table 5.2 Thermal boundary conditions for closed insulated side walls stairwell case.

(a) 300 W heat input rate.
(b) 600 W heat input rate.

Grid size	region X1	region X2	region X3	region X4	region Y1	regior Y2
56 X 37	7	10	24	15	28	9
68 X 50	7	10	36	15	41	9
68 X 55	7	10	36	15	41	14

Table 5.3 The number of grid lines adopted in various regions of the stairwell (see Figure 5.2).

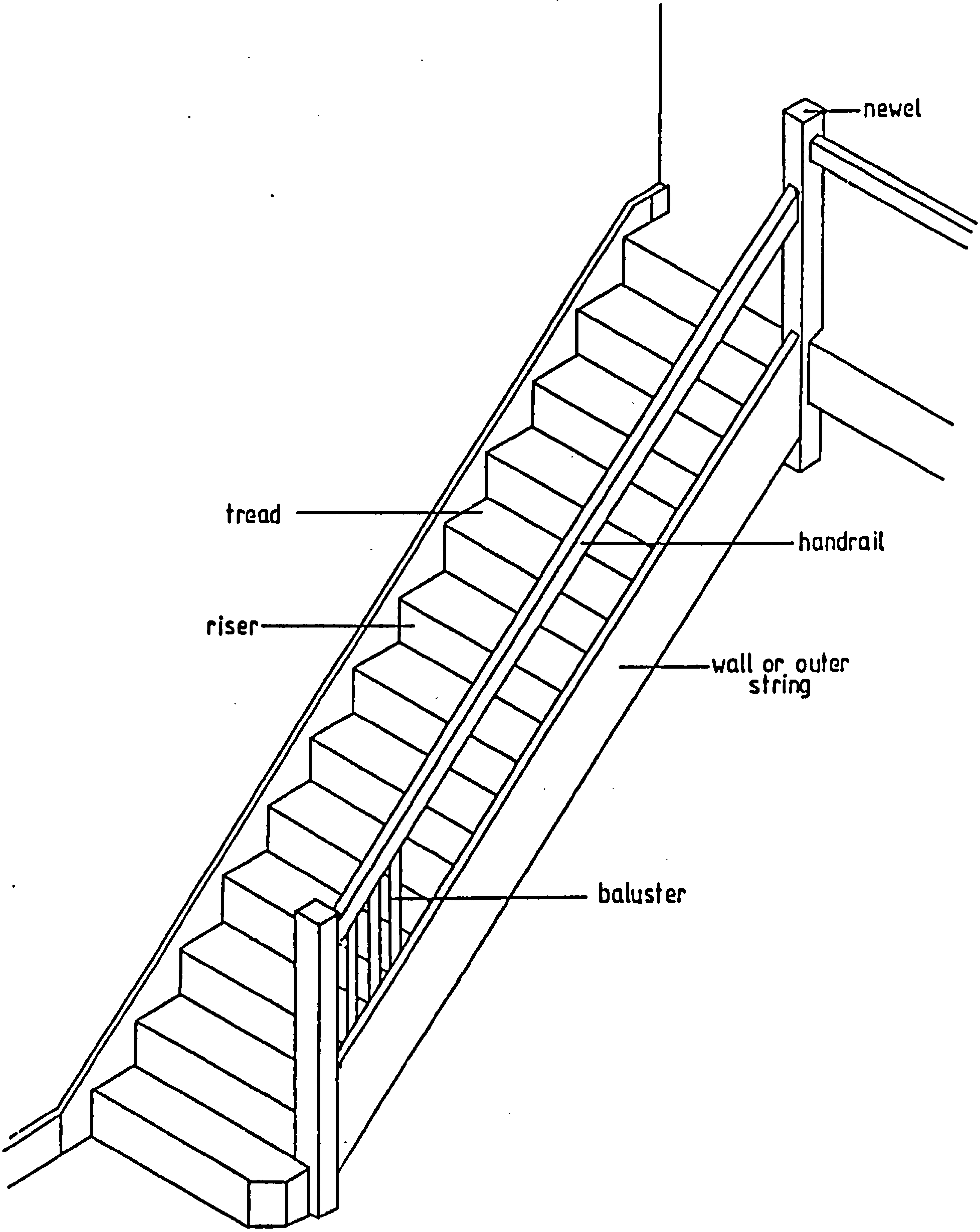

Figure 1. Straight-flight stairwell.

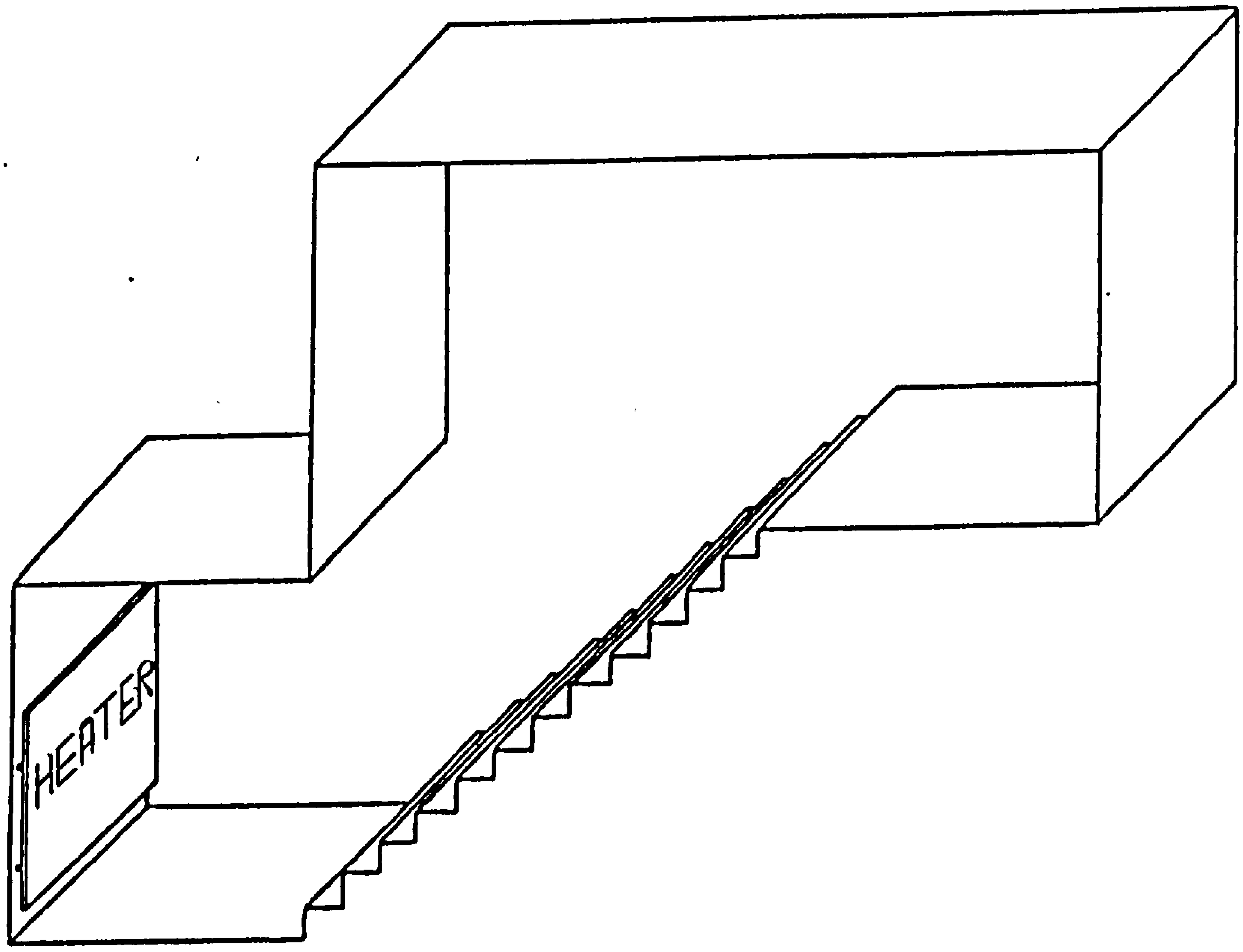

Figure 2.1. Schematic diagram of the stairwell model.

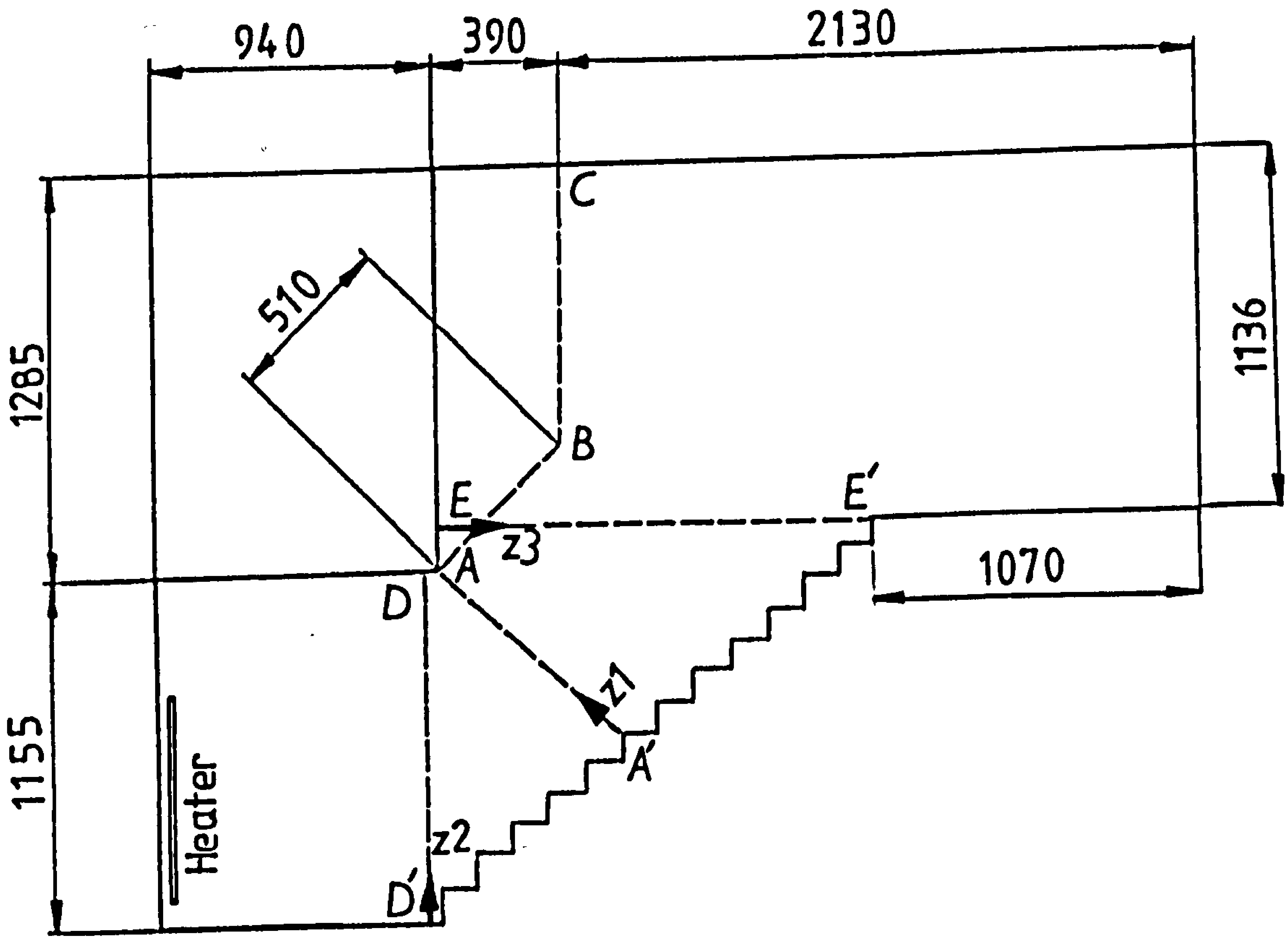

Figure 2.2. Non-sloping ceiling, and sloping-ceiling (shown by broken lines ABC) geometries. AA' indicates the throat area DD' and EE' indicate two other cross-sections in which the temperatures were measured.
(Dimensions are in mm).

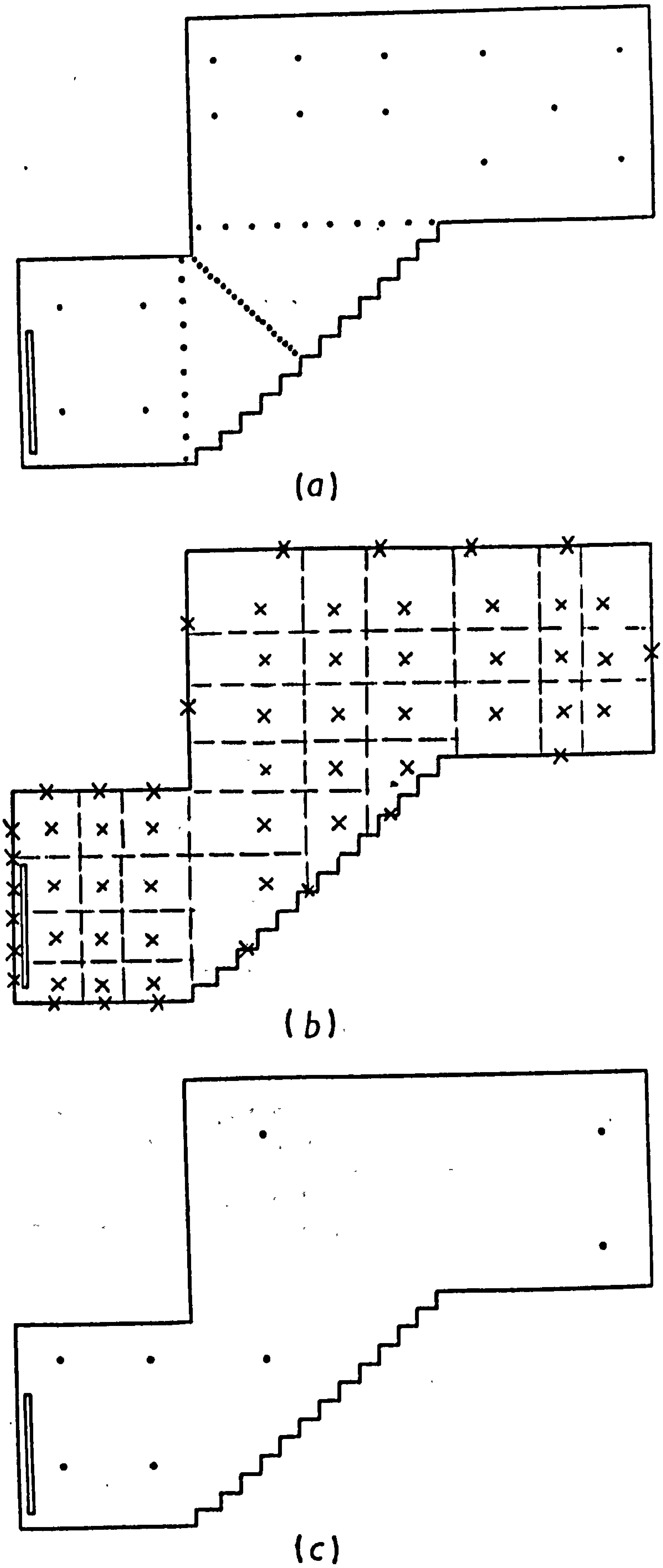

Figure 2.3. Measurement position. (a) velocity and temperature probes; (b) thermocouples fixed to the walls; (c) concentration sampling points.

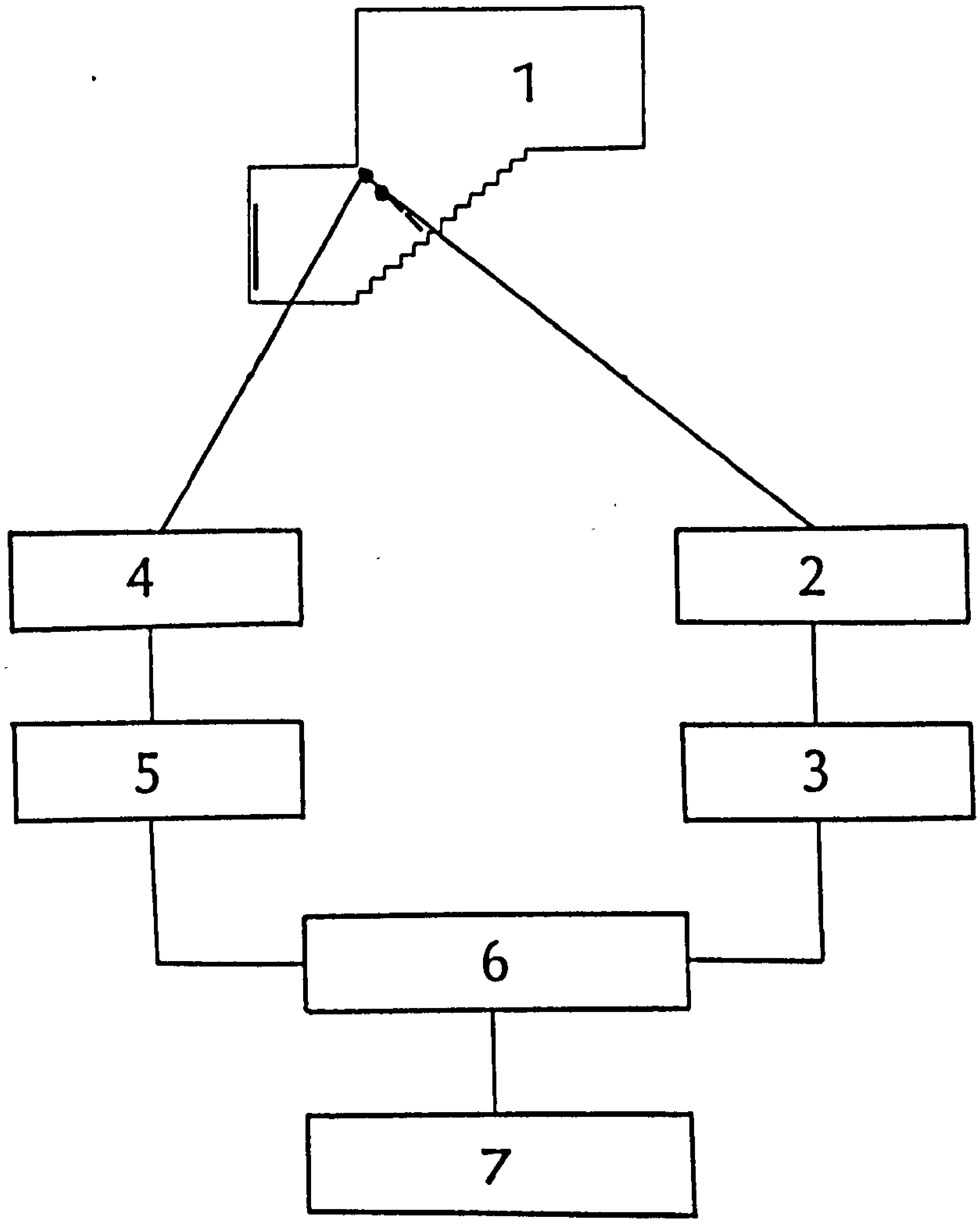

Figure 2.4. Schematic diagram of the rig.
(1) Stairwell; (2,4) Signal conditioning electronics for velocity and temperature measurements;
(3,5) Analogue-to-Digital Converters; (6) Apple computer; (7) Printer.

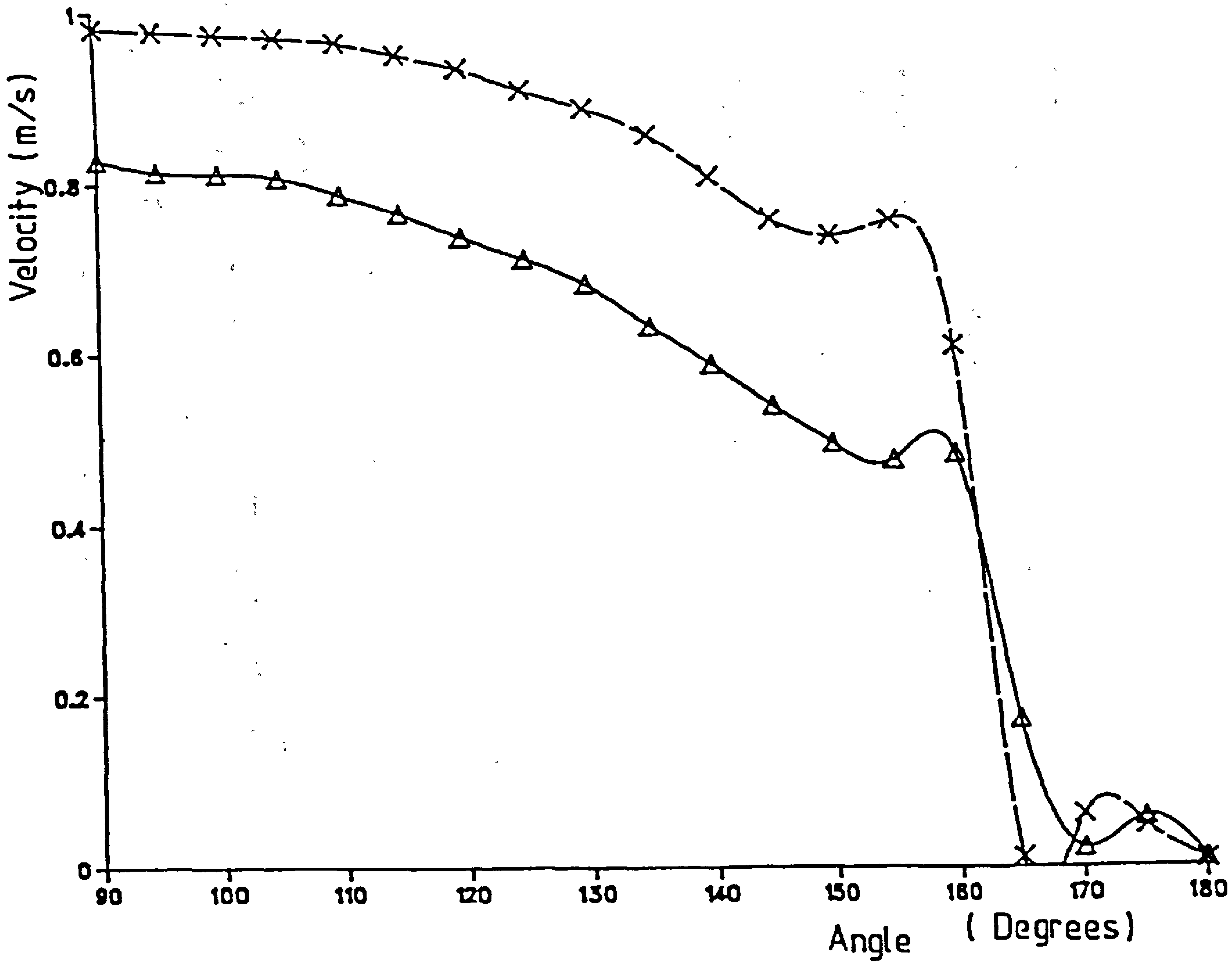

Figure 2.5. Variation of the velocity versus probe-angle rotation (based on wind-tunnel tests): Δ and X represent different air speeds in the wind tunnel.

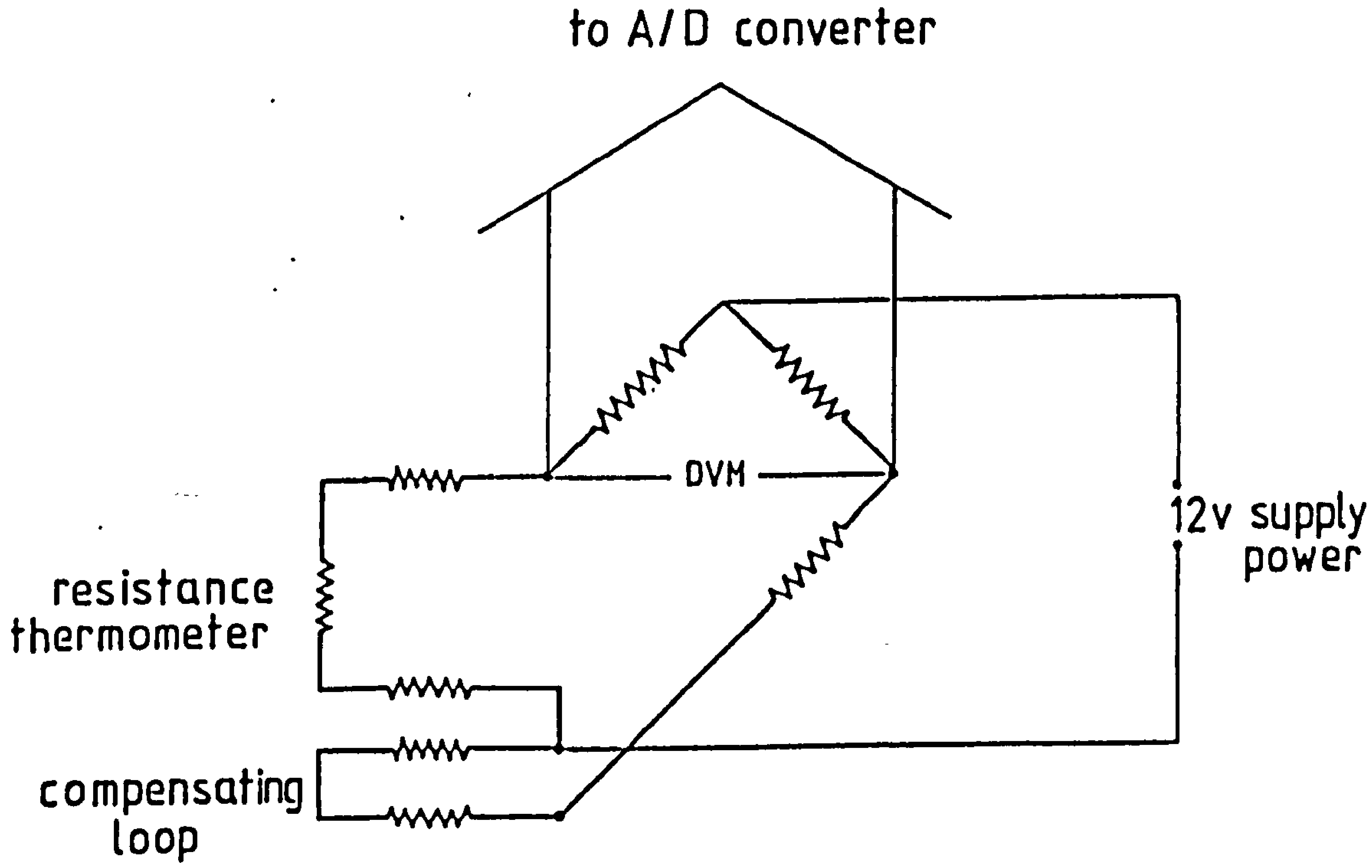

Figure 2.6. Circuit diagram of platinum resistance thermometer of the temperature measuring system.

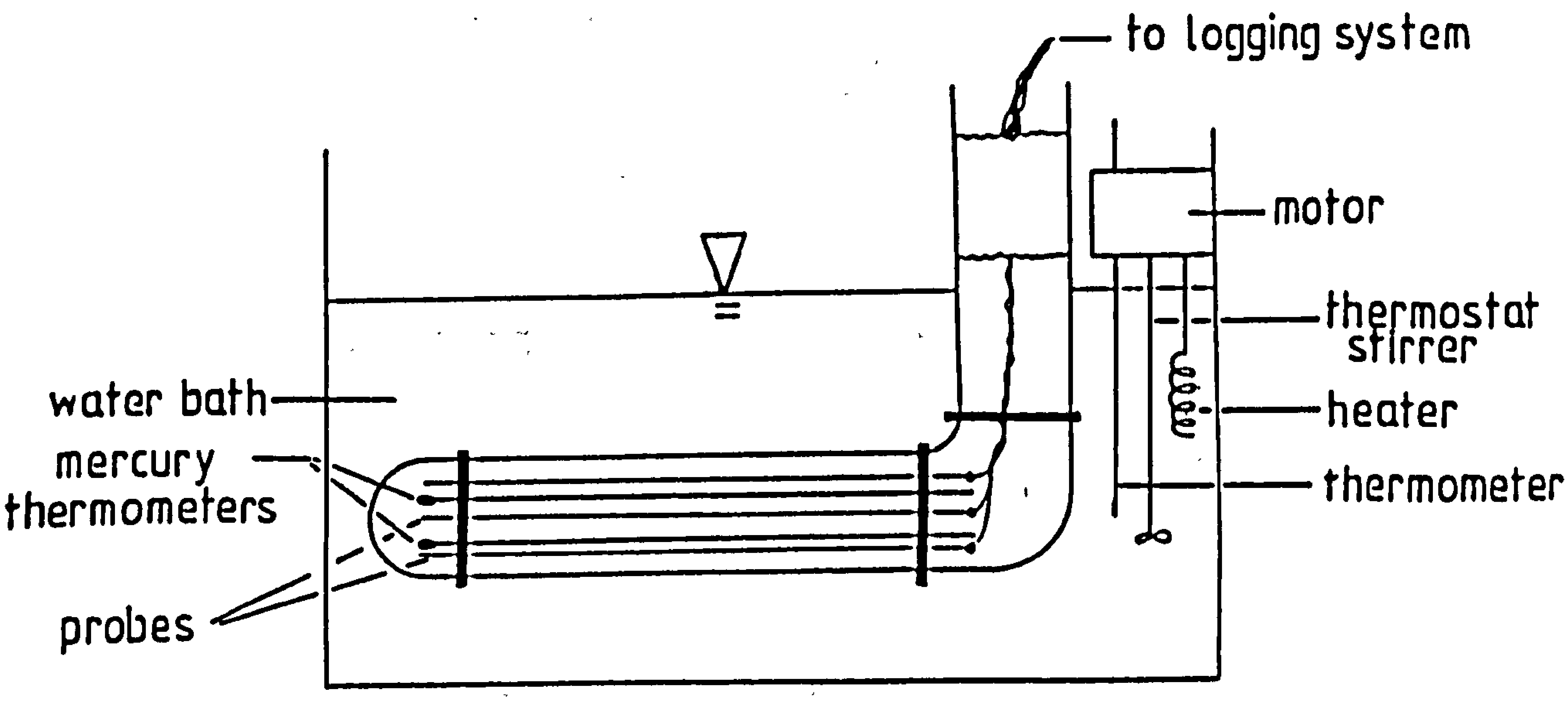

Figure 2.7. Calibration set up of the platinum resistance thermometer.

Figure 2.8. Flow chart for data-acquisition system.

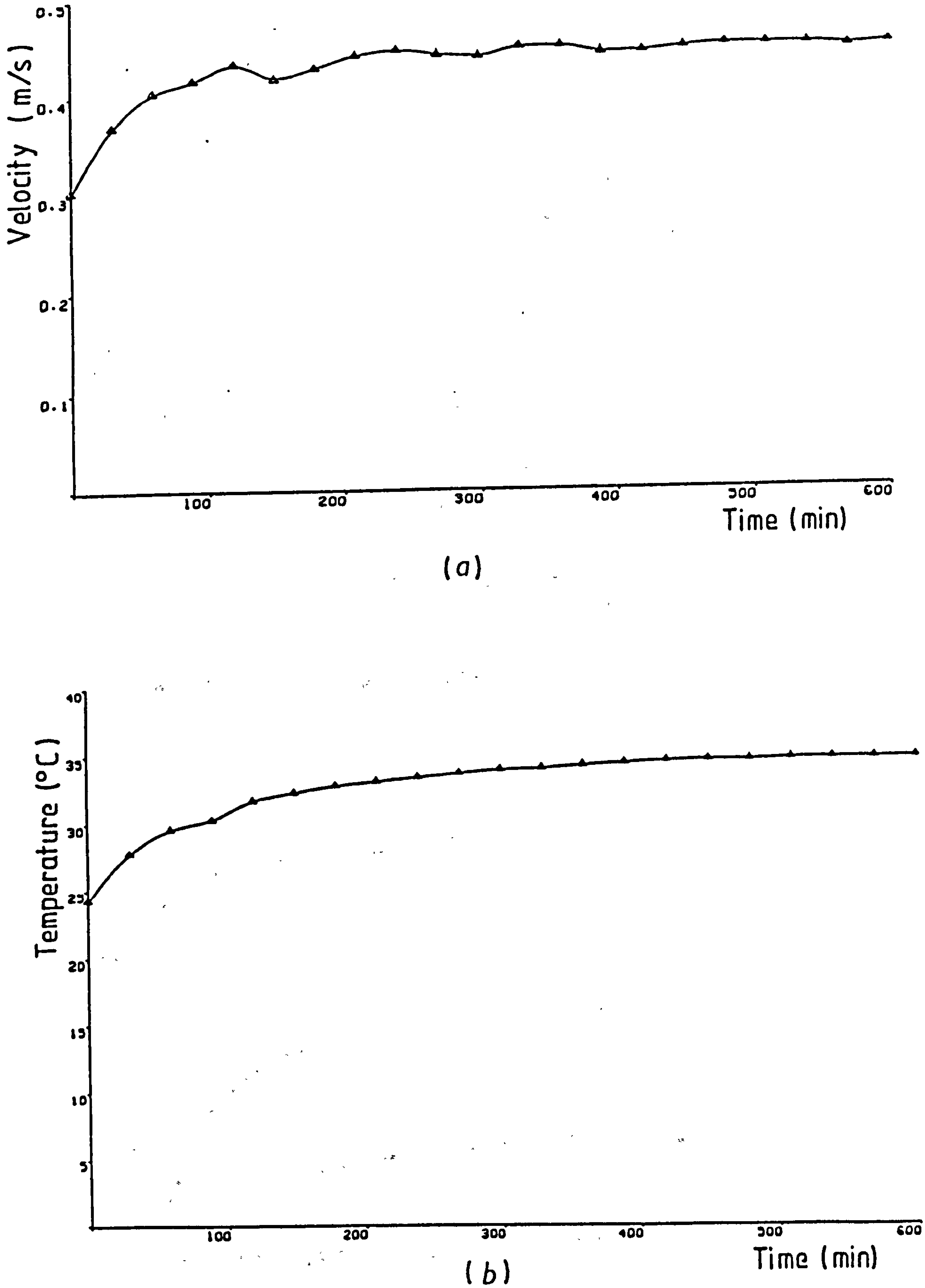

Figure 2.9. Variation of velocity and temperature with time.
(a) - Velocity
(b) - Temperature

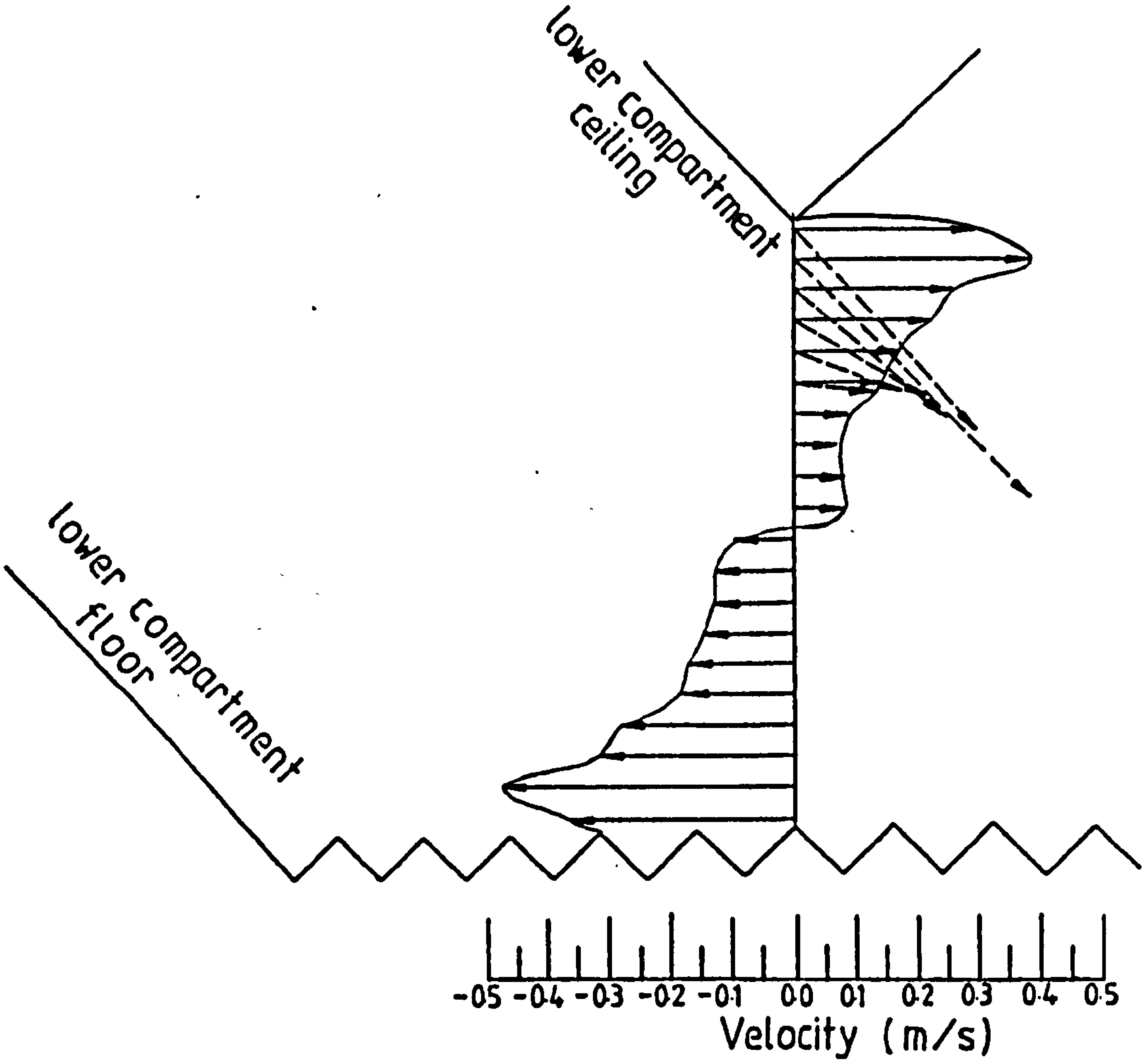

Figure 2.10. A typical velocity profile at the throat area.

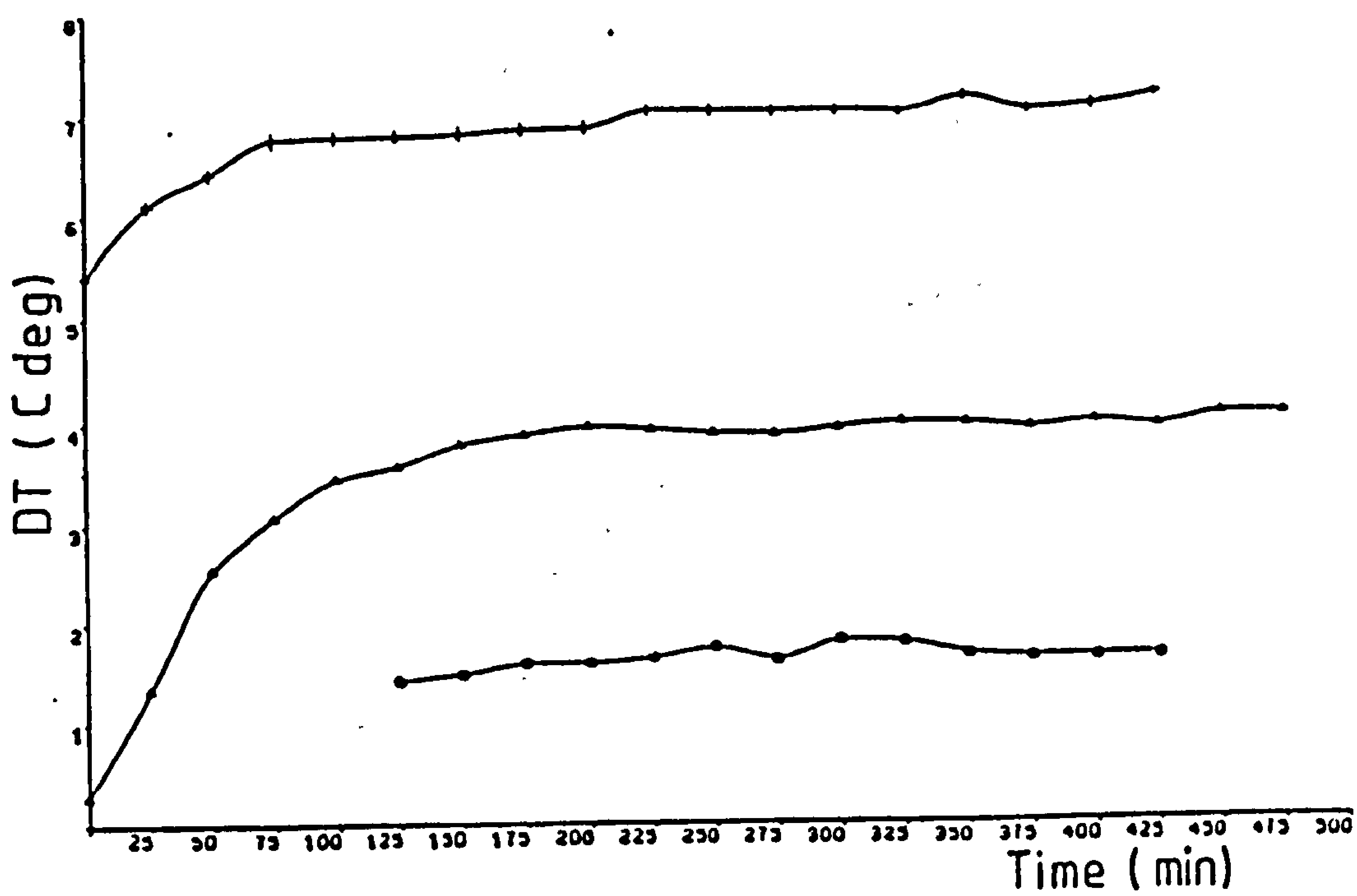

Figure 2.11. Differential temperatures at the throat area versus time for various heat input rates:
O 100 W ; Δ 300 W ; + 600 W.

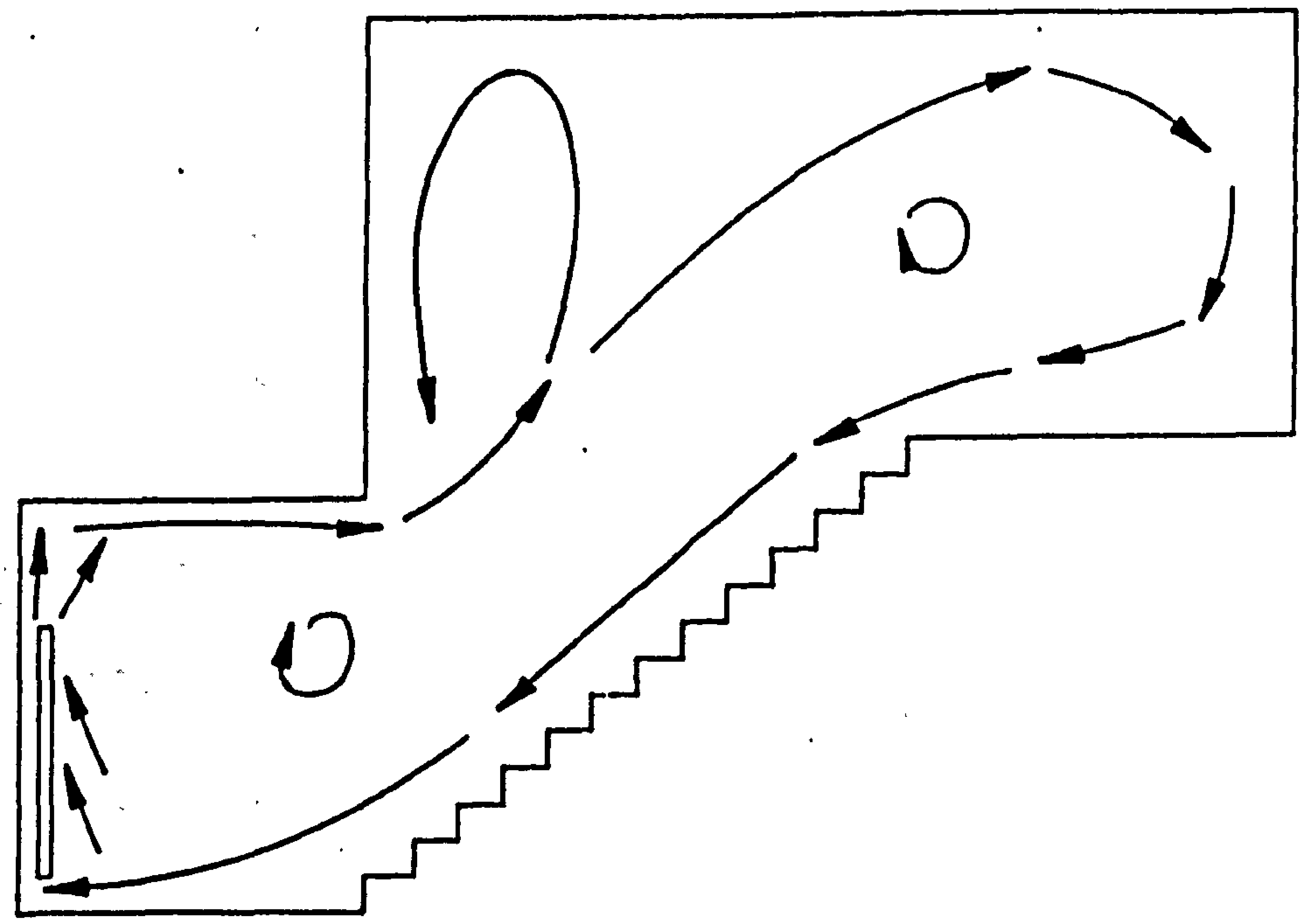

Figure 3.1. A two-dimensional view of the flow pattern in the closed stairwell.

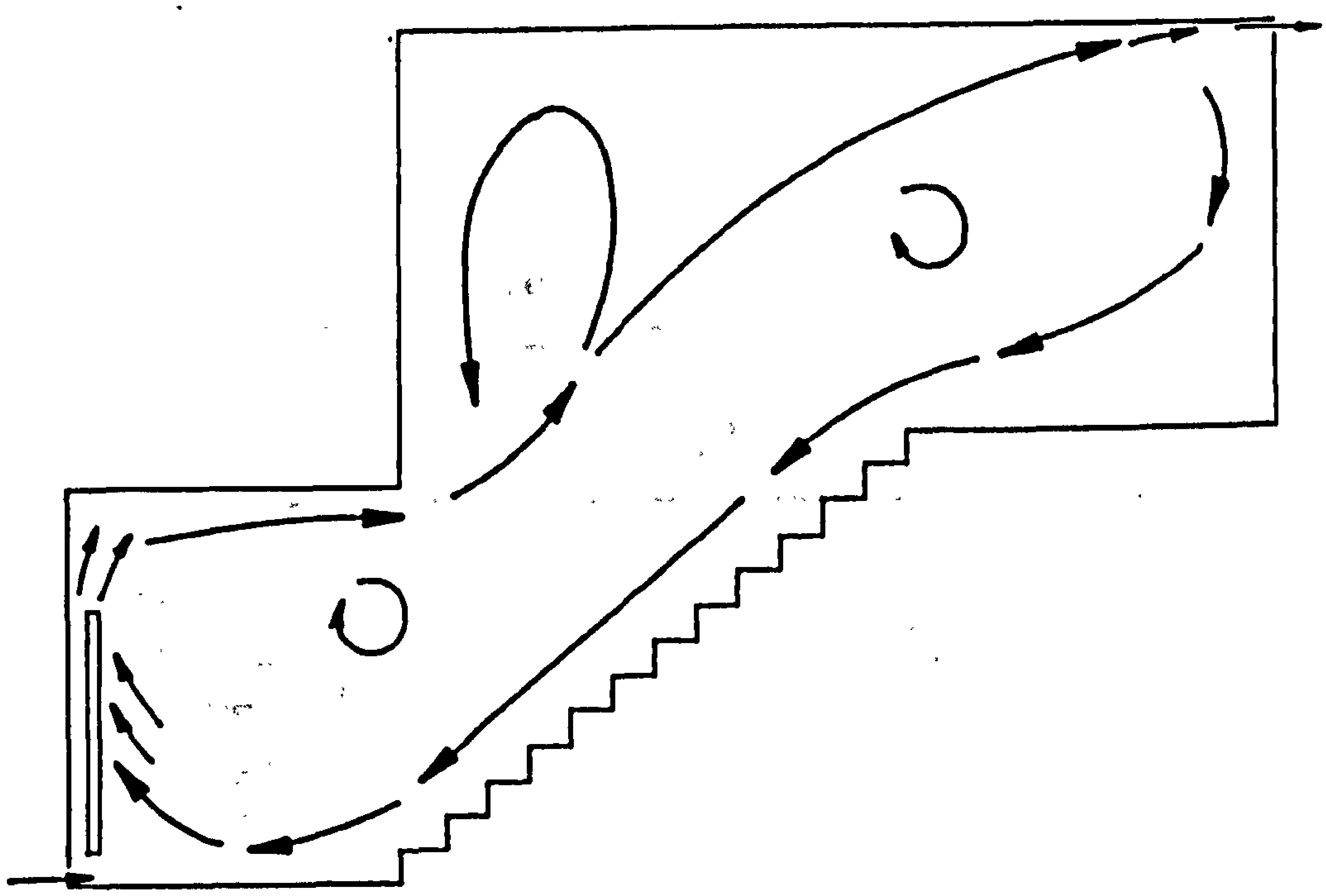

Figure 3.2. A two-dimensional view of the flow pattern in the open stairwell.

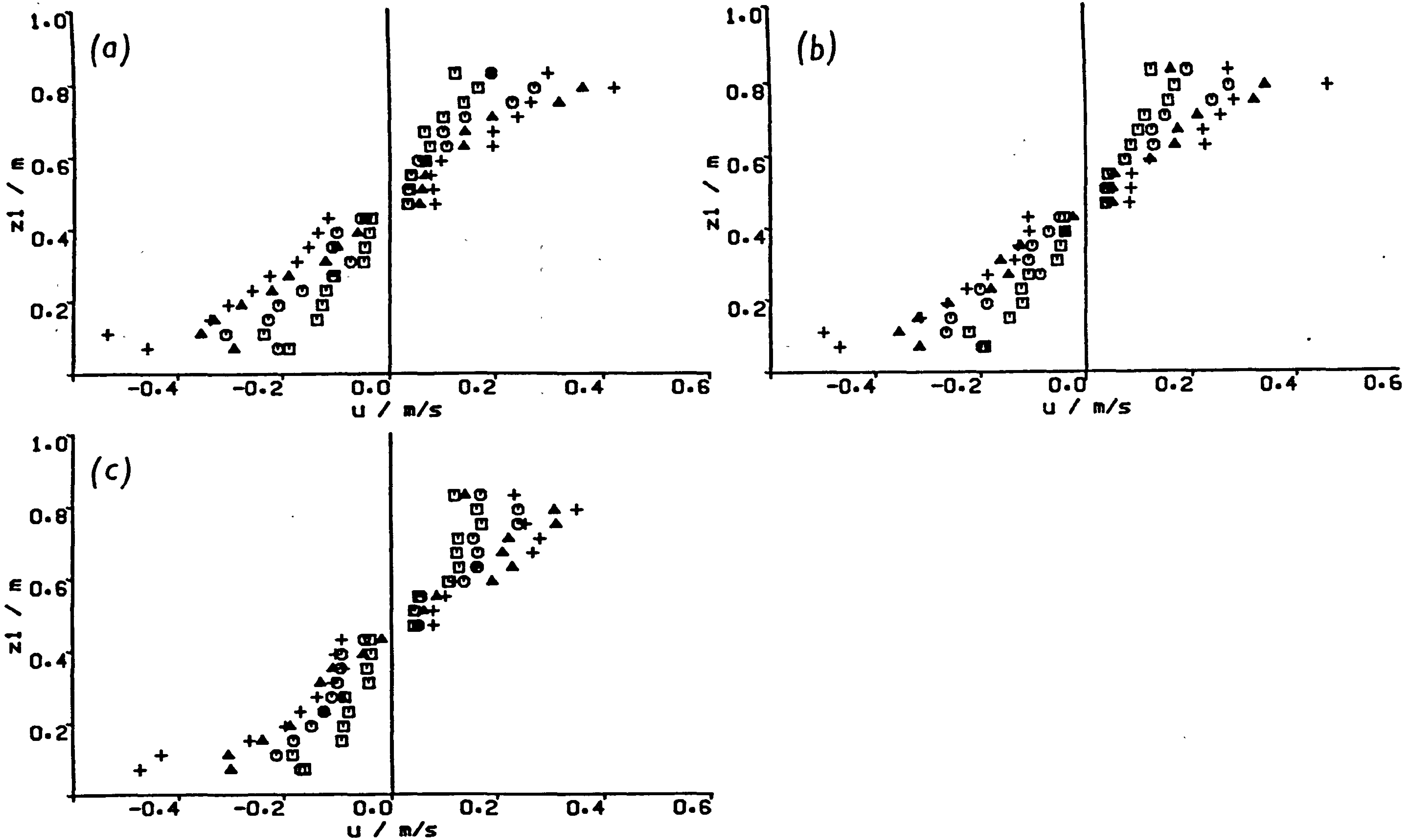

Figure 3.3. Velocity profiles at various distances from the side wall for various heat input rates (closed stairwell case):
(a) w/2 ; (b) w/3 ; (c) w/6.
□ 100 W ; ○ 300 W ; Δ 600 W ; + 900 W.

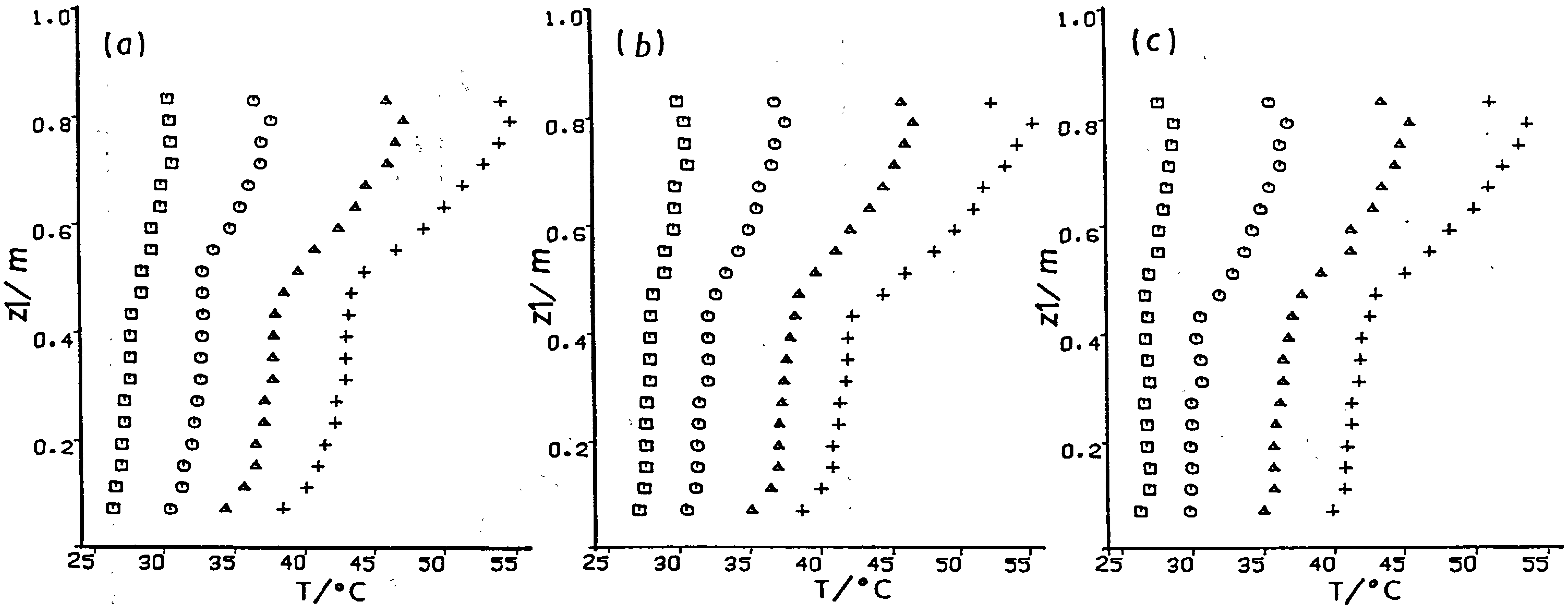

Figure 3.4. Temperature distributions at various distances from the side wall, for various heat input rates (closed stairwell case):
(a) w/2 ; (b) w/3 ; (c) w/6.
□ 100 W; ○ 300 W ; Δ 600 ; + 900 W.

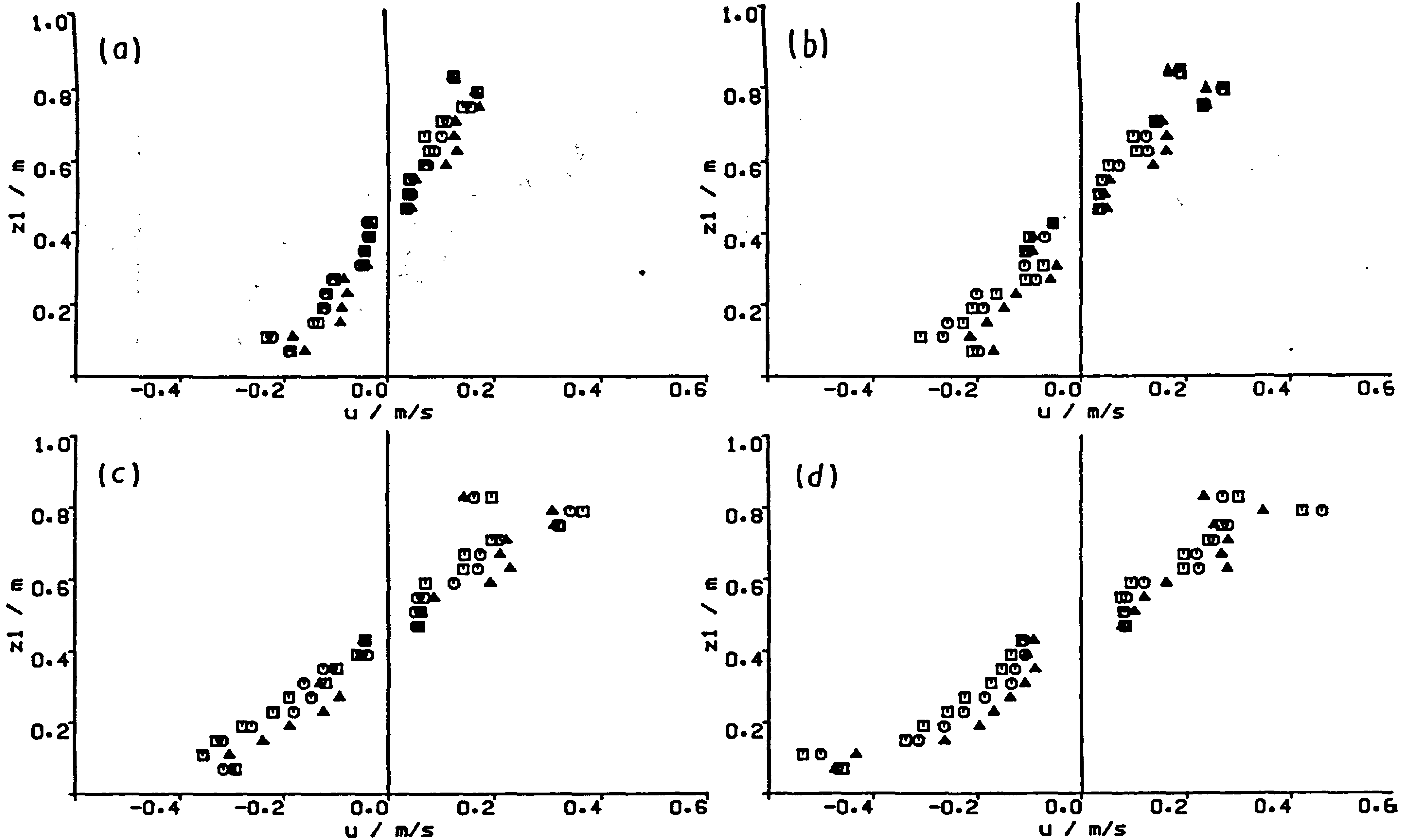

Figure 3.5. Velocity profiles for various heat input rates, at various distances from the side wall (closed stairwell case):
(a) 100 W ; (b) 300 W ; (c) 600 W ; (d) 900 W.
o w/2 ; □ w/3 ; Δ w/6.

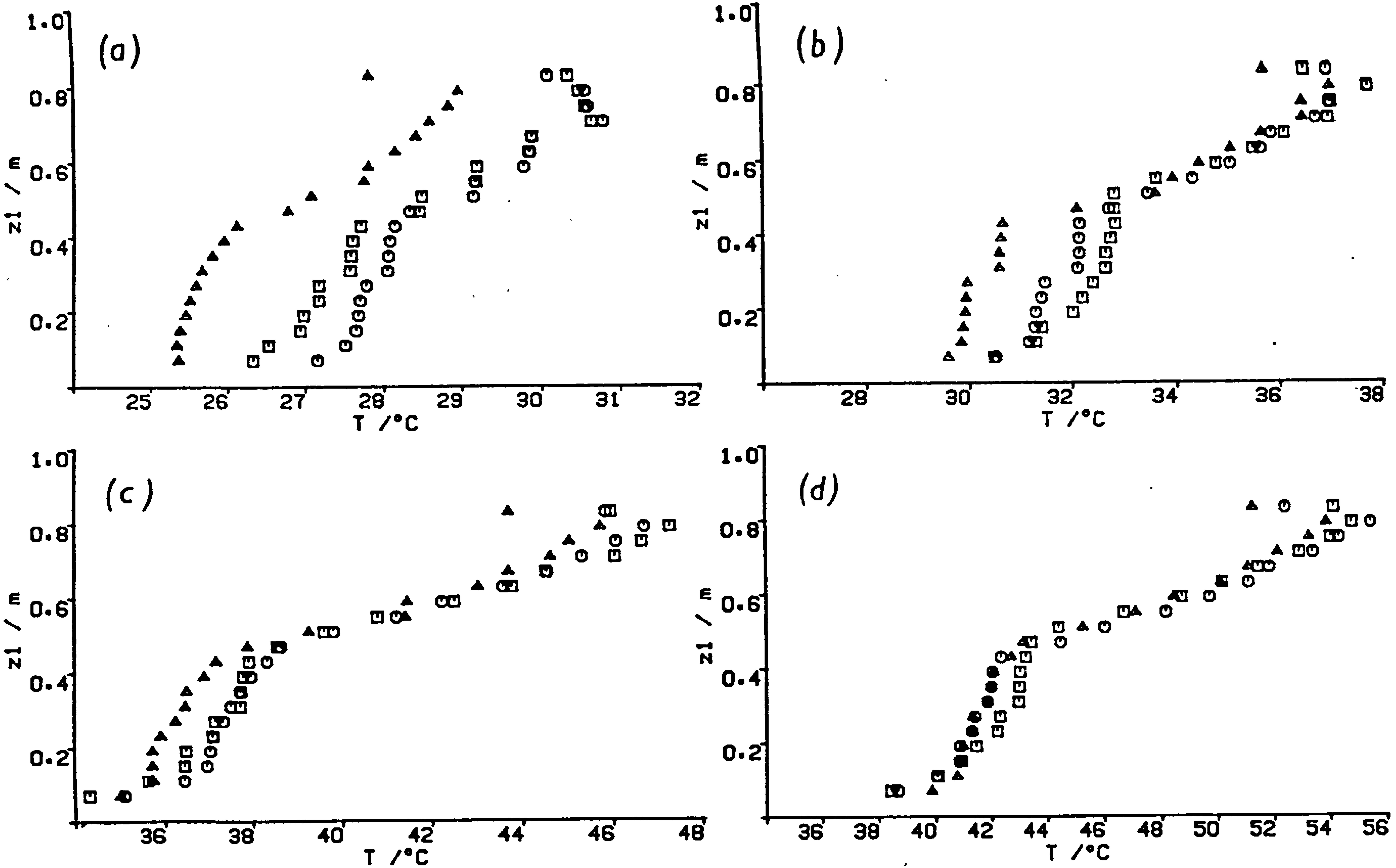

Figure 3.6. Temperature distributions for various heat input rates, at various distances from the side wall (closed stairwell case):
(a) 100 W ; (b) 300 W ; (c) 600 W ; (d) 900 W
○ w/2 ; □ w/3 ; Δ w/6.

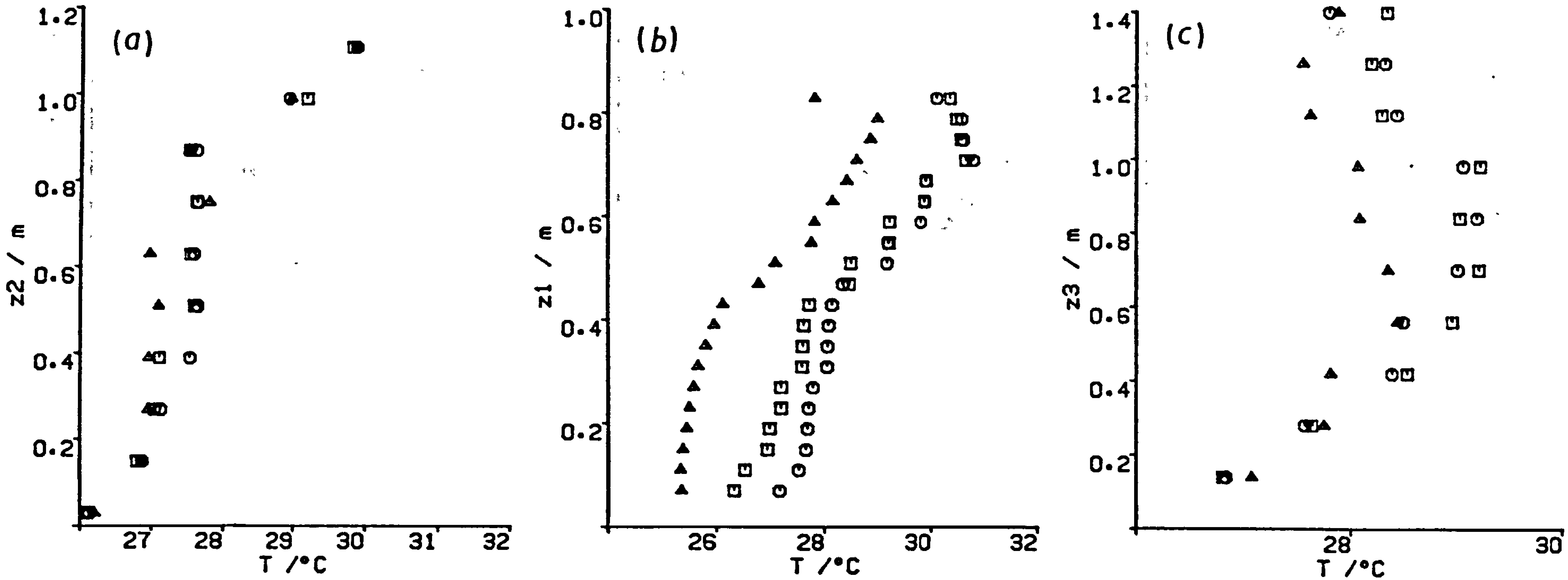

Figure 3.7. Temperature profiles at various distances from the side wall, at cross-sections DD', AA' and EE' for closed stairwell case. (Heat input rate = 100 W):
o w/2 ; □ w/3 ; Δ w/6.
(a) DD' ; (b) AA' ; (c) EE'.

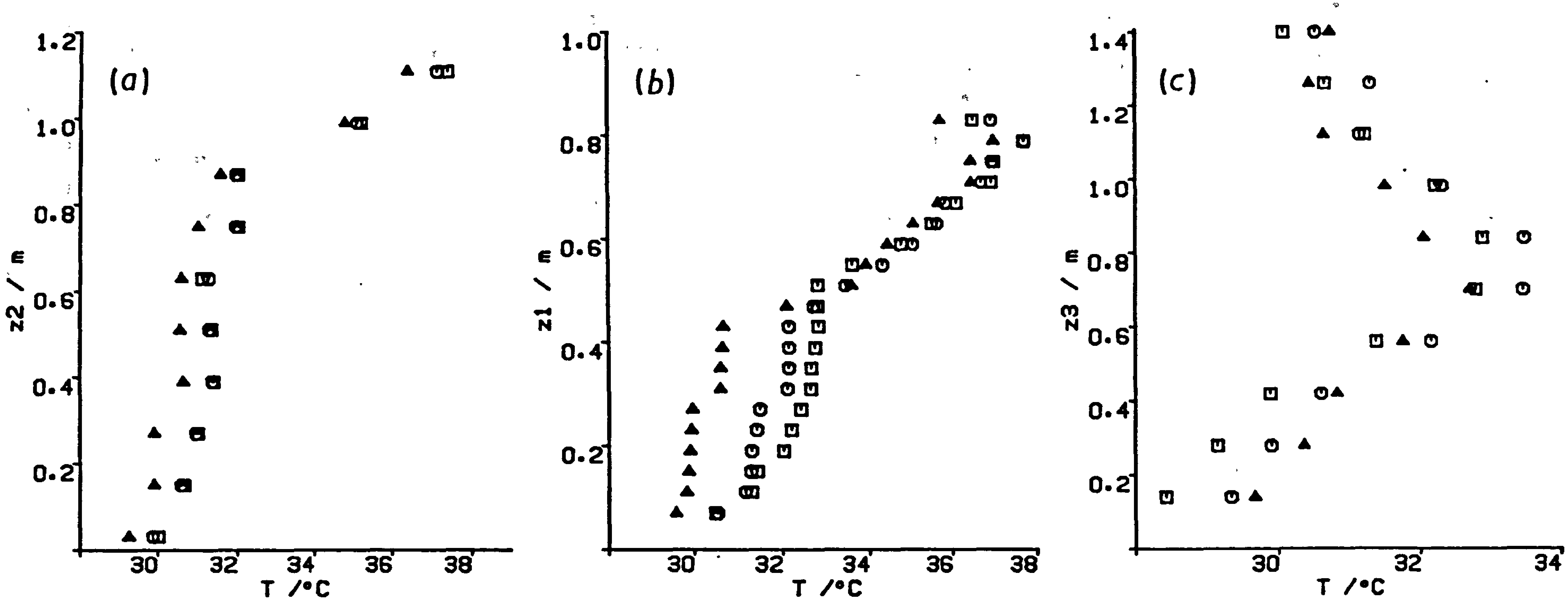

Figure 3.8. Temperature profiles at various distances from the stairwell side wall, at cross-sections DD', AA' and EE' for closed stairwell case. (Heat input rate = 300 W):
o w/2 ; □ w/3 ; Δ w/6.
(a) DD' ; (b) AA' ; (c) EE'.

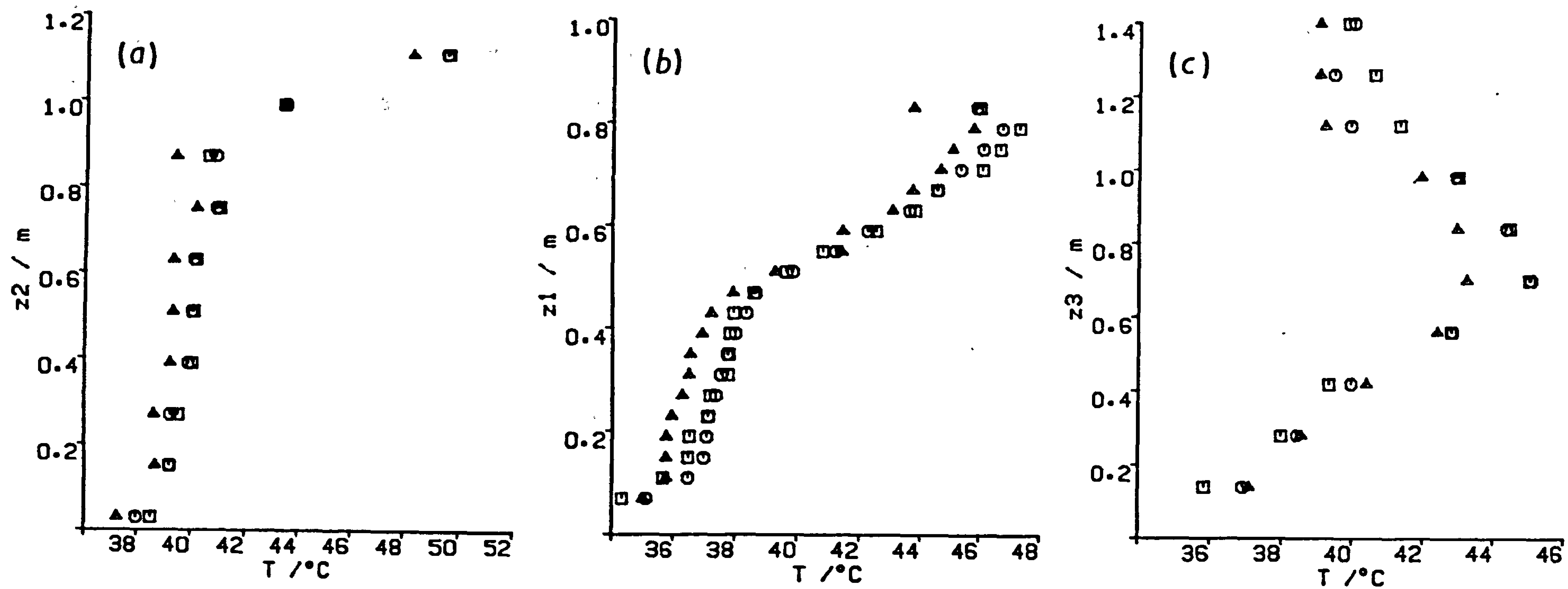

Figure 3.9. Temperature profiles at various distances from the stairwell side wall, at cross-sections DD', AA' and EE' for closed stairwell case. (Heat input rate = 600 W):
o w/2 ; □ w/3 ; Δ w/6.
(a) DD' ; (b) AA' ; (c) EE'.

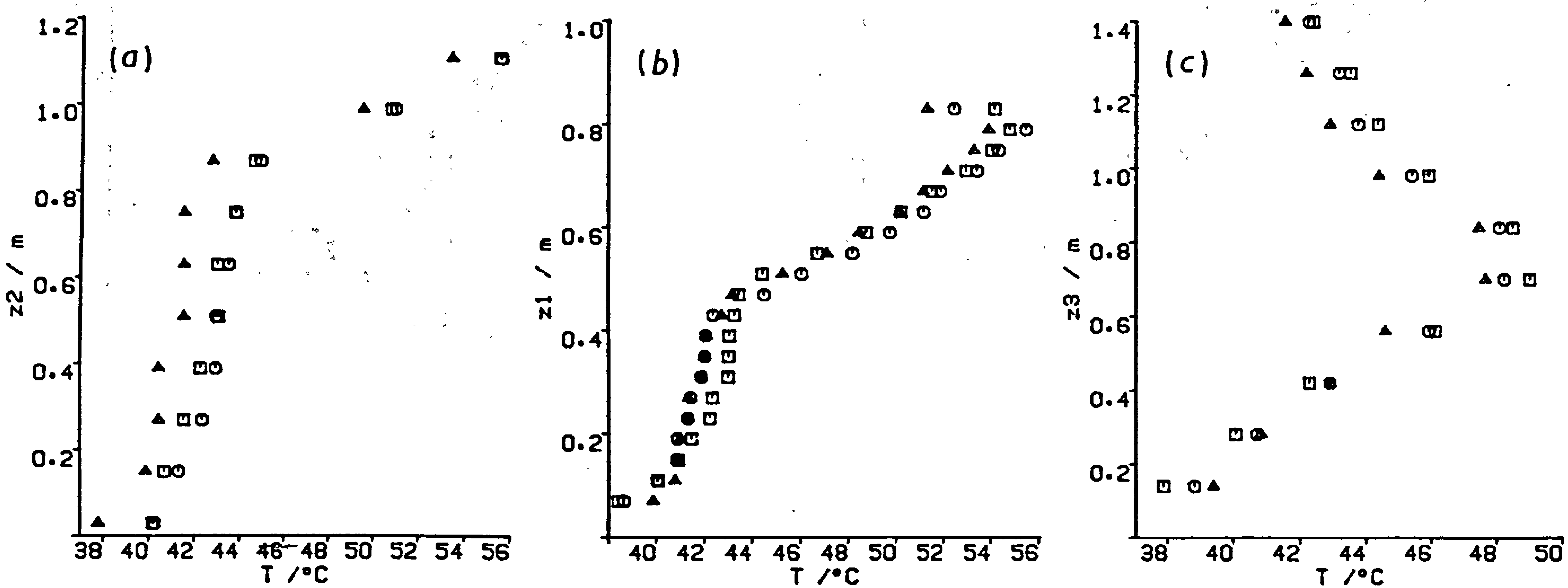

Figure 3.10. Temperature profiles at various distances from the stairwell side wall, at cross-sections DD'.
(Heat input rate = 900 W) :
o w/2 ; □ w/3 ; Δ w/6.
(a) DD' ; (b) AA' ; (c) EE'.

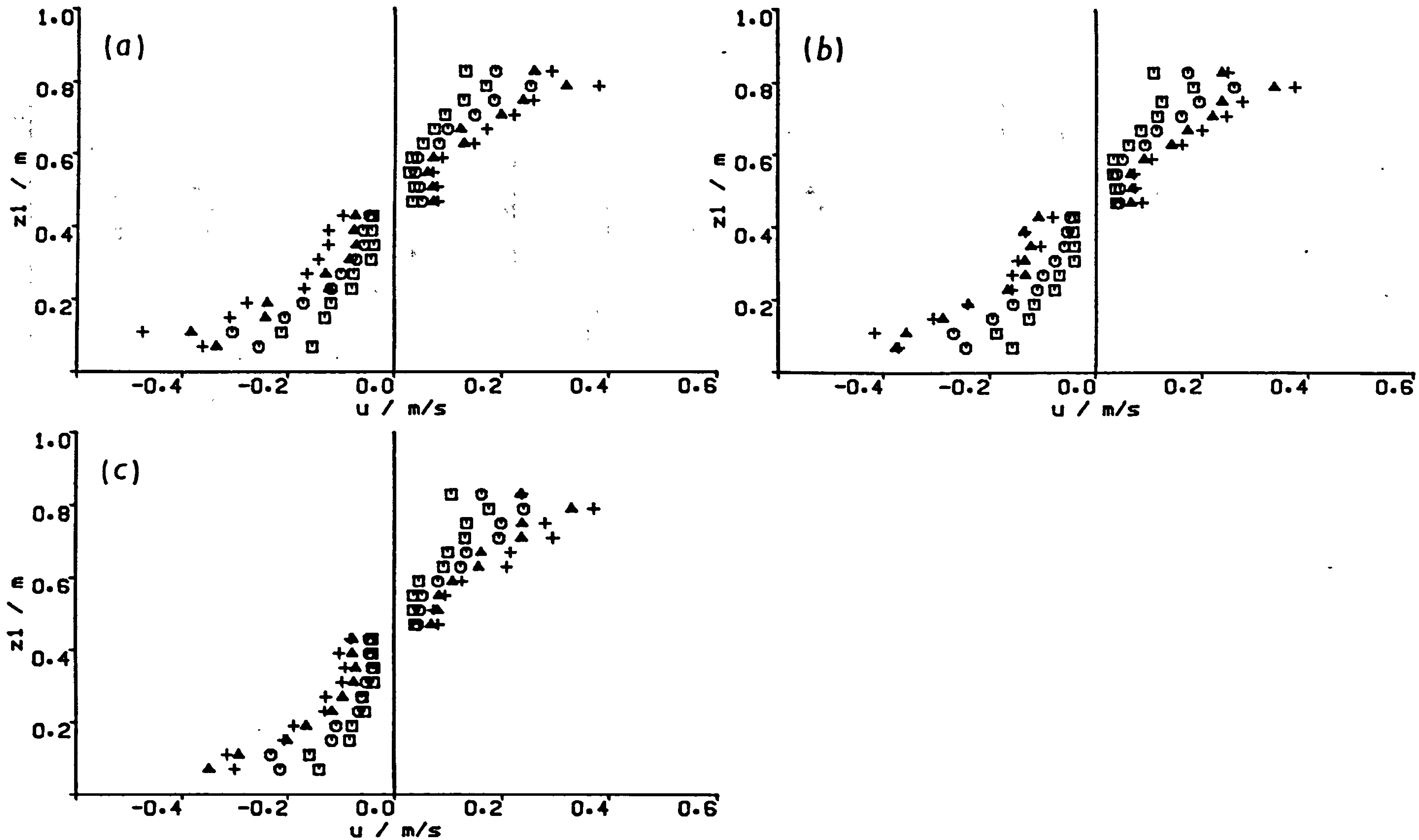

Figure 3.11. Velocity profiles at various distances from the side wall for various heat input rates (open stairwell case):
(a) w/2 ; (b) w/3 ; (c) w/6.
□ 100 W ; O 300 W ; Δ 600 W ; + 900 W.

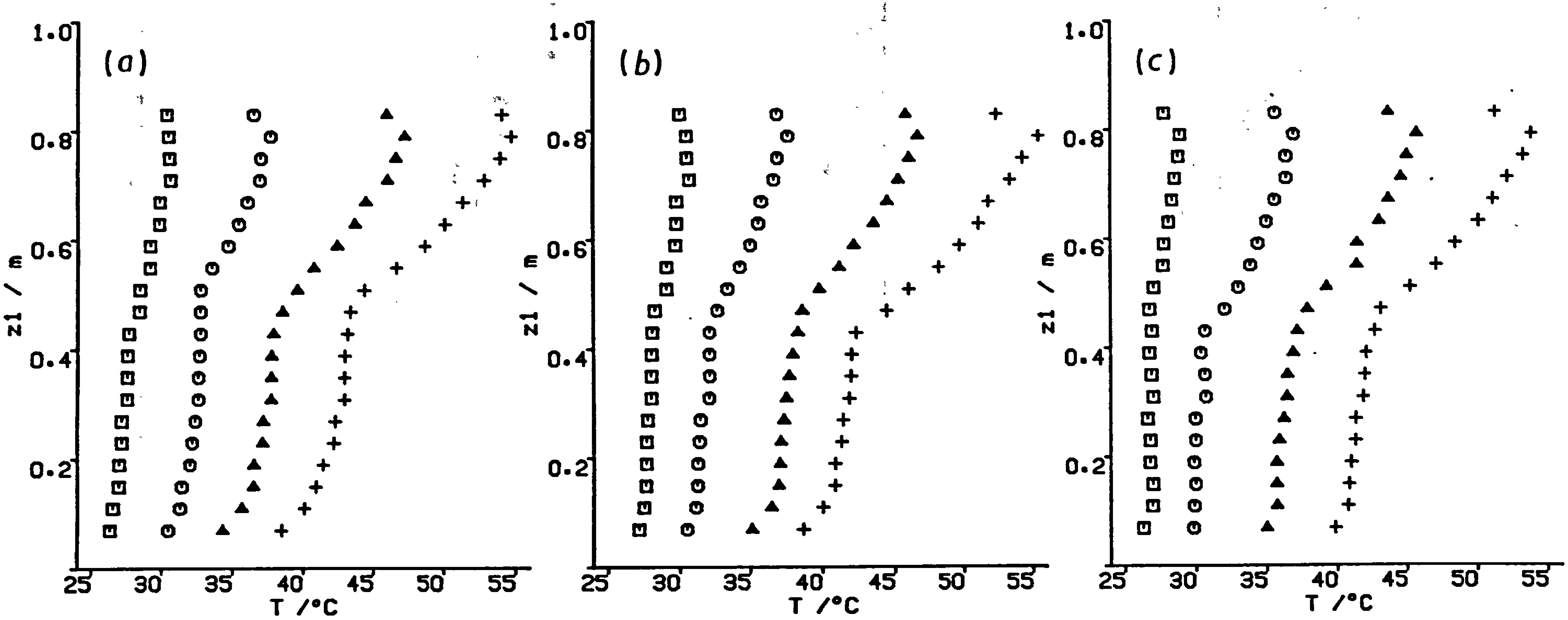

Figure 3.12. Temperature distributions at various distances from the side wall for various heat input rates (open stairwell case):
(a) w/2 ; (b) w/3 ; (c) w/6.
□ 100 W ; o 300 W ; Δ 600 W ; + 900 W.

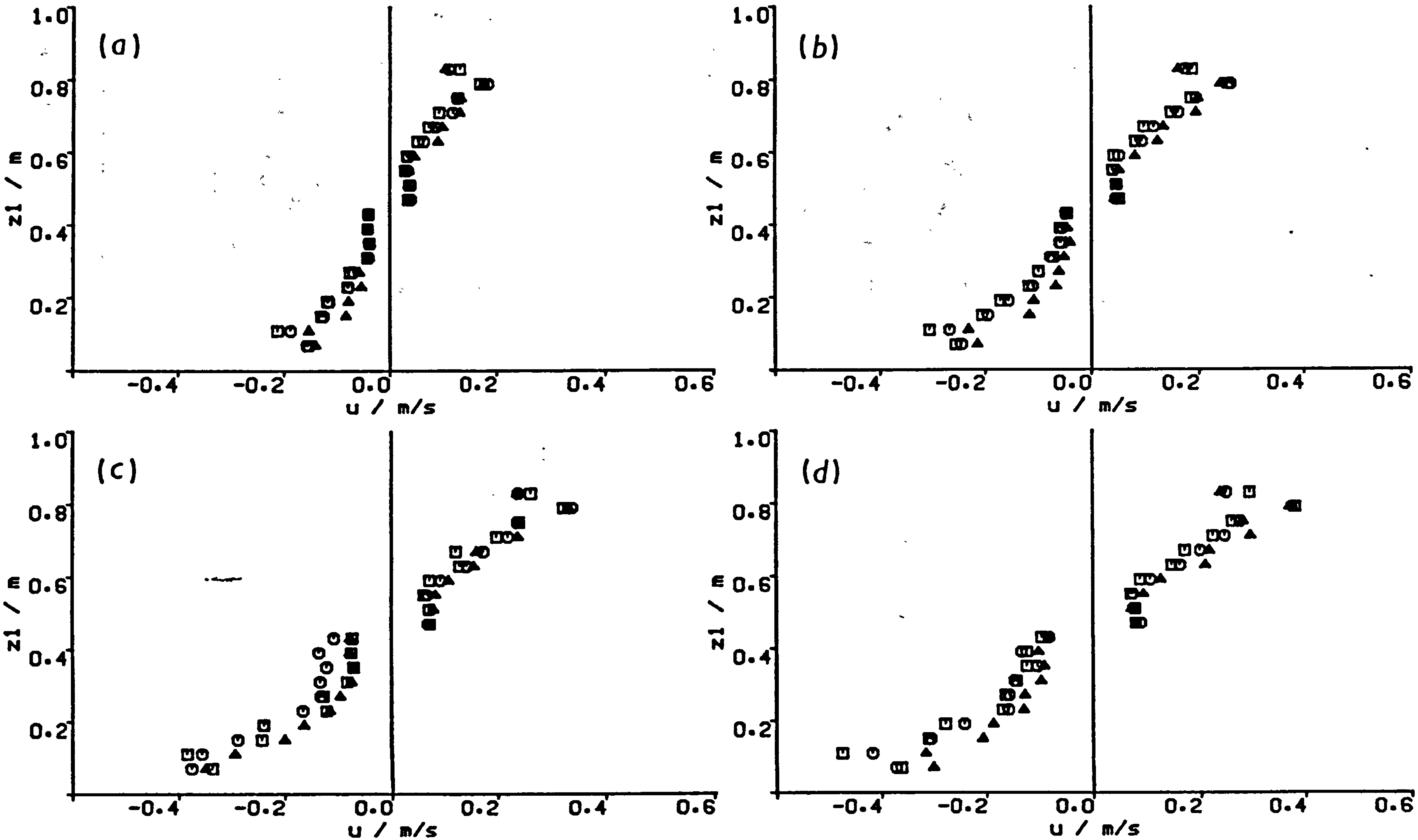

Figure 3.13. Velocity distributions for various heat input rates, at various distances from the side wall
(open stairwell case):
(a) 100 W ; (b) 300 W ; (c) 600 W ; (d) 900 W.
o w/2 ; □ w/3 ; Δ w/6.

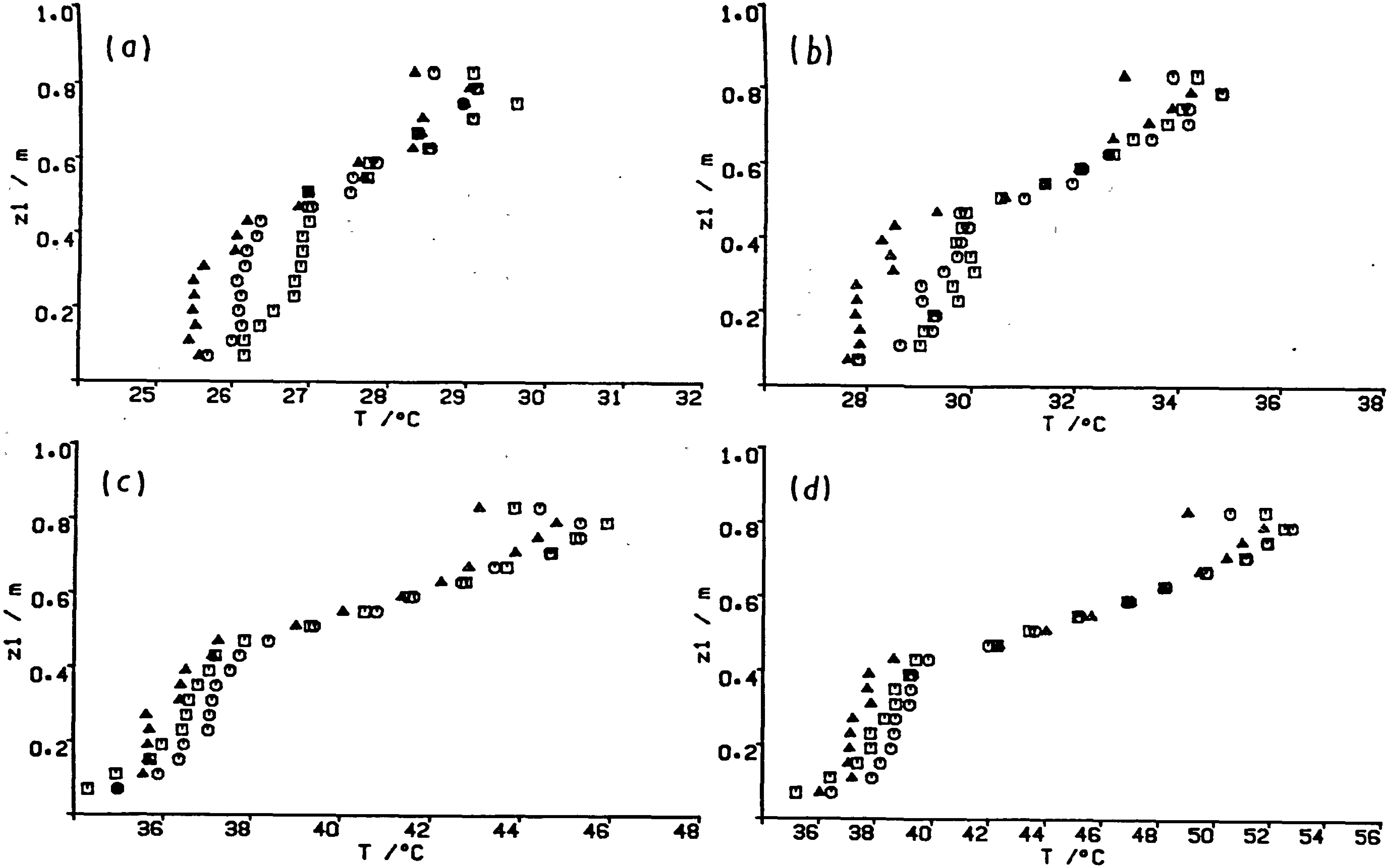

Figure 3.14. Temperature profiles for various heat input rates, at various distances from the side wall (open stairwell case) :
(a) 100 W ; (b) 300 W ; (c) 600 W ; (d) 900 W.
o w/2 ; □ w/3 ; Δ w/6.

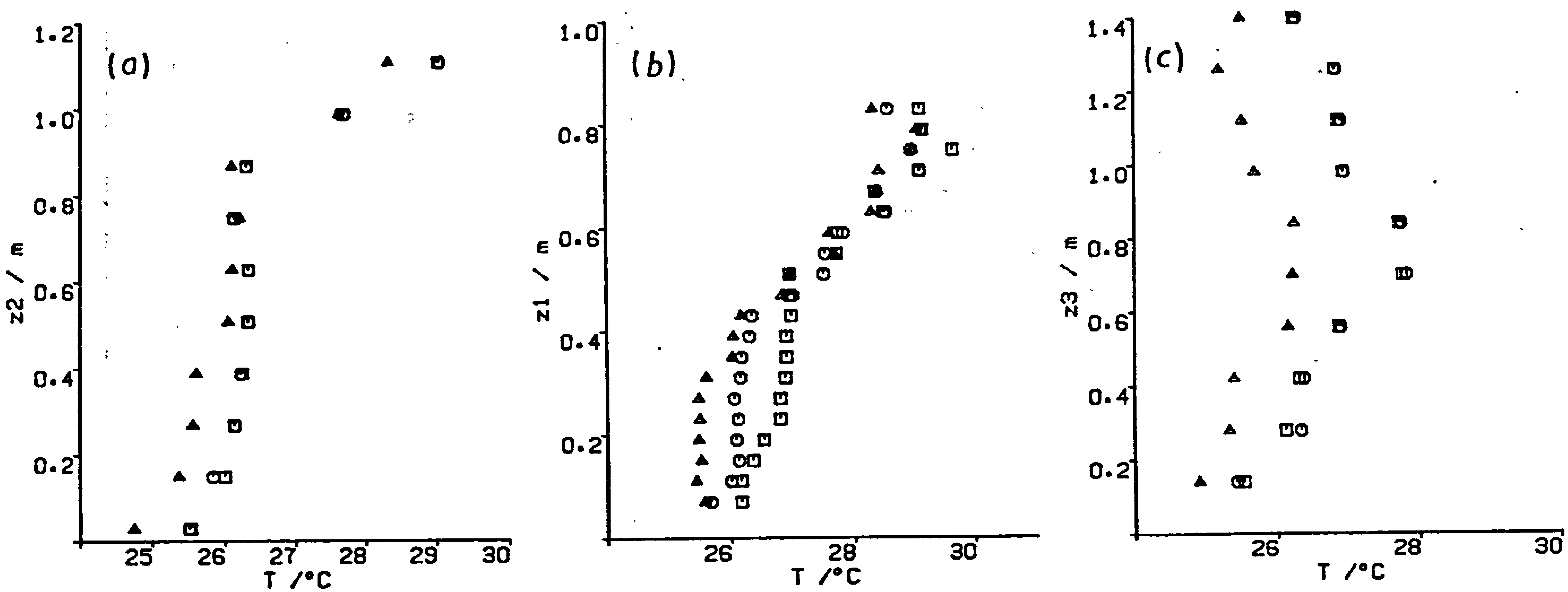

Figure 3.15. Temperature profiles at various distances from the stairwell side wall, at cross-sections DD', AA' and EE' for open stairwell case.
(Heat input rate = 100 W) :
o w/2 ; □ w/3 ; Δ w/6.
(a) DD' ; (b) AA' ; (c) EE'.

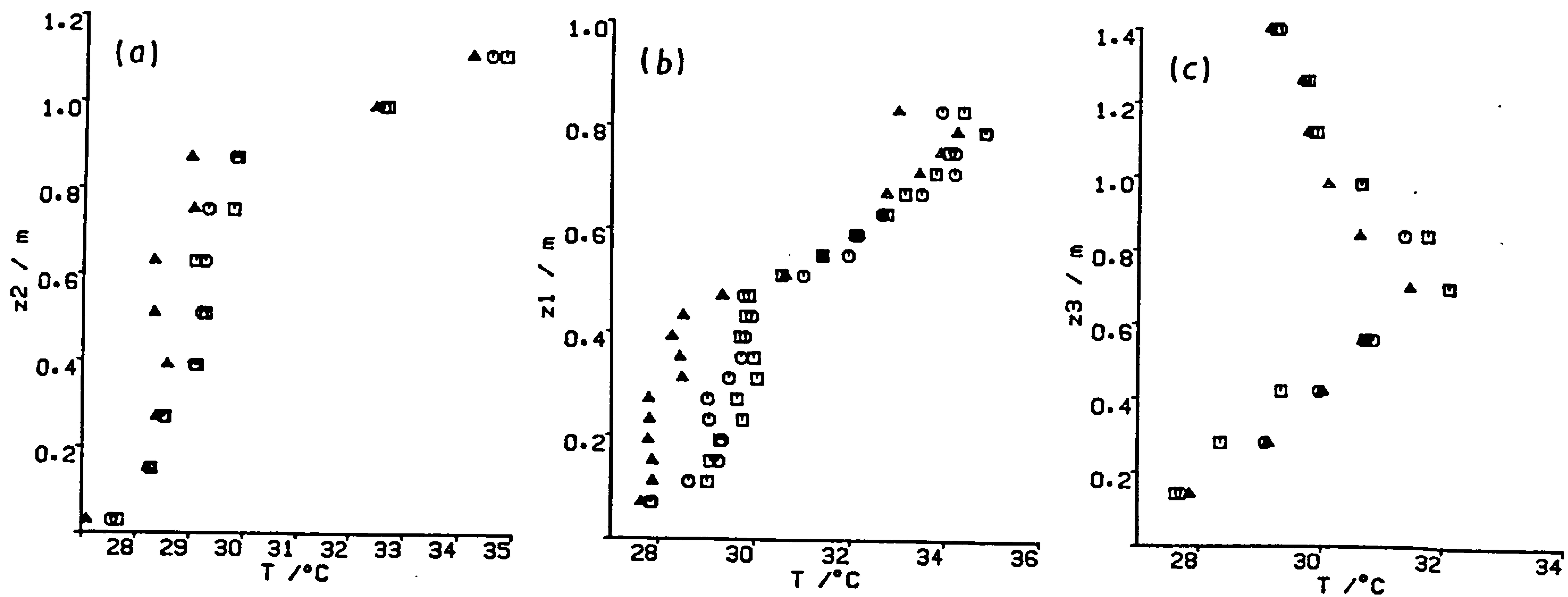

Figure 3.16. Temperature profiles at various distances from the stairwell side wall, at cross-sections DD', AA' and EE' for open stairwell case.
(Heat input rate = 300 W) :
○ w/2 ; □ w/3 ; Δ w/6.
(a) DD' ; (b) AA' ; (c) EE'.

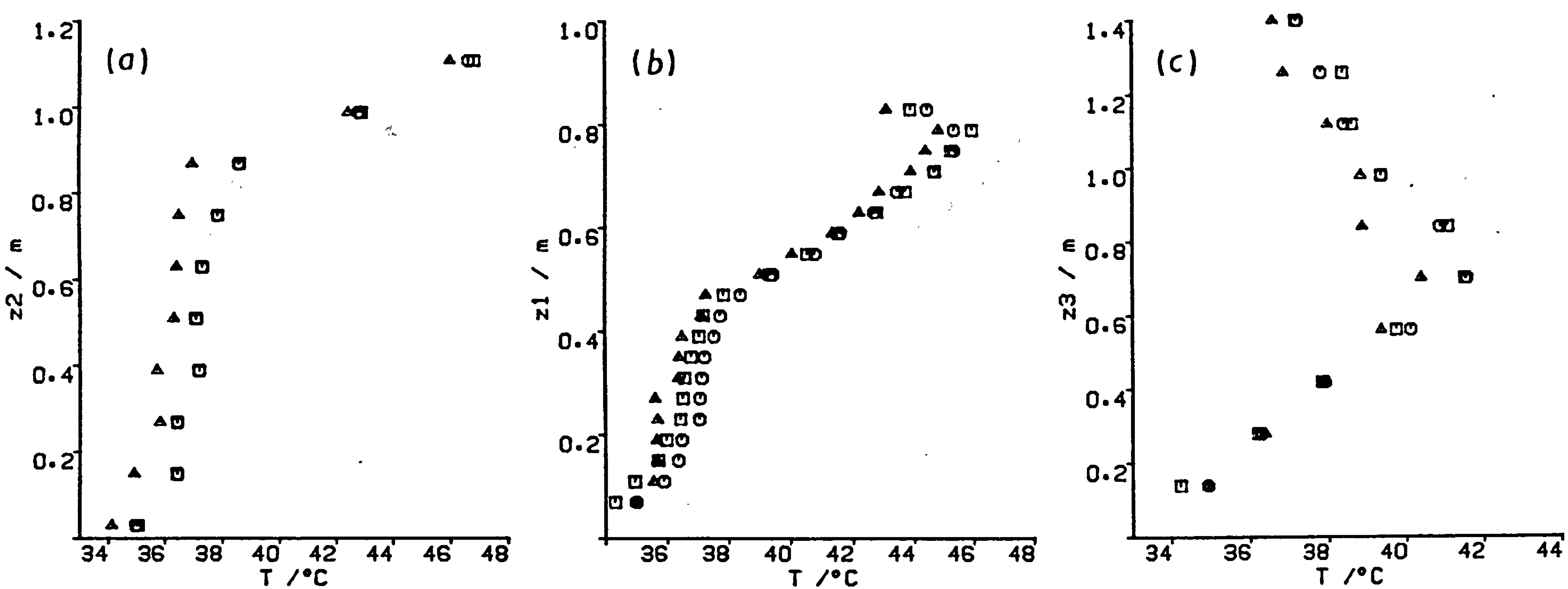

Figure 3.17. Temperature profiles at various distances from the stairwell side wall, at cross-sections DD', AA' and EE' for open stairwell case.
(Heat input rate = 600 W):
o w/2 ; □ w/3 ; Δ w/6.
(a) DD' ; (b) AA' ; (c) EE'.

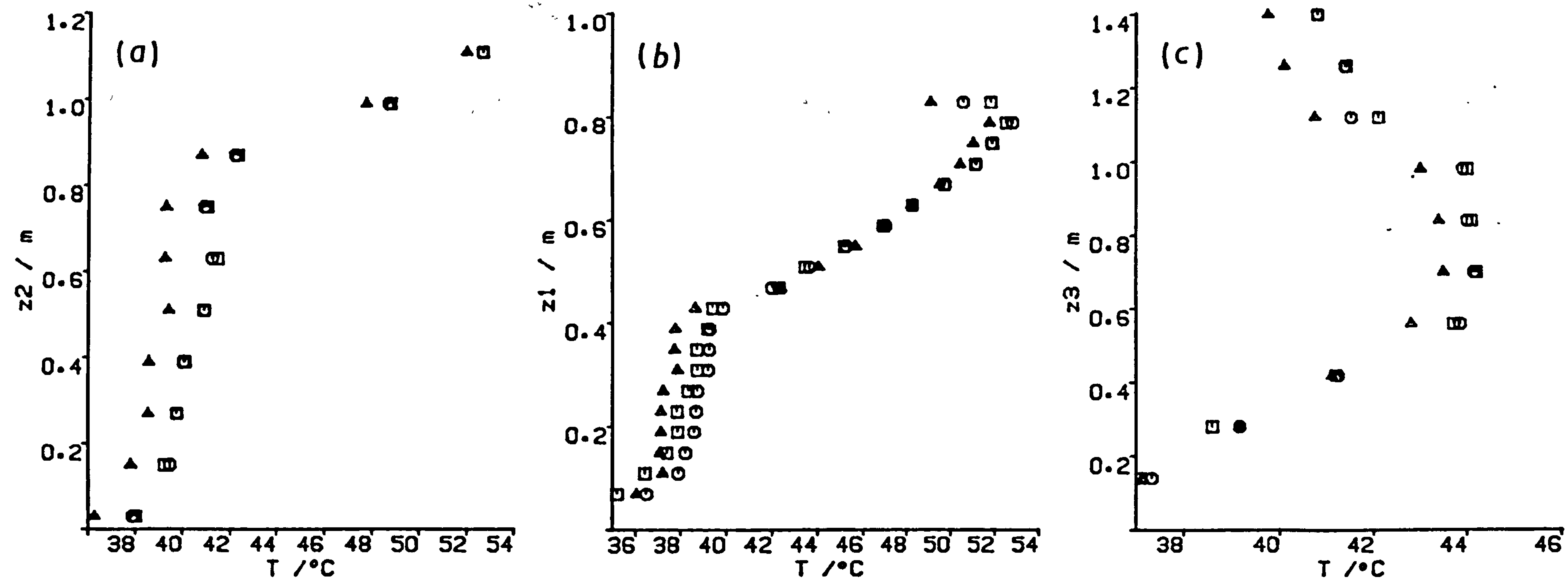

Figure 3.18. Temperature profiles at various distances from the stairwell side wall, at cross-sections DD', AA' and EE' for open stairwell case.
(Heat input rate = 900 W):
O w/2 ; □ w/3 ; Δ w/6.
(a) DD' ; (b) AA' ; (c) EE'.

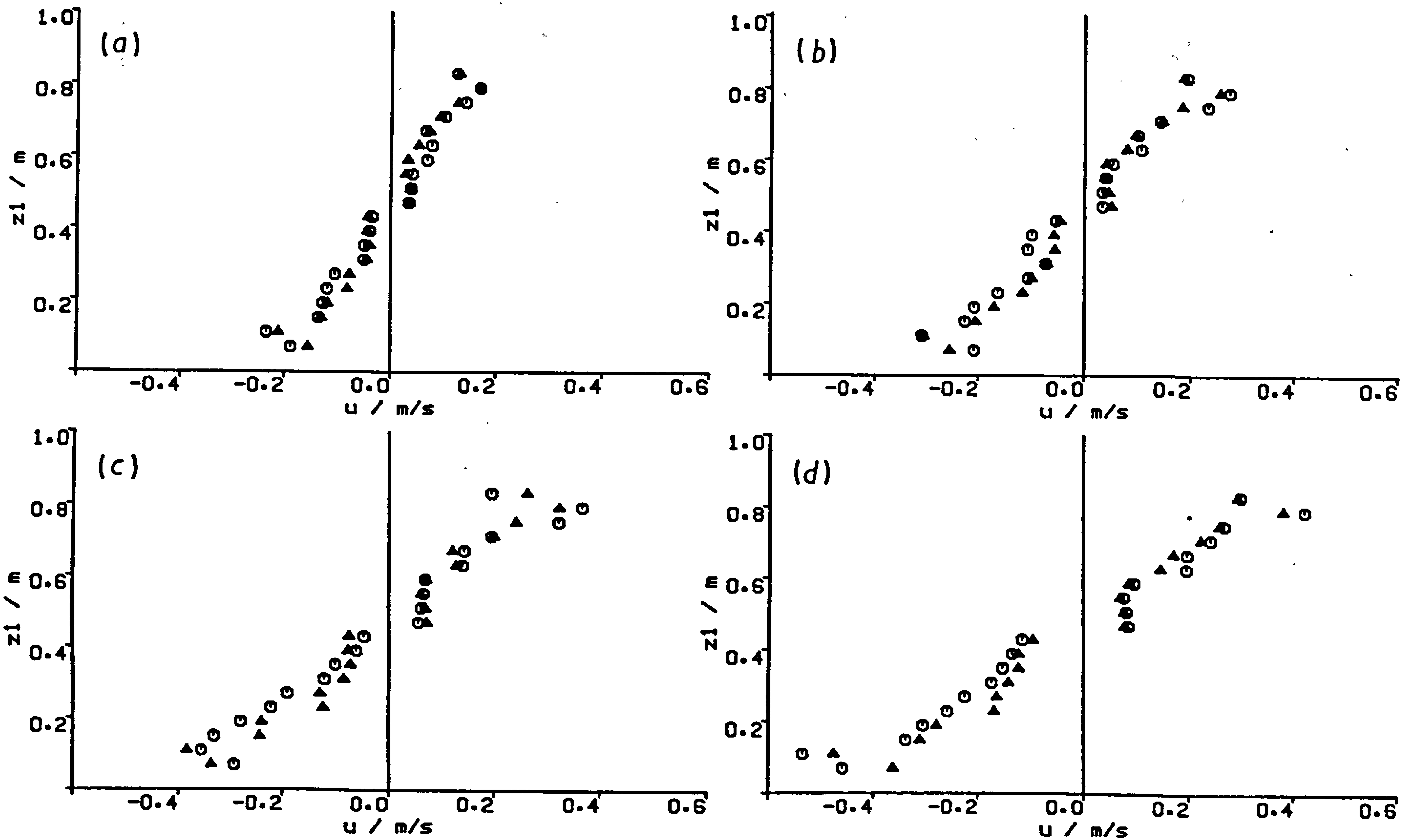

Figure 3.19. Comparison between the velocity profiles for open and closed stairwell case (at one-half width of the stairwell) :
(a) 100 W ; (b) 300 W; (c) 600 W ; (d) 900 W.
Δ open stairwell ; o closed stairwell.

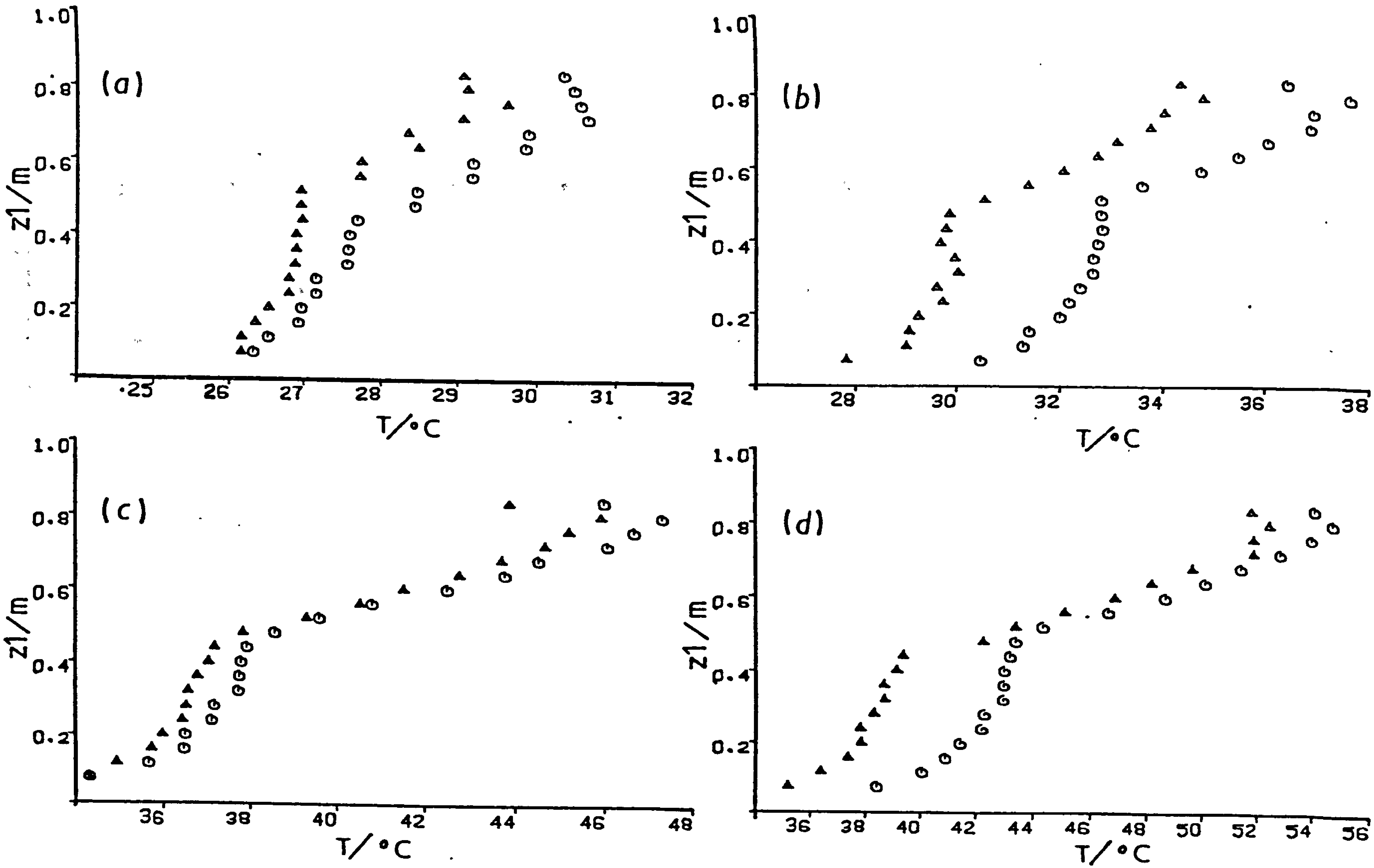

Figure 3.20. Comparison between the temperature profiles for open and closed stairwell cases (at one-half width of the stairwell):
(a) 100 W ; (b) 300 W ; (c) 600 W ; (d) 900 W.
Δ open stairwell ; O closed stairwell.

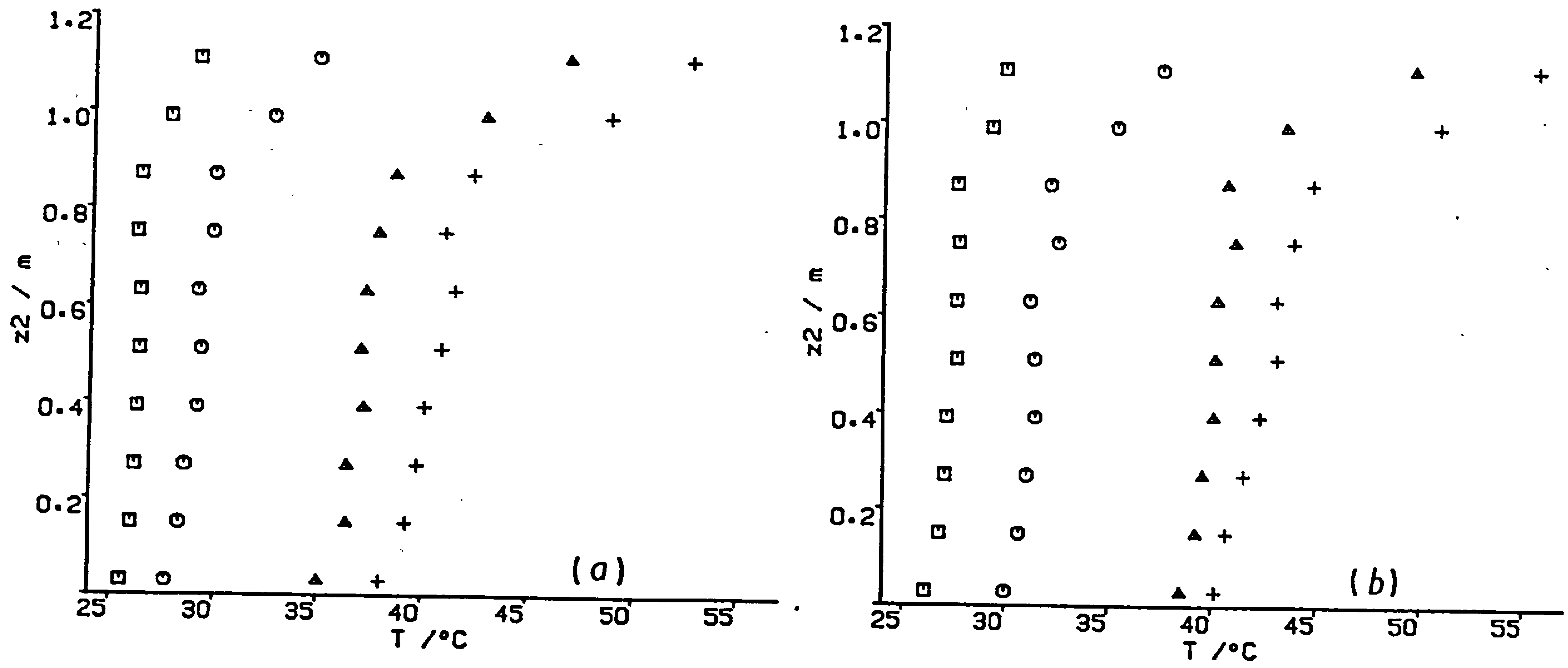

Figure 3.21. Temperature profiles for various heat input rates, at cross sections DD' and at one-half width of the stairwell model(as shown in Figure 2.2):
(a) closed stairwell case
(b) open stairwell case
□ 100 W ; O 300 W ; Δ 600 W ; + 900 W.

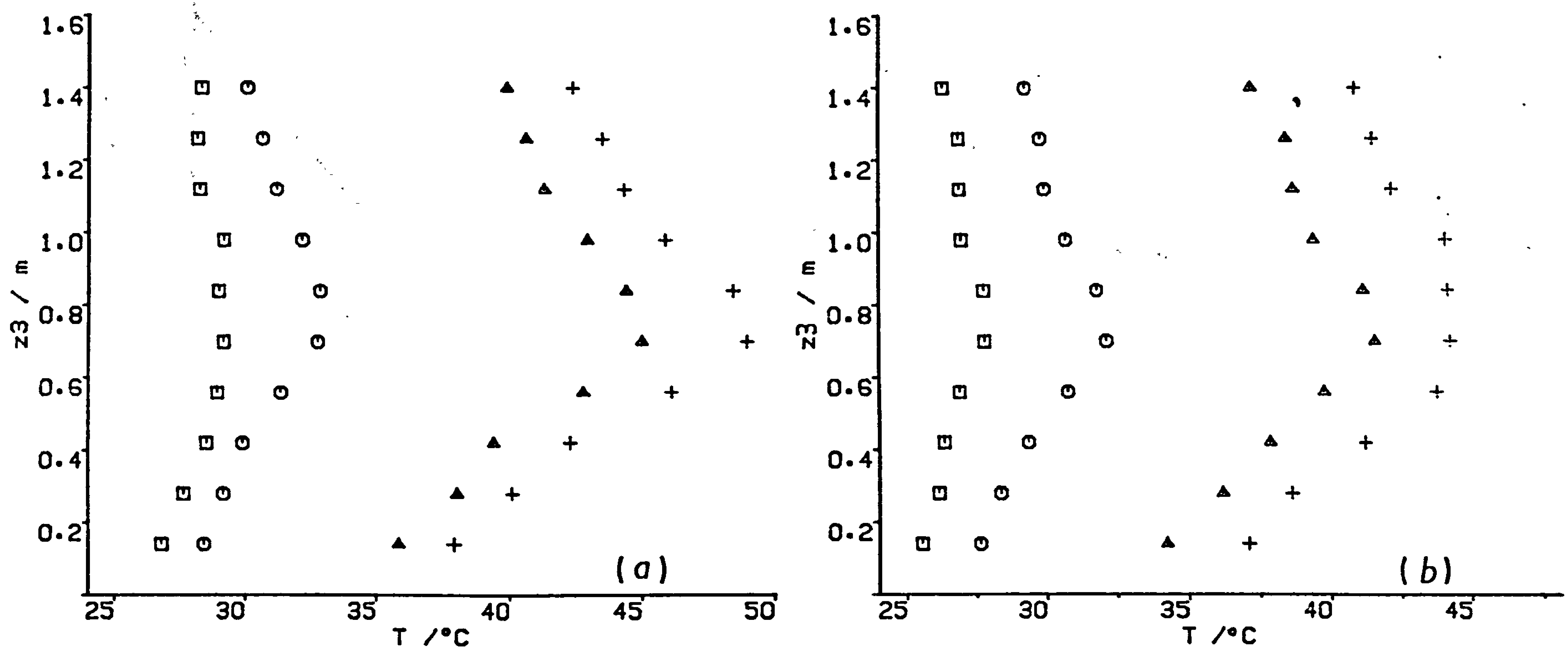

Figure 3.22. Temperature profiles for various heat input rates, at cross-sections EE' and at one-half width of the stairwell (as shown in Figure 2.2):
(a) closed stairwell case
(b) open stairwell case
□ 100 W ; O 300 W ; Δ 600 W ; + 900 W.

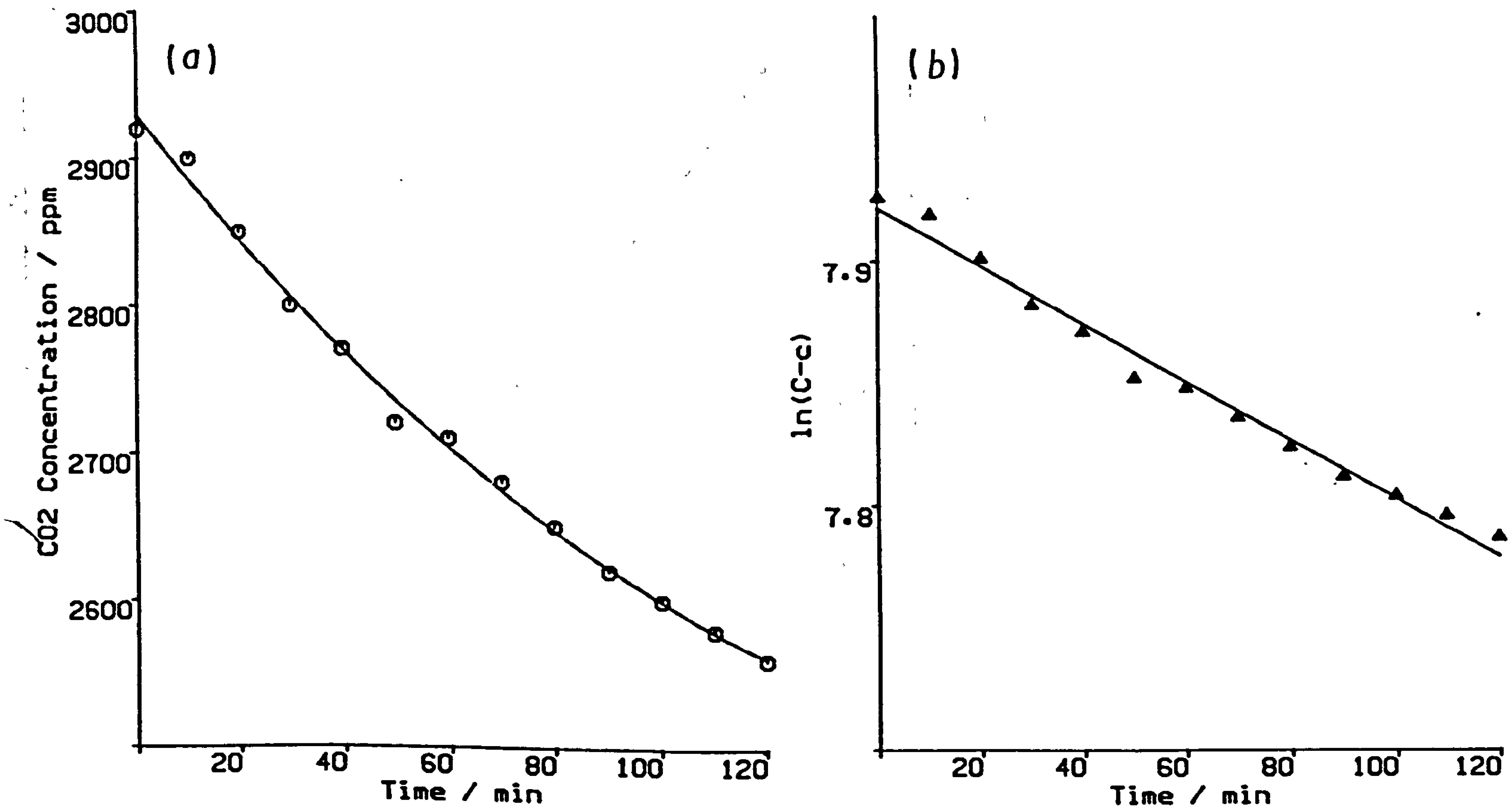

Figure 3.23. Typical curve of CO_2 tracer gas concentration against time.
(Heat input rate = 100 W).

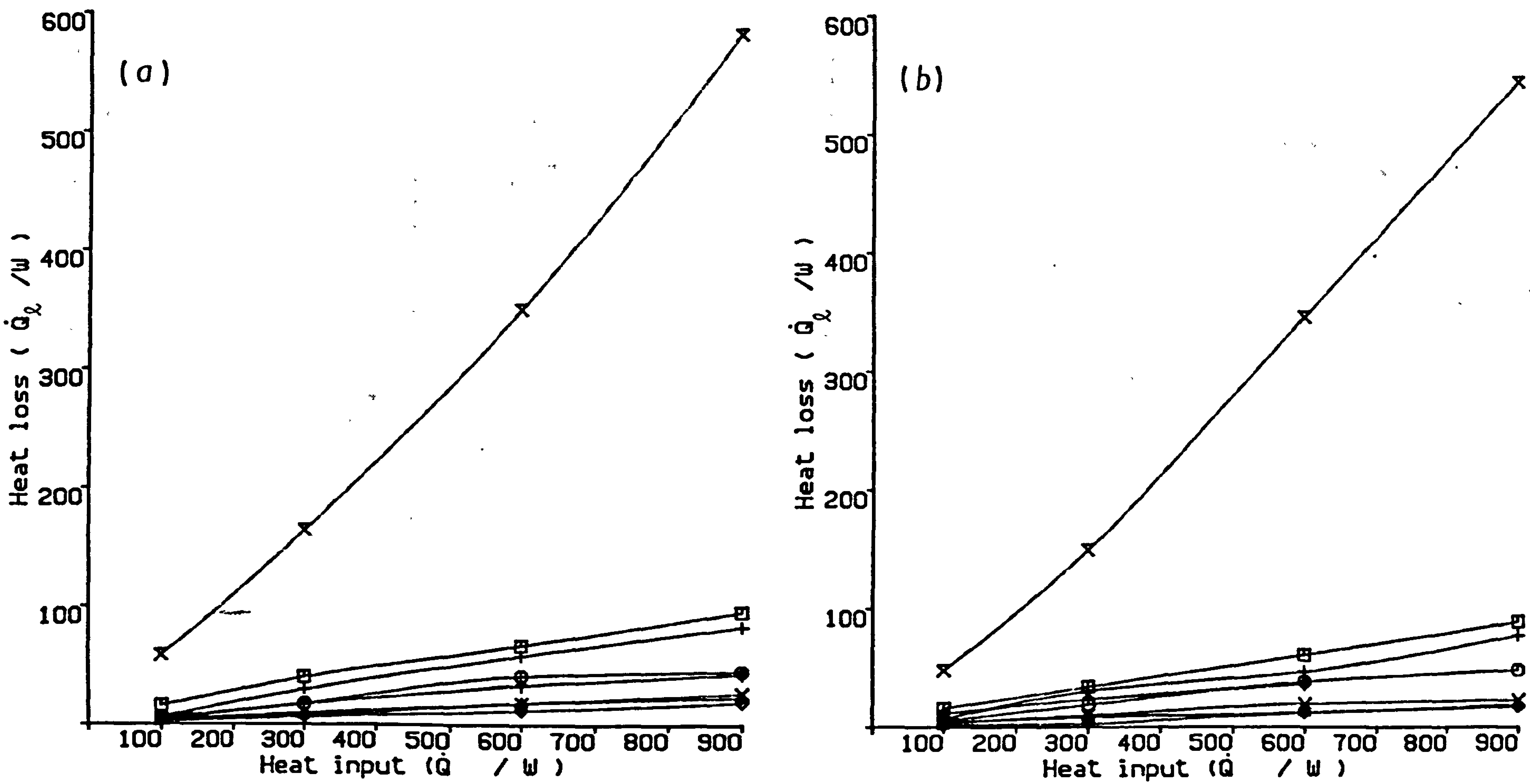

Figure 3.24. Rate of heat loss from the stairwell at various heat input rates. (See Figure 5.2 for corresponding walls):
(a) closed stairwell case
(b) open stairwell case.
□ wall AC ; O wall CD ; Δ wall DE ;
+ wall EF ; X wall FG ; ◇ wall GH ;
↑ wall HI+IA ; X side walls.

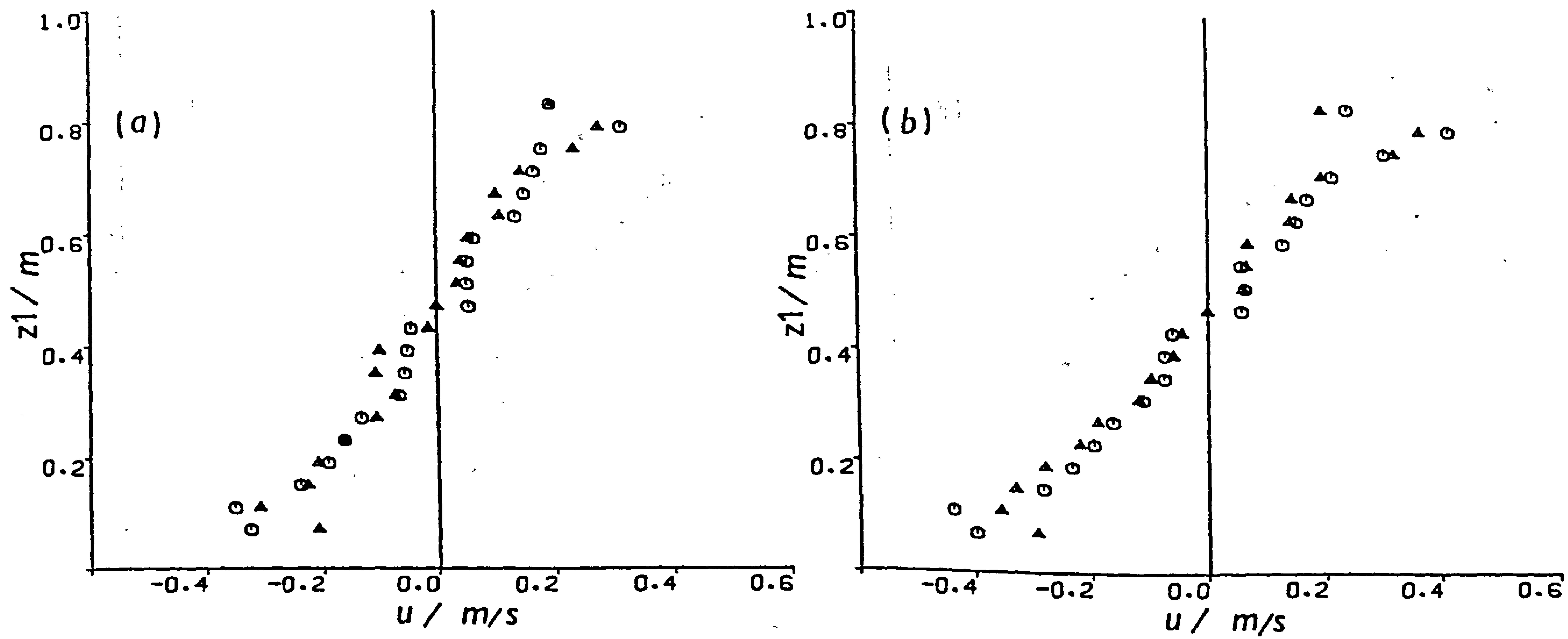

Figure 3.25. Effect of heat transfer rate through the side walls, on velocity profiles at the throat area (closed stairwell case):
(a) 300 W ; (b) 600 W.
o insulated side walls
Δ not insulated side walls.

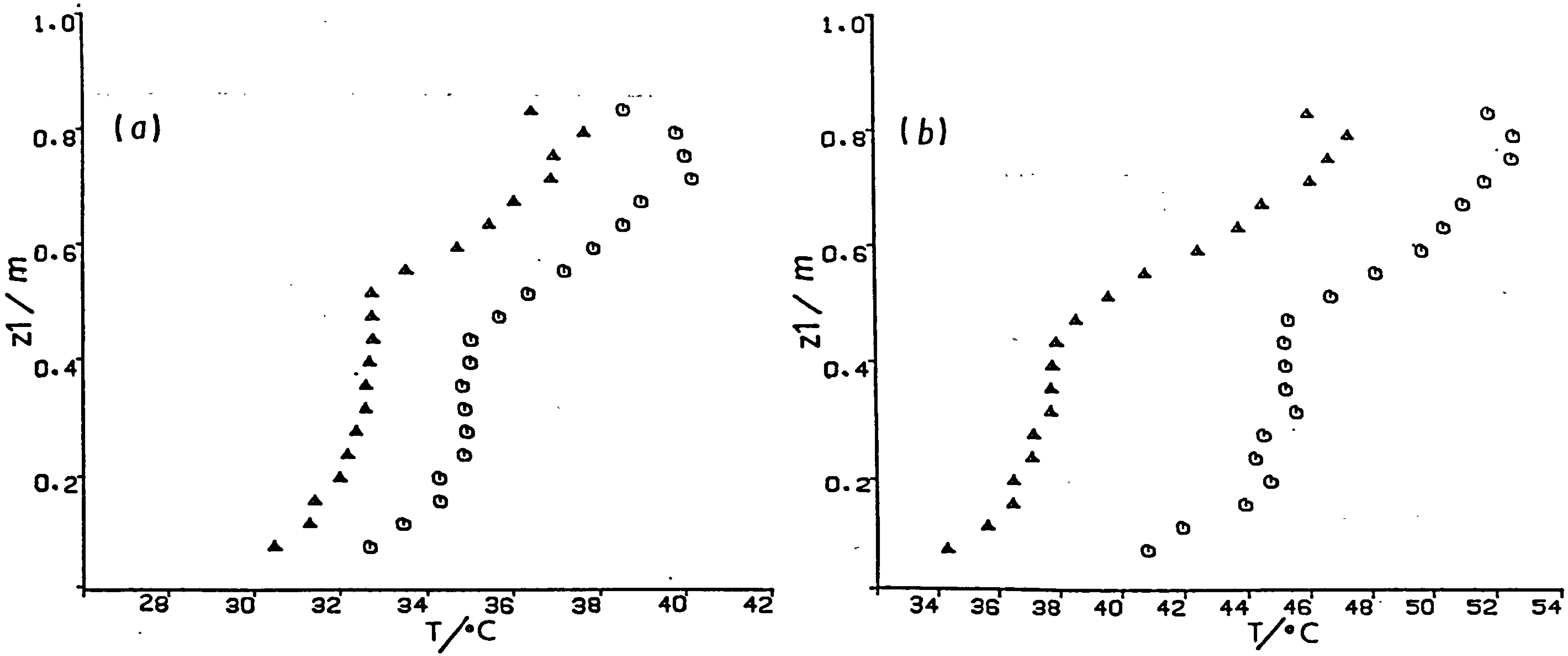

Figure 3.26. Effect of heat transfer rate through the side walls, on temperature profiles at the throat area (closed stairwell case):
(a) 300 W ; (b) 600 W.
o insulated side walls.
Δ not insulated side walls.

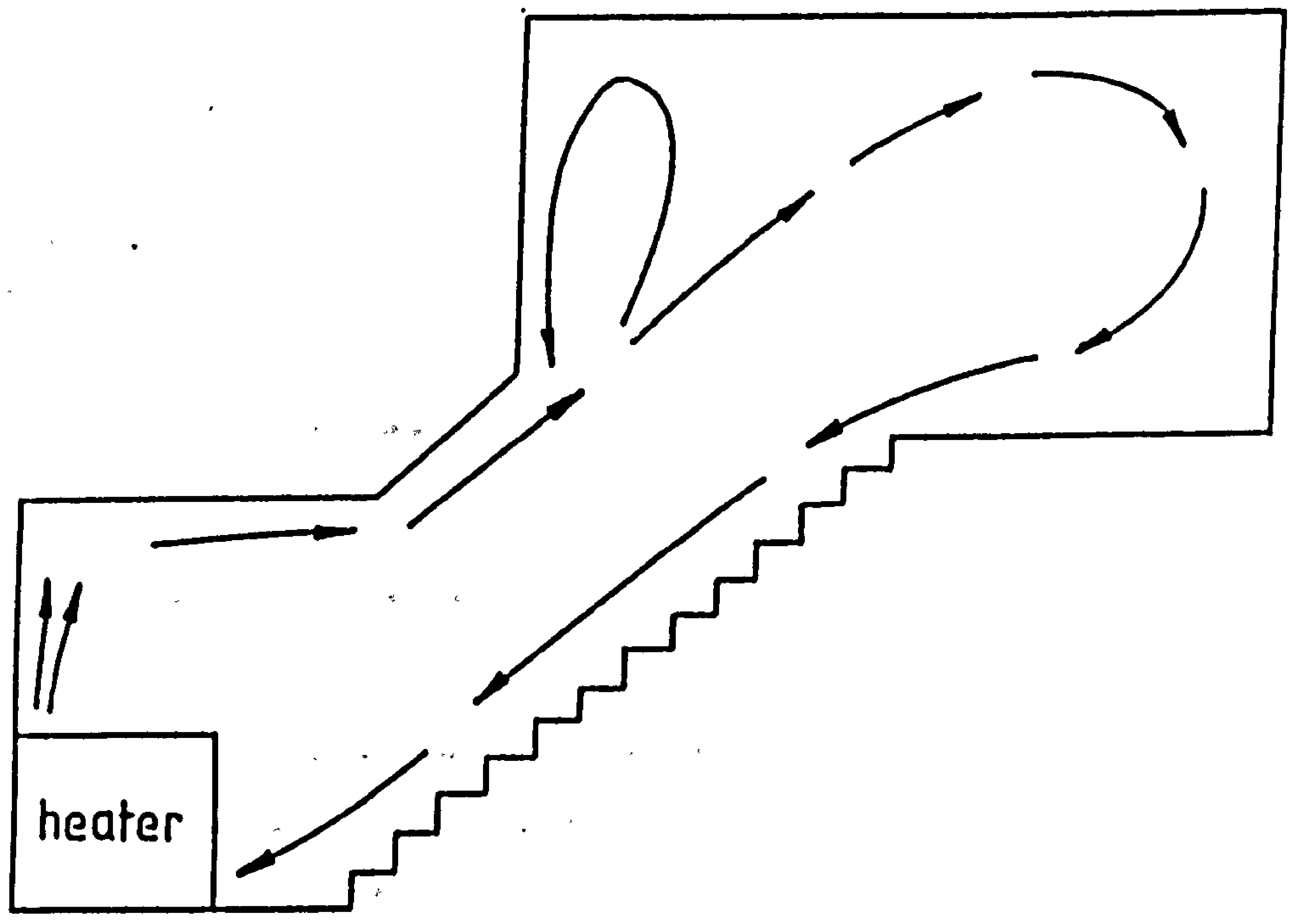

Figure 4.1. A two-dimensional view of the flow pattern in the sloping-ceiling geometry.

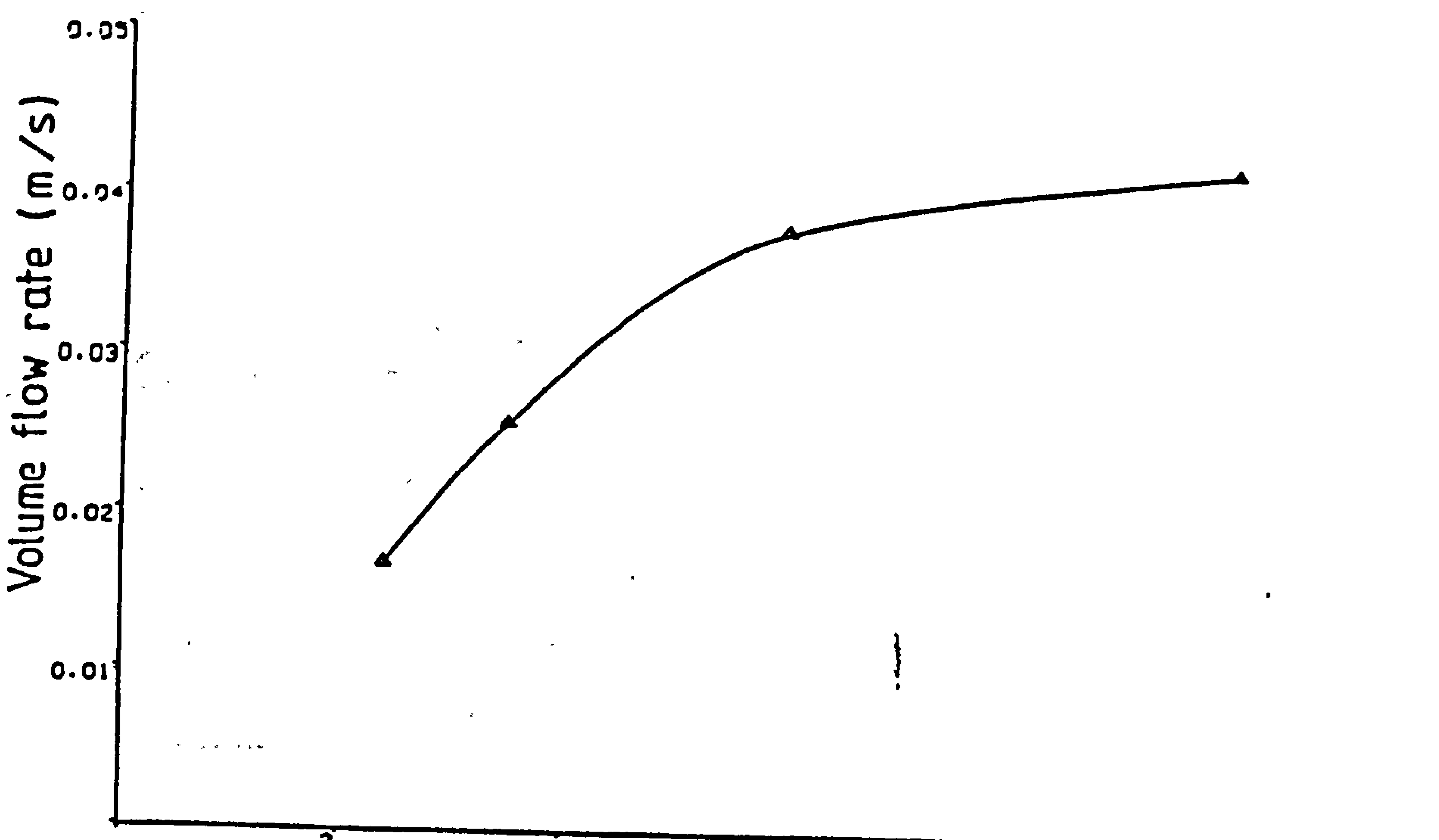

Figure 4.2. Volume flow rate versus differential temperature, DT (open stairwell case).

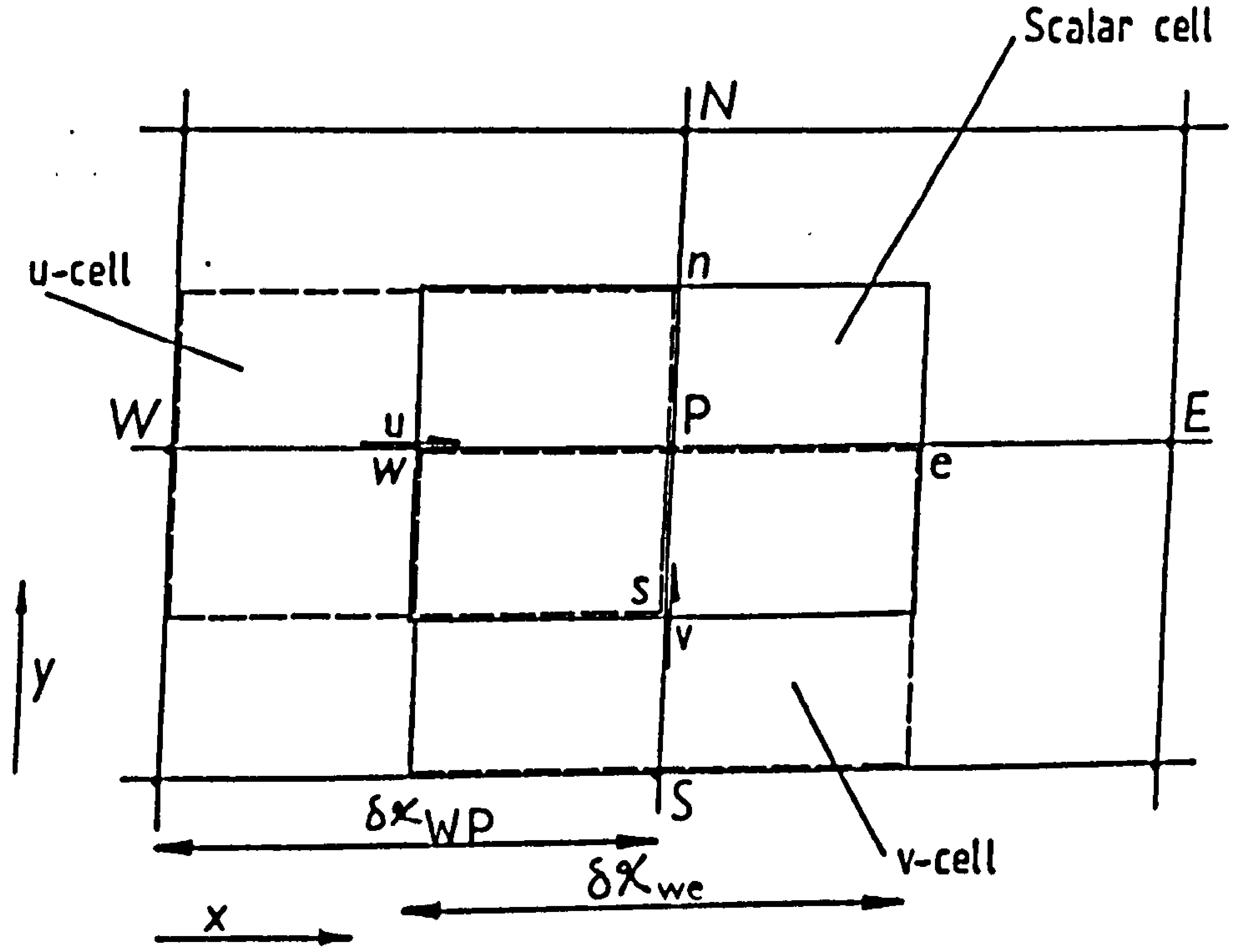

Figure 5.1. Control volumes of the staggered-grid system.

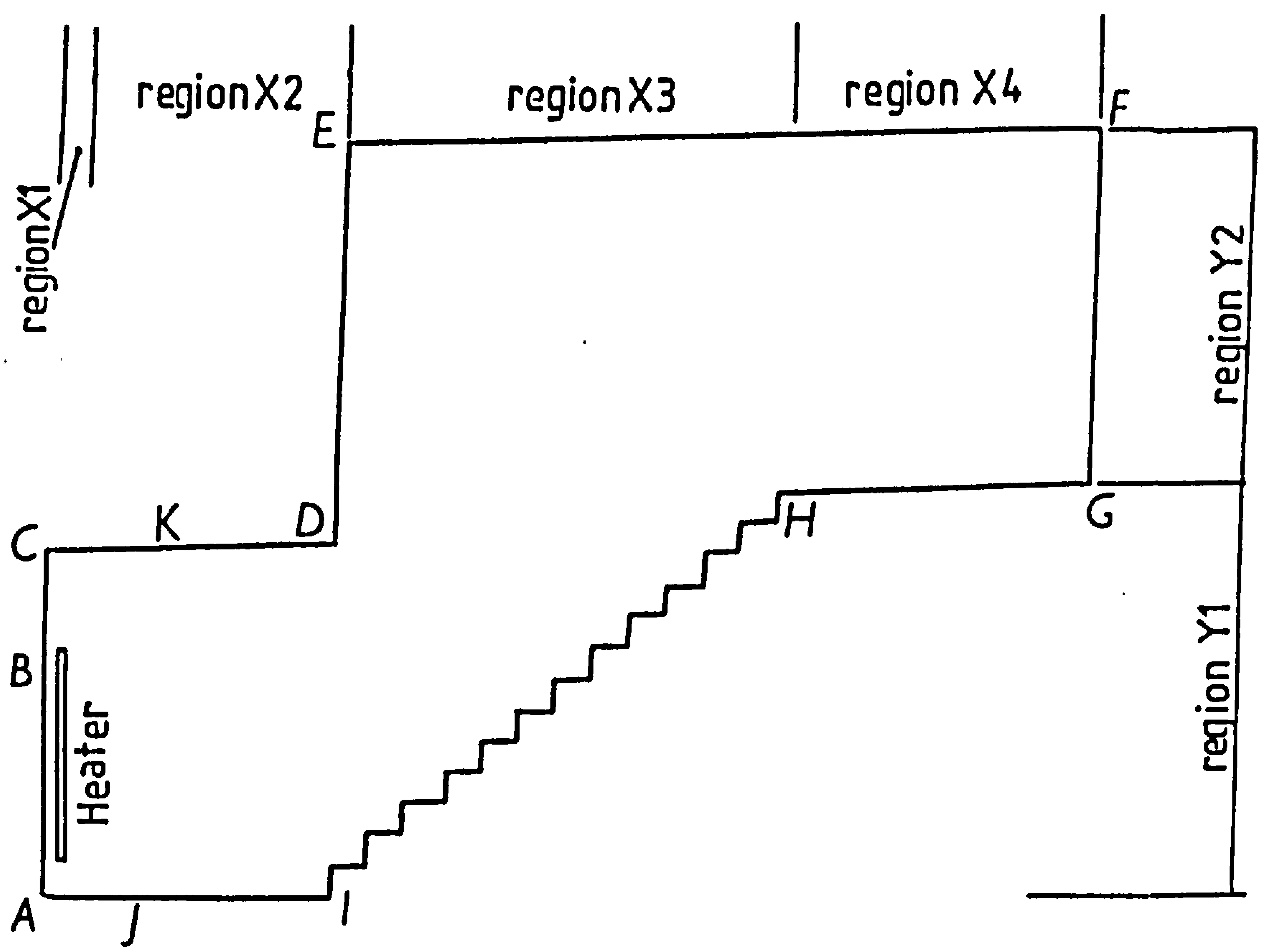

Figure 5.2. Definition of various walls and regions in the stairwell.

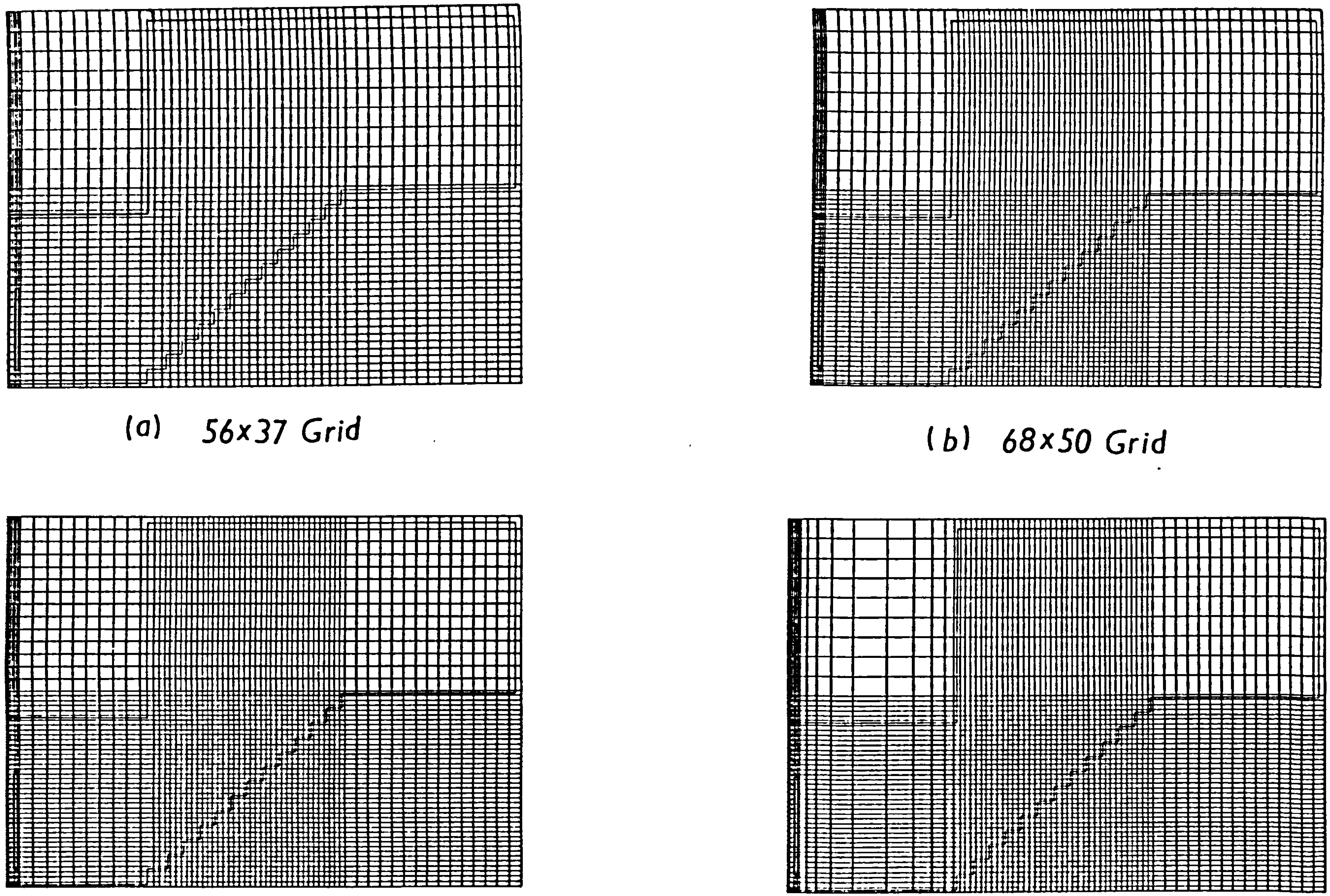

(a) 56x37 Grid

(b) 68x50 Grid

(c) 68x55 Grid

(d) 68x50 Grid

Figure 5.3. Illustration of the various computational grids.

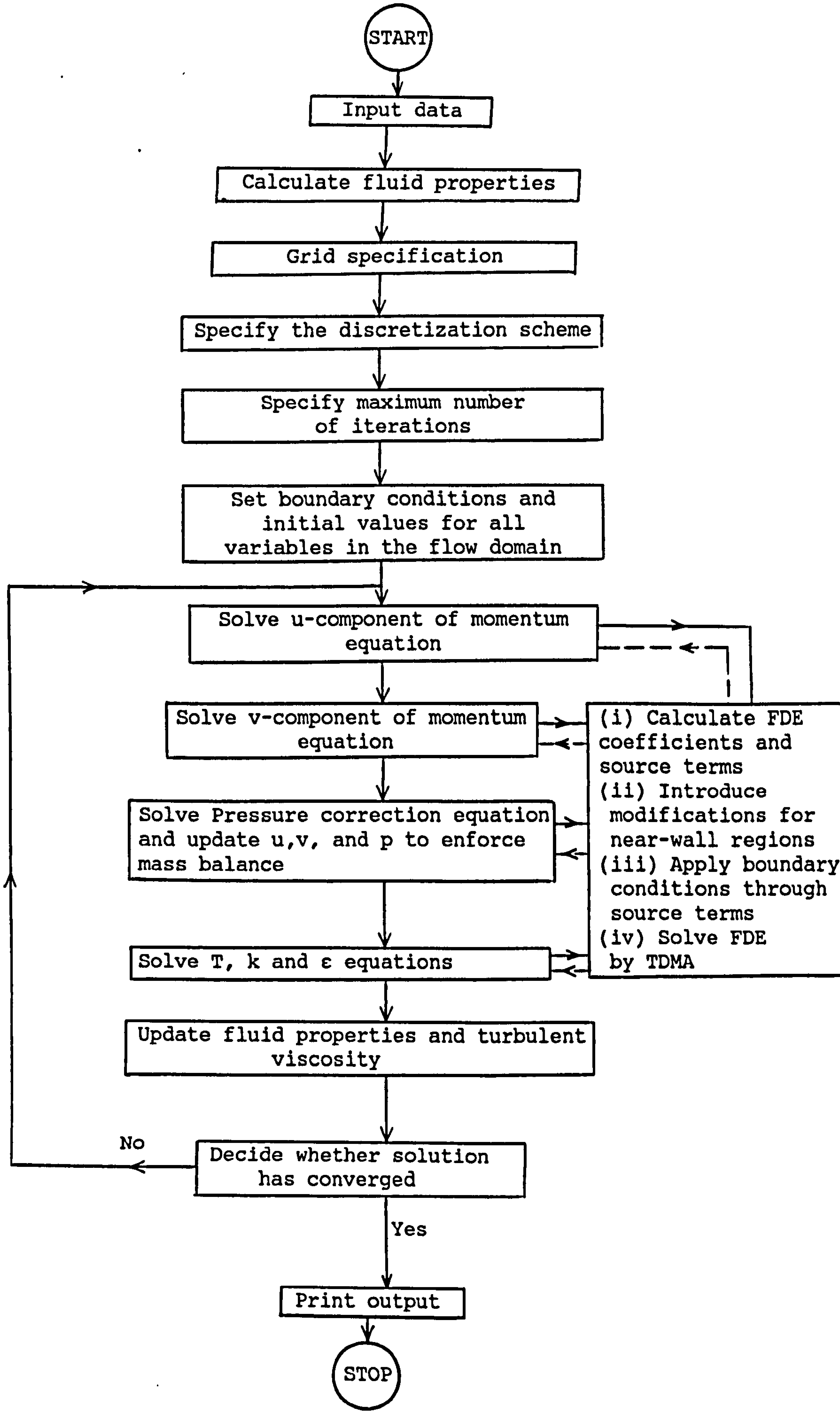

Figure 5.4. Flow-chart of 2D solution sequence.

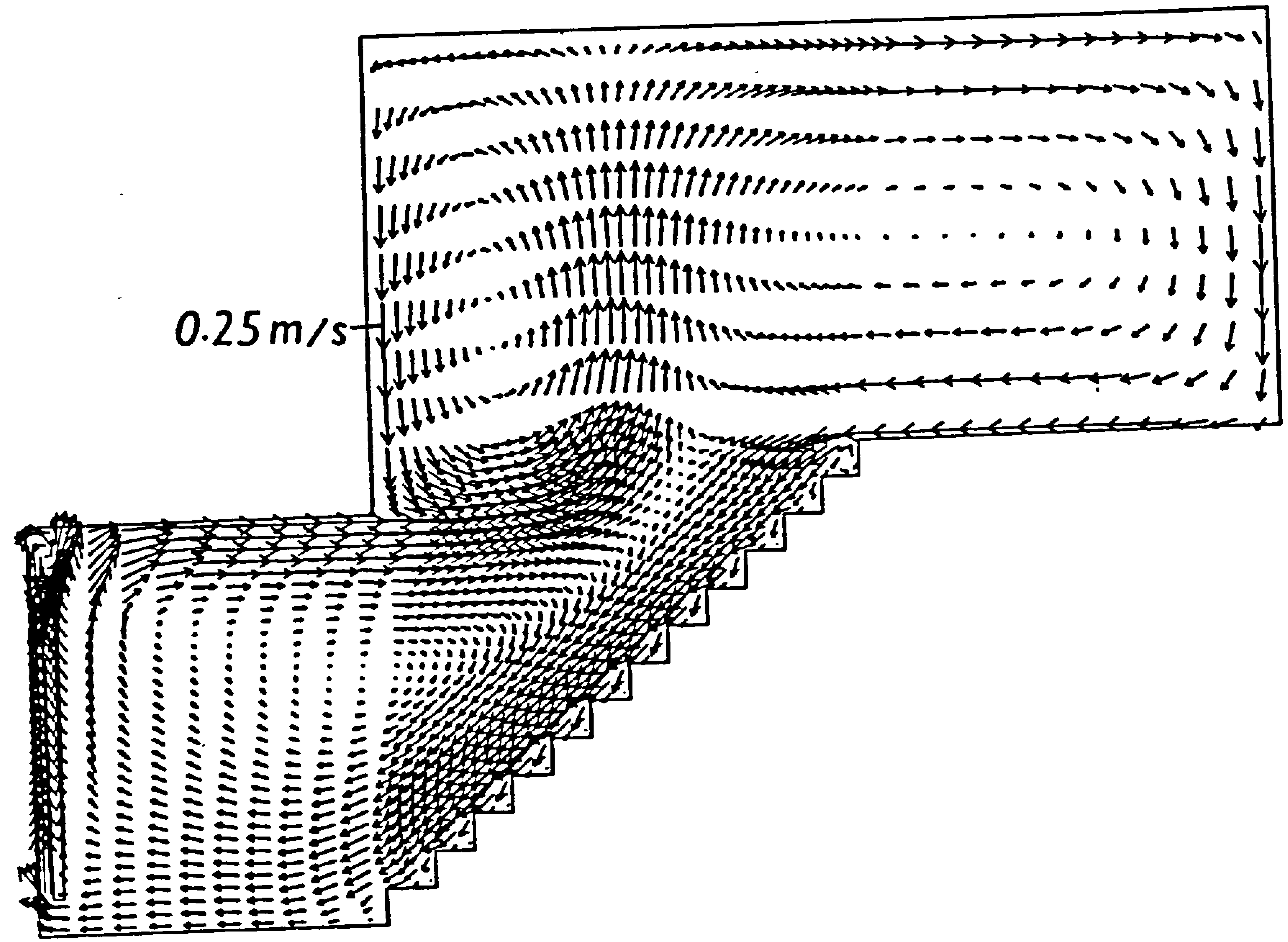

Figure 5.5. Vector plot of the predicted flow field. (300 W heat input rate).

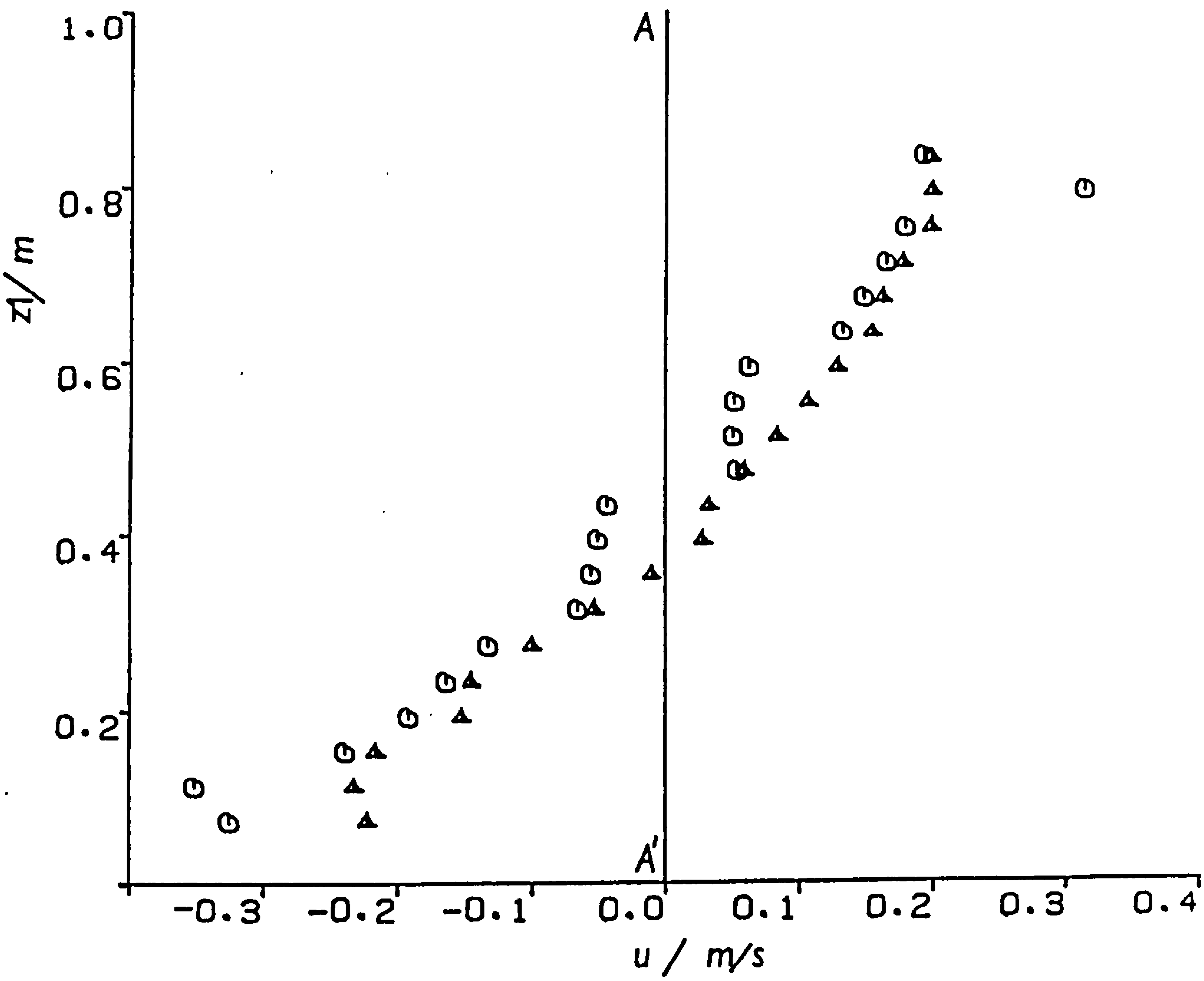

Figure 5.6. Predicted and measured profiles of the component of the velocity (perpendicular to AA') at the throat area. (Heat input rate = 300 W) :
Δ prediction; o experiment.

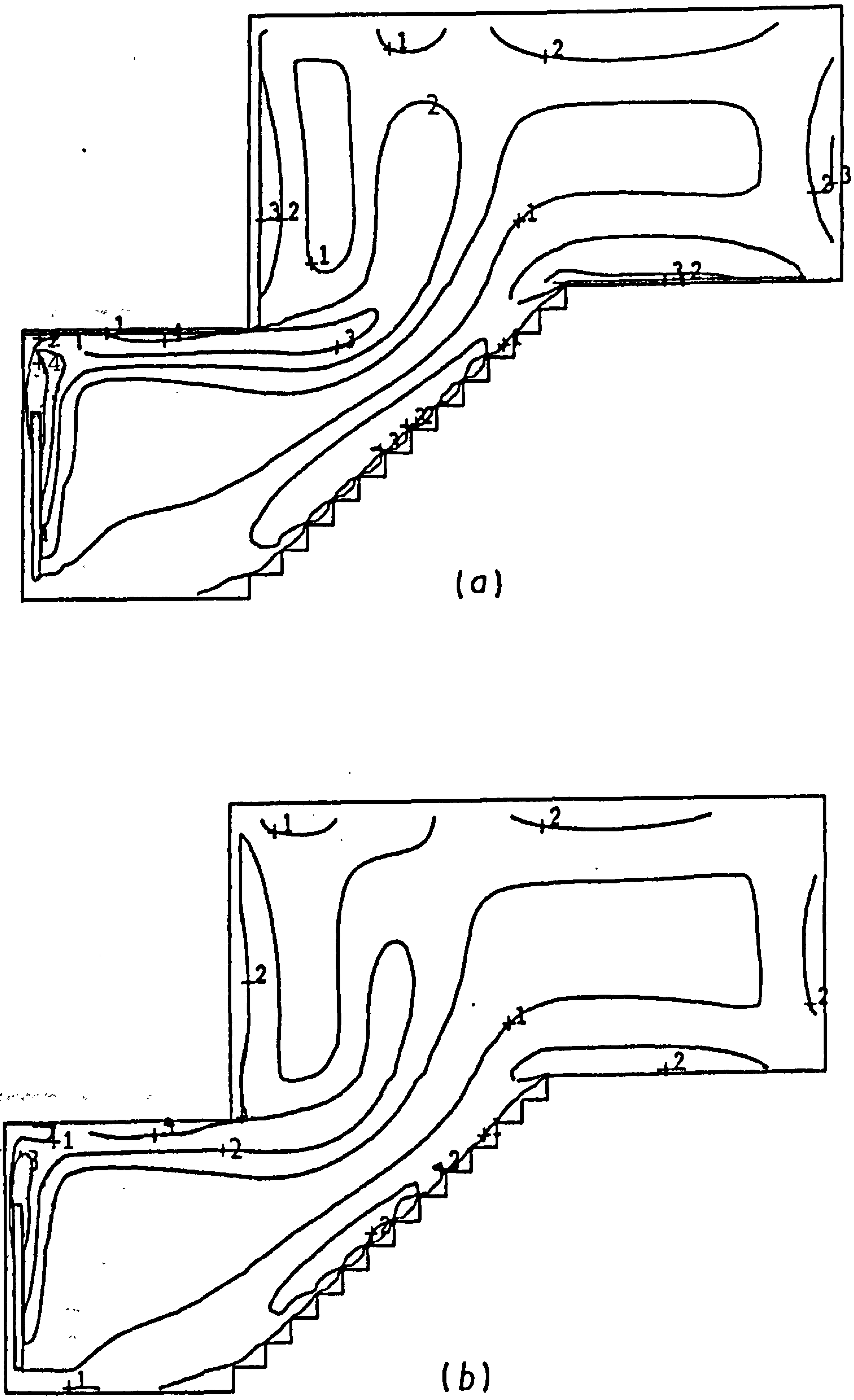

Figure 5.7. Contour plot of the predicted velocity (10^{-1} ms^{-1}):
(a) 600 W heat input rate
(b) 300 W heat input rate

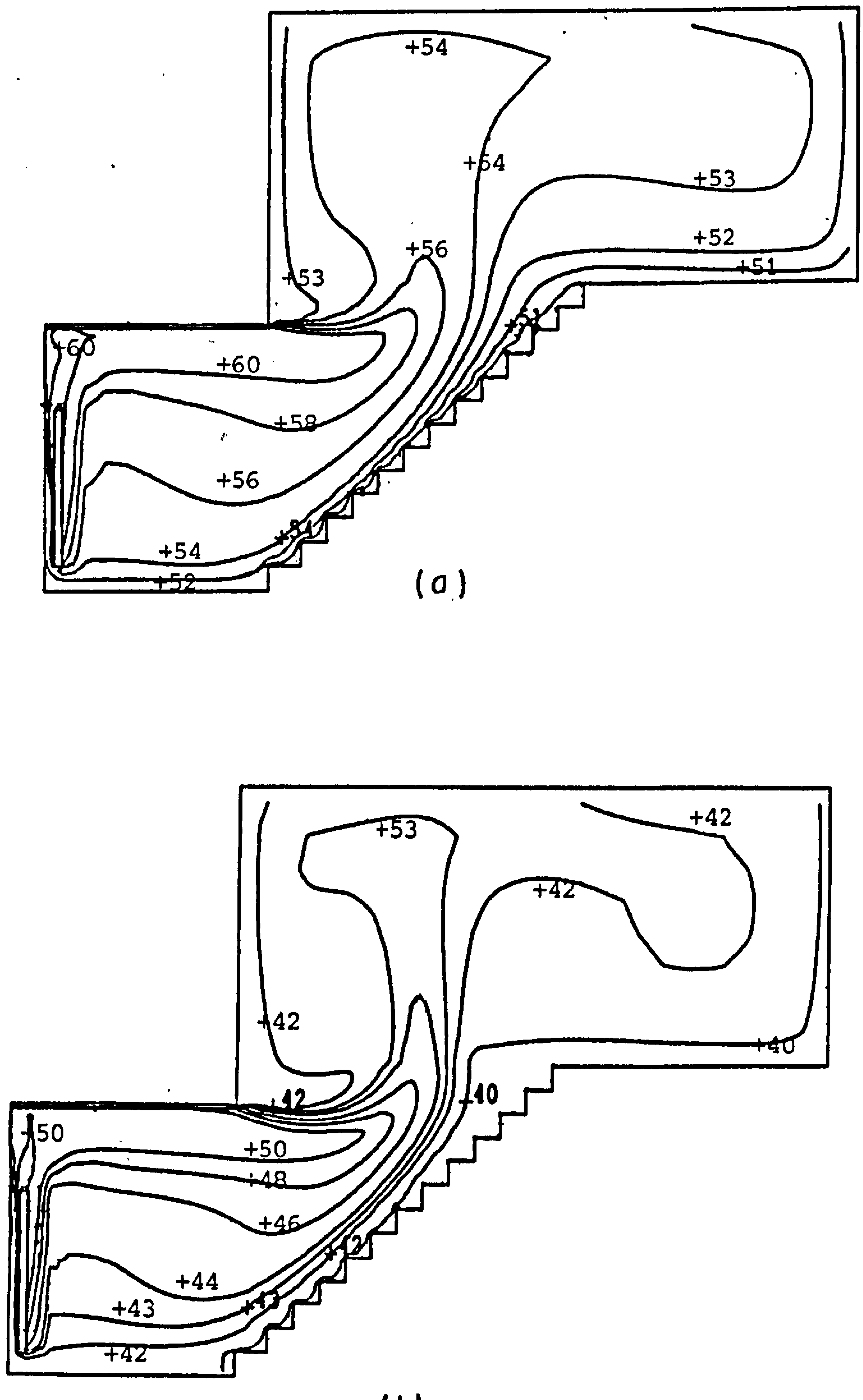

Figure 5.8. Contour plot of the predicted temperature field (^{o}C):
(a) 300 W heat input rate ($f_\varepsilon = 1.0$)
(b) 300 W heat input rate ($f_\varepsilon = 0.05$).

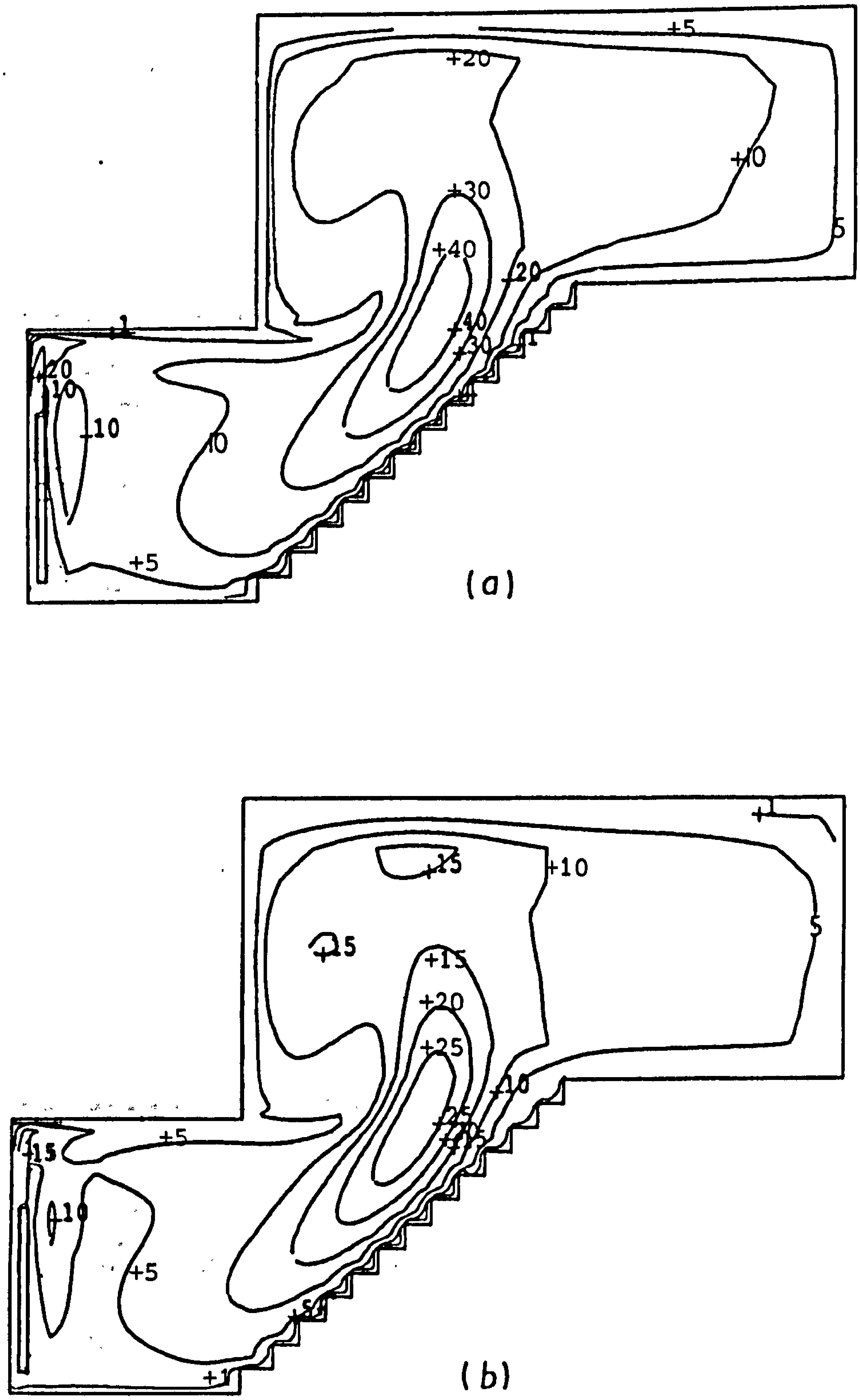

Figure 5.9. Contour plot of the predicted turbulence energy (10^{-3} Nm kg^{-1})
(a) 600 W heat input rate
(b) 300 W heat input rate.

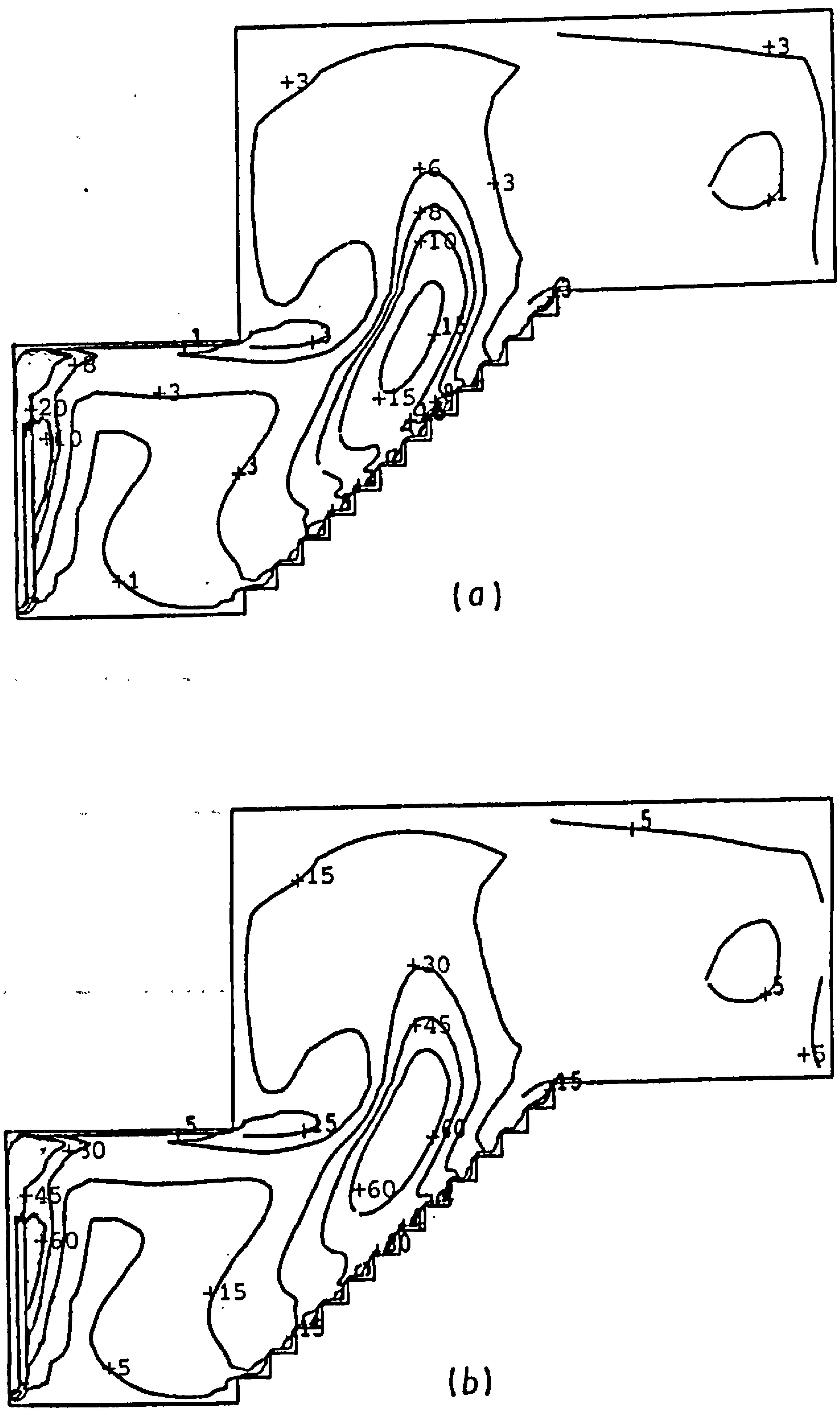

Figure 5.10. Contour plot of the predicted energy dissipation:
(a) 600 W heat input rate (10^{-3} Nm kg^{-1})
(b) 300 W heat input rate (10^{-4} NM kg^{-1})

APPENDIX A: Velocity probe calibration Results

velocity ($m\ s^{-1}$)	probe 212 (volt)	probe 214 (volt)	probe 215 (volt)	probe 216 (volt)	probe 225 (volt)
0.0	0.0	0.0	0.0	0.0	0.0
0.1	0.945	0.676	0.822	0.362	0.430
0.2	1.952	1.740	2.065	1.510	1.457
0.3	3.071	2.889	3.232	2.670	2.624
0.4	4.084	4.092	4.387	3.864	3.799
0.5	5.205	5.233	5.377	5.000	4.962
0.6	6.241	6.203	6.275	6.017	6.163
0.7	7.096	7.094	6.601	7.027	7.170
0.8	7.988	8.022	7.730	8.037	8.159
0.9	9.009	8.949	8.983	9.072	9.245
1.0	-	9.875	10.00	10.12	-

(a)

velocity ($m\ s^{-1}$)	probe 209 (volt)	probe 211 (volt)	probe 258 (volt)	probe 223 (volt)	probe 224 (volt)
0.0	0.0	0.0	0.0	0.0	0.0
0.1	0.643	0.630	0.616	0.464	0.331
0.2	1.768	1.798	1.827	1.562	1.645
0.3	2.859	2.803	2.078	2.844	2.914
0.4	4.093	4.103	4.220	4.093	4.137
0.5	5.231	5.158	5.262	5.258	5.338
0.6	6.249	6.258	6.205	6.275	6.253
0.7	7.157	7.152	7.140	7.202	7.171
0.8	8.069	8.095	7.940	7.949	8.025
0.9	9.016	9.097	9.009	8.913	9.045
1.0	10.04	10.09	-	9.959	10.01

(b)

Table A (a-b) Calibration results for the velocity probes.

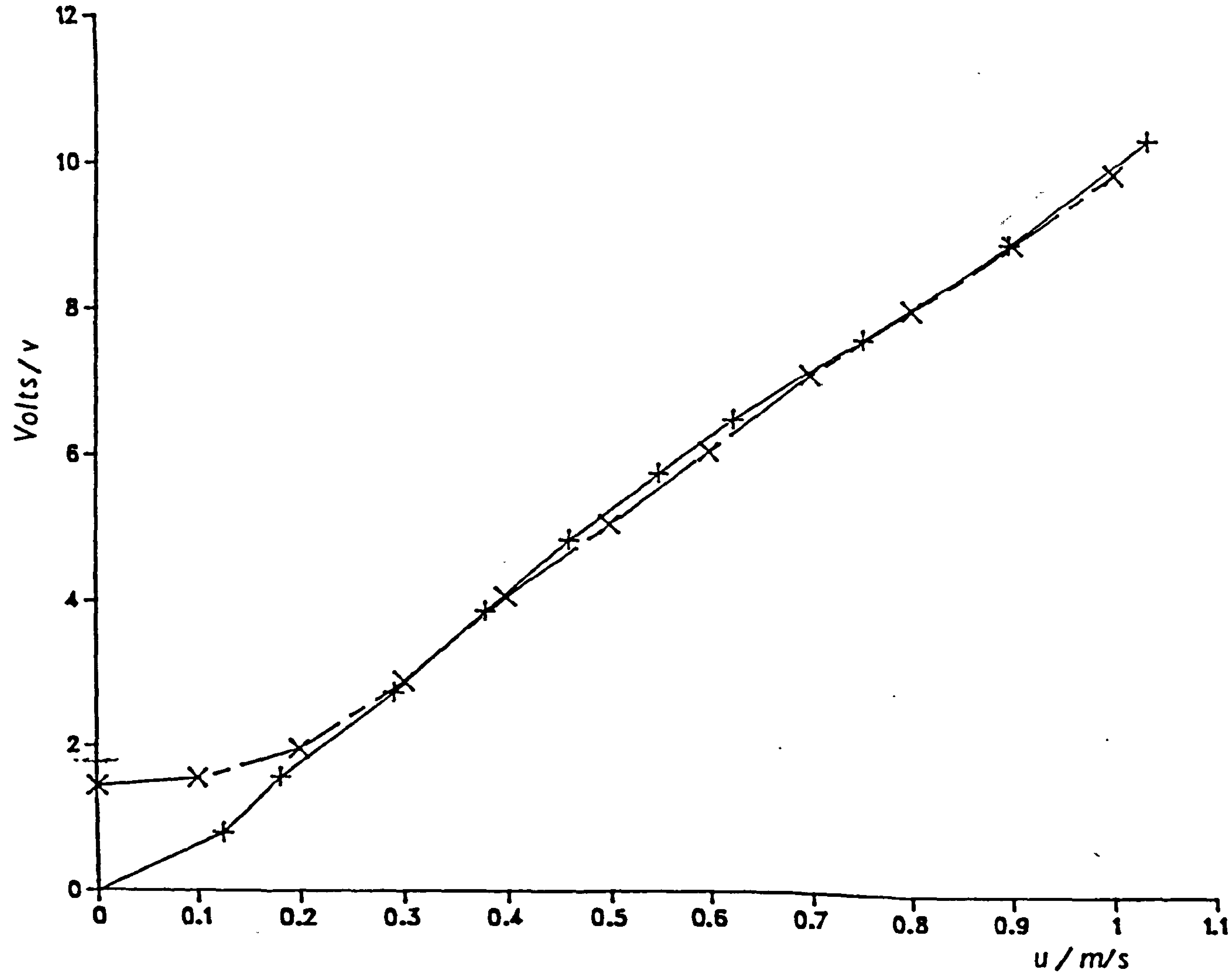

Figure A.1. Typical calibration curves for a velocity probe.
X initial calibration
+ subsequent calibration

APPENDIX B: A Typical recalibration result for a velocity probe

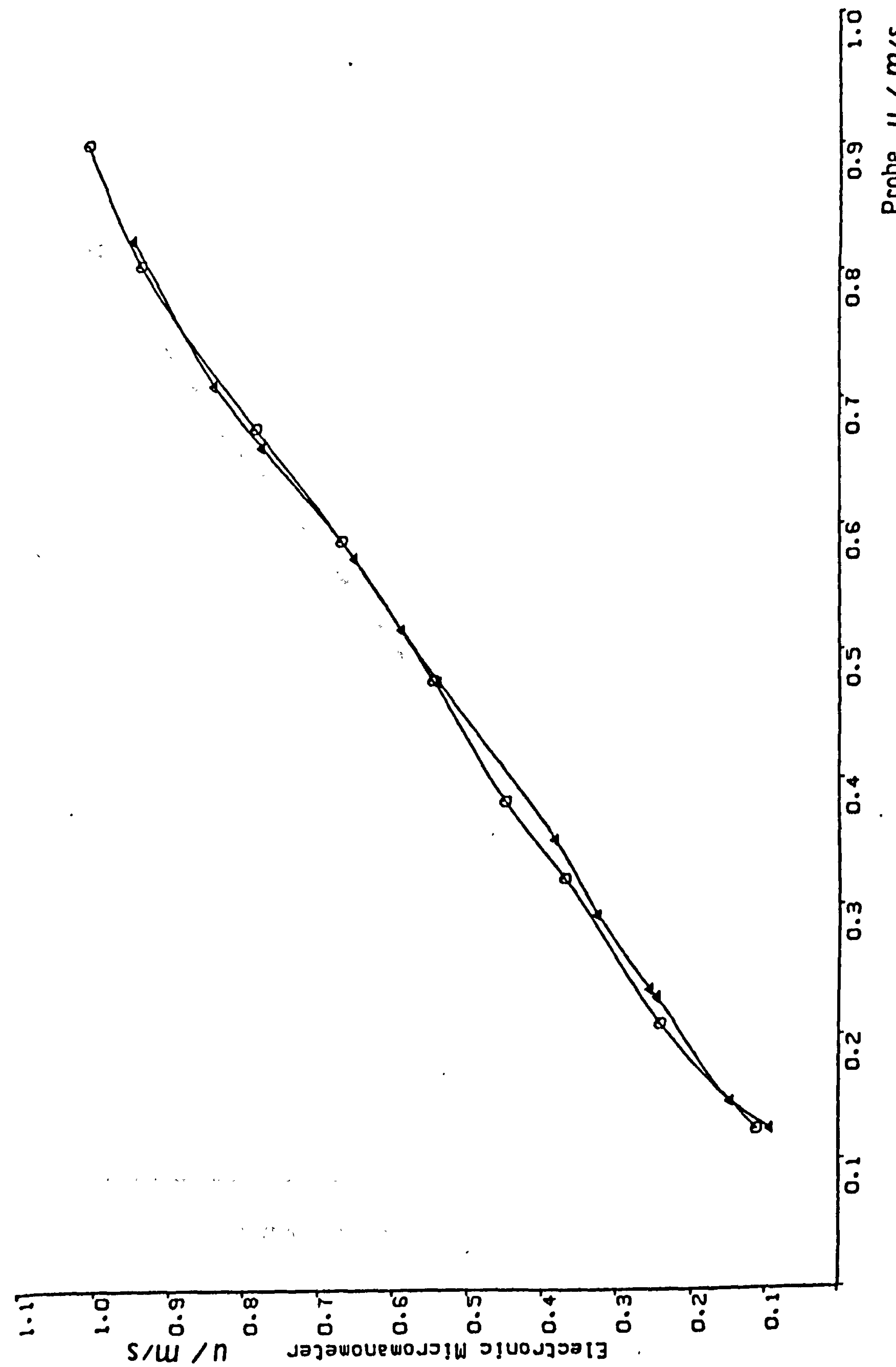

Figure B.1. Typical calibration curves for a velocity probe. Calibration was carried out in the wind tunnel against electronic micromanometer.
Δ before tests
O after tests.

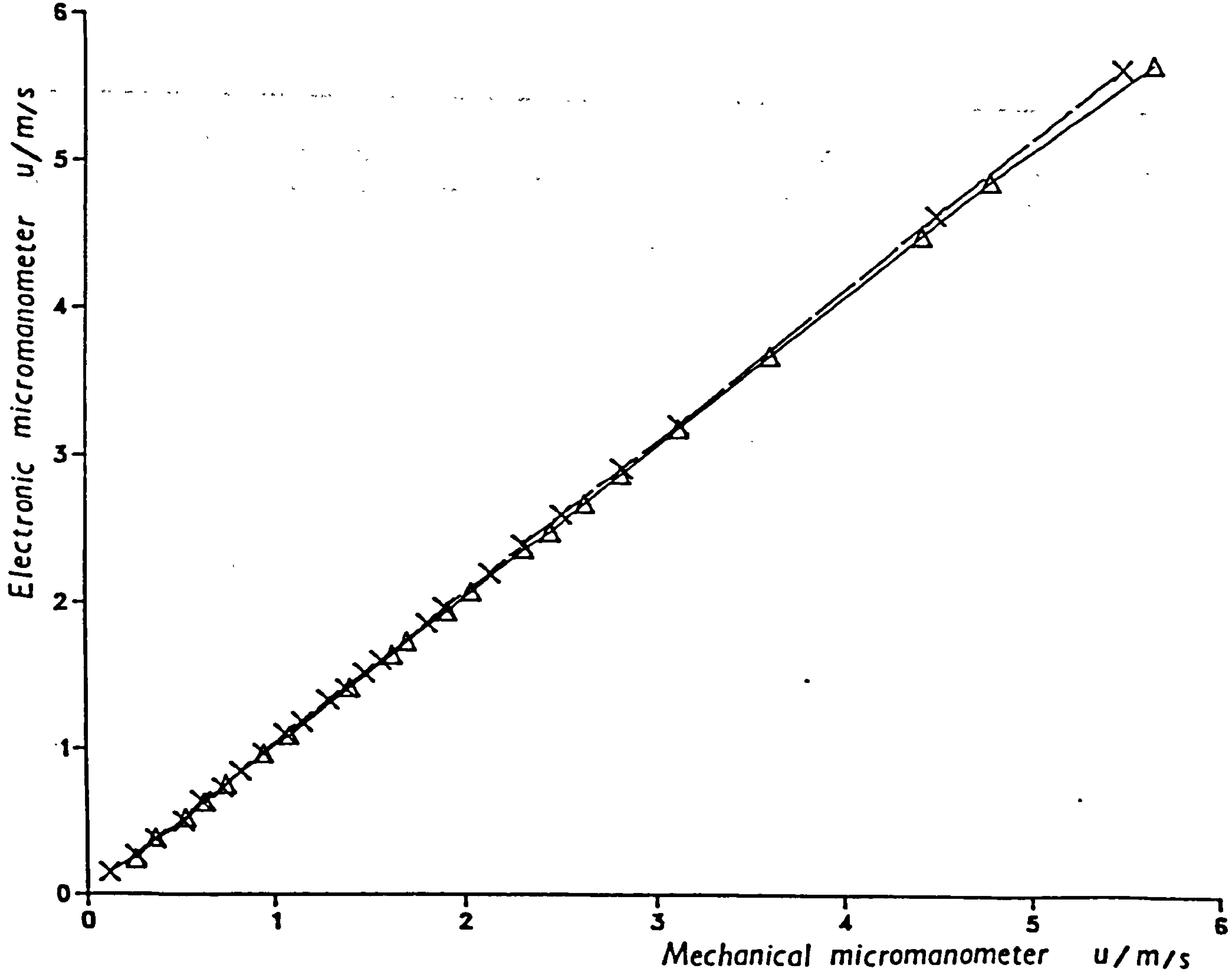

Figure B.2. Calibration curve for the electronic micromanometer against mechanical micromanometer.
Δ electronic micromanometer
X mechanical micromanometer

APPENDIX C: Temperature probe calibration results

mercury thermometer (°C)	probe (1) (°C)	probe (2) (°C)	probe (3) (°C)	probe (4) (°C)	probe (5) (°C)
18.8	18.71	18.92	18.86	18.74	18.83
20.2	20.09	20.29	20.25	20.11	20.21
22.8	22.71	22.91	22.87	22.74	22.82
24.6	24.51	24.72	24.67	24.53	24.61
27.0	26.84	27.04	27.00	26.86	26.93
29.8	29.57	29.79	29.73	29.59	29.67
32.0	31.74	31.95	31.91	31.77	31.84
34.1	33.87	33.81	33.96	33.94	34.03
37.2	36.85	36.81	37.02	36.93	37.01
39.1	38.76	39.00	38.94	38.80	38.88
41.1	40.79	41.01	40.96	40.82	40.89
44.2	43.83	44.06	44.02	43.88	43.95
46.6	46.14	46.38	46.33	46.19	46.26
48.9	48.37	48.60	48.55	48.40	48.48
50.4	49.75	49.98	49.94	49.80	49.87

(a)

mercury thermometer (°C)	probe (6) (°C)	probe (7) (°C)	probe (8) (°C)	probe (9) (°C)	probe (10) (°C)
18.0	17.74	18.38	18.05	18.05	18.43
20.3	20.14	20.77	20.45	20.88	20.83
20.5	20.29	20.95	20.59	21.06	20.99
21.3	21.07	21.75	21.36	21.85	21.77
24.2	24.03	24.73	24.32	24.84	24.75
27.5	27.31	28.03	27.61	28.14	28.04
30.1	29.91	30.60	30.21	30.70	30.62
33.7	33.60	34.26	33.84	34.36	34.27
37.7	37.61	38.33	37.90	38.43	38.33
40.7	40.59	41.35	40.88	41.45	41.33
44.3	44.14	44.92	44.41	45.01	44.89
47.7	47.49	48.29	47.78	48.39	48.25
50.1	49.89	50.68	50.18	50.77	50.63

(b)

Table C (a-b) Calibration results of the platinum resistance thermometers.

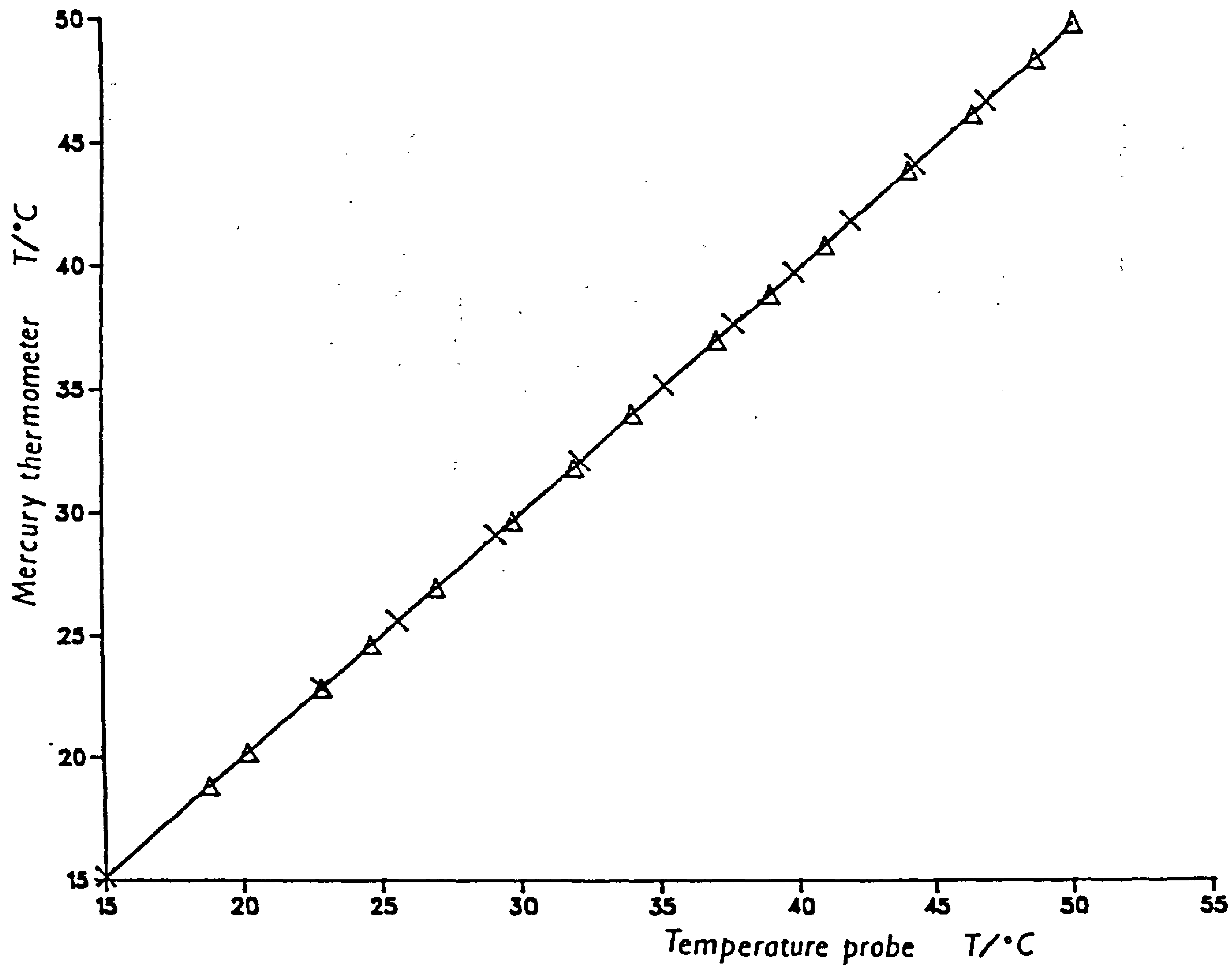

Figure C.1. A typical calibration curve for platinum resistance thermometer.
X before tests
Δ after tests.

APPENDIX D: DERIVATION OF TRACER GAS TECHNIQUE EQUATION

Concentration Decay Method

In this method a one-time injection of tracer gas is made. The gas was allowed to mix with the internal air of the stairwell model, using a small electric fan. The concentration of gas, over a given time interval, was then monitored with the gas analyser.

The generalised tracer gas continuity equation can be written as (See also Charlesworth [1988]):

$$V \frac{dC}{dt} = \dot{Q}_s (c - C) + P \tag{D.1}$$

V : Effective enclosure volume (m^3)

$\dot{Q}_s$: Specific air flow rate through enclosure ($m^3 s^{-1}$)

c : External concentration of tracer gas

C : Internal concentration of tracer gas

P : Production rate of tracer by all sources within the enclosure

Following injection of tracer gas, assuming there are no additional sources of tracer, the continuity equation, (D.1) reduces to:

$$V \frac{dC}{dt} = - \dot{Q}_s (C - c) \quad \text{or} \quad \frac{dC}{(C-c)} = - \frac{\dot{Q}_s}{V} \, dt \tag{D.2}$$

Assuming a constant flow rate, $\dot{Q}_s$, and integrating from both sides:

$$\int_{C_o}^{C_t} \frac{dC}{(C-c)} = - \frac{\dot{Q}_s}{V} \int_{t=0}^{t=t} dt \tag{D.3}$$

Where C_o and C_t are concentration of tracer gas at time t=0 and t=t, respectively.

Hence:

$$\ell n\ (C_t - c) - \ell n\ (C_o - c) = - \frac{\dot{Q}_s\ t}{V} \tag{D.4}$$

Or

$$\frac{\dot{Q}_s}{V} = \frac{\ell n\ (C_o - c) - \ell n\ (C_t - c)}{t} \tag{D.5}$$

Where $\dot{Q}_s/V$ = Air change rate

If the actual volumetric air leakage rate is required, then the determined value of $\dot{Q}_s/V$ must be multiplied by the volume of the enclosure.

APPENDIX E: Changes in dimensionless parameters from one-half scale model to full scale. The following information has been extracted from Reynolds (1986).

Fr_m/Fr	1	1.3	1.4	1.6
Re_m/Re	0.354	0.460	0.495	0.566
Gr_m/Gr	0.0442	0.0971	0.1213	0.1817
St_m/St	0.354	1.010	1.358	2.320
$\dot{V}_m/\dot{V}$	0.1768	0.2298	0.2401	0.4096
$\dot{Q}_m/\dot{Q}$	0.0625	0.1785	0.2401	0.4096
T_m/T	0.354	0.777	0.970	1.448
u_m/u	0.707	0.919	0.990	1.131

APPENDIX F: Calculation of air density and specific heat at constant pressure

(a) - Calculation of Air Density

The air density can be calculated from (Porges [1971])

$$\rho = 0.348\ (p_a - 0.378\ p)\ /\ (T + 273) \qquad (F.1)$$

where $p = p' - 6.66 \times 10^{-4}\ p_a\ (T - t_w)$ (F.2)

where p vapour pressure (mbar)

p' saturation vapour pressure at the wet-bulb temperature (mbar)

p_a atmospheric pressure (mbar)

T temperature (°C)

t_w wet bulb temperature (°C)

A simpler relationship for density has been suggested by Porges (1971)

$$\rho = 0.470\ p_a /\ (T + 273) \qquad (F.3)$$

Calculations for air temperatures between 20°C and 50°C and relative humidities within the range of 38 per cent to 70 per cent showed that equation (F.3) overestimates the density by up to 3 per cent, compared with values obtained using equation(F.1). Therefore, the above equation (F.3) was corrected and the density was obtained from the following equation:

$$\rho = 0.470 \frac{P_a}{(T + 273)} - 0.22 \tag{F.4}$$

This equation yields the density, for the above range of temperatures and humidities, with an error of less than 0.3 per cent.

(b) - Calculation of Specific Heat Capacity

The specific heat capacity at constant pressure was calculated from (see Jones [1973])

$$c_p = 1.012 + 1.89\ g \tag{F.5}$$

Where g is moisture content in kg/kg of dry air

However, omission of the term including g, for the range of temperatures and relative humidities mentioned in part (a) above, resulted in an error in the specific heat of less than 1 per cent. Therefore a single value of 1.025 kJ kg^{-1} $°C^{-1}$ was chosen for the specific heat.

APPENDIX G: List of some of the computer software in the field of Computational Fluid Dynamics.

1. HARWELL-FLOW3D

This program has been developed at Harwell, Oxfordshire, Great Britain. It is based on finite-volume technique, for the prediction of laminar and turbulent single-phase flows, and heat transfer, in two and three-dimensions. This program can handle complex geometries using body fitted co-ordinates, steady state or transient flows, buoyancy, compressibility and conduction in solid regions.

2. TEACH-T

This program has been developed by Gosman and Ideriah at Imperial College, London. It is a general computer program for 2-D laminar and turbulent recirculating flows. It is mainly for elliptic or separated flow applications. It uses Cartesian or cylindrical coordinates system.

3. FIDAP

This program has been developed by Fluid Dynamics International, Illinoise, USA. It is a general purpose computer program for the prediction of two and three dimensional incompressible fluid flows and heat transfer. It is based on finite-element technique. It can be applied to isothermal Newtonian and non-Newtonian flows, turbulent flows, free and forced mixed convection flows, environmental and atmospheric flows, swirling flows, flows in rotating frames of reference, flows with a free and moving surfaces, thermal flows, solid-fluid phase change, conjugate heat transfer. The program includes pre-processing mesh generation, file conversion and post-processing.

4. FLOW.FORTRAN

This program has been developed by M.R. Mokhtarzadeh-Dehghan, Mechanical Engineering Department, Brunel University. FLOW.FORTRAN is a program for 2-D, steady, single-phase, laminar and turbulent heat transfer and fluid flows. It solves the conservation equations of thermal energy and momentum using finite-volume technique. It is based on the two-equation eddy-viscosity k-ε model of turbulence. It uses Cartesian or curvilinear-orthogonal coordinates system and grid. It includes grid-generation and graphics routines for the presentation of the contour and vector plots. It is user friendly, easily adaptable to different problems.

5. FLUENT

This program has been developed in Sheffield University, but is marketed in USA by Creare Inc., and is distributed in Europe and UK by Flow Simulation Limited, Sheffield, Great Britain. It is a general purpose package, which can be used to analyse 2-D and 3-D laminar and turbulent flows with and without heat transfer. It solves the steady and unsteady fluid flow equations using a finite-difference technique. For turbulent flow problems, two turbulent flow models can be employed. These are the well-established k-ε model and algebraic stress model. It employs Cartesian or cylindrical coordinates systems.

6. PHOENICS

PHOENICS has been developed by CHAM Limited, London, Great Britain. It is a general-purpose one, two or three dimensional computer code, which can be used to simulate fluid flow, heat transfer and chemical reaction processes problems. It solves the conservation equations of mass, momentum and energy equations, using finite volume method. It incorporates the k-ε turbulence model. PHOENICS can provide Cartesian and cylindrical polar coordinate system. In addition a body-fitted-co-ordinate system is also available. Typical applications of PHOENICS are internal-combustion engines, air movement within an enclosed space (including in the presence of a fire), plume disposal in the atmosphere, external hydrodynamics and aerodynamics of cars, ships and buildings, thermal-hydraulics of nuclear reactors.